MULTI-DIMENSIONAL ANALYSIS OF HDL: AN APPROACH TO UNDERSTANDING ATHEROGENIC HDL

A Dissertation

by

JEFFERY DEVOYNE JOHNSON JR.

Submitted to the Office of Graduate Studies of
Texas A&M University
in partial fulfillment of the requirements for the degree of

DOCTOR OF PHILOSOPHY

December 2008

Major Subject: Chemistry

MULTI-DIMENSIONAL ANALYSIS OF HDL: AN APPROACH TO UNDERSTANDING ATHEROGENIC HDL

A Dissertation

by

JEFFERY DEVOYNE JOHNSON JR.

Submitted to the Office of Graduate Studies of
Texas A&M University
in partial fulfillment of the requirements for the degree of

DOCTOR OF PHILOSOPHY

Approved by:

Chair of Committee,	Ronald D. Macfarlane
Committee Members,	David H. Russell
	Gyula Vigh
	Stephen B. Smith
Head of Department,	David H. Russell

December 2008

Major Subject: Chemistry

ABSTRACT

Multi-Dimensional Analysis of HDL: An Approach

to Understanding Atherogenic HDL.

(December 2008)

Jeffery Devoyne Johnson Jr., B.S., Texas A&M University

Chair of Advisory Committee: Dr. Ronald D. Macfarlane

Density gradient ultracentrifugation (DGU) is a powerful method for analyzing lipoprotein particles in great detail. It yields considerable amounts of information regarding the density distribution of these particles when coupled with fluorometric analysis and is an invaluable tool in determining their relative abundance. This union allows relationships between subclasses of lipoproteins to be established that gives researchers a more focused path to aid them in developing methods to predict the early onset of coronary artery disease (CAD). The research presented here focuses on the pairing of DGU with post-separatory techniques including matrix-assisted laser desorption mass spectrometry (MALDI-MS), liquid chromatography mass spectrometry (LC-MS), capillary electrophoresis (CE), isoelectric focusing (IEF) and apoptosis studies involving cell cultures.

It is becoming clearer that cholesterol concentrations themselves do not provide sufficient data to assess the quality of cardiovascular health. As a result, research is becoming more focused on identifying better markers that may be indicative of development of CAD in a patient. Of specific interest is group of particles known as high density lipoproteins (HDL). Classically, this molecule is considered the "good cholesterol", but literature from the last decade suggests that there may be atherogenic variants to this group. By utilizing DGU as a preparatory method for secondary analyses, new dimensions can be added to the density distribution analysis to allow a

better determination of markers of cardiovascular health. The aim of this work is to utilize the principles involved with these various techniques to develop a comprehensive set of methods to aid in the detection of potential risk markers.

In this study, the properties of metal ion complexes of EDTA as solute systems for analysis of lipoproteins by DGU are analyzed. We show that by varying the complexing ion and counter-ion of these metal-ion complexes, we gain the ability to control the separation of lipoprotein subclasses for subsequent analyses. Qualitative and quantitative data is presented that describes the analysis of different density regions of HDL for apolipoprotein content. Trends between control and atherogenic samples are also described and a clinical link between the biological activity of these regions and the chemical analysis is discussed.

DEDICATION

To my parents Jeff and Cindi Johnson, my brothers Joshua and Christopher Johnson, and my loving friends and family that have provided support over the years.

ACKNOWLEDGEMENTS

I would like to acknowledge my research advisor Dr. Ronald D. Macfarlane for his guidance and support throughout the course of my undergraduate and graduate career and for helping me to "see the bigger picture" outside of my own research.

I would also like to thank my past and present colleagues, Brian Hosken, Leticia Espinosa, Richa Chandra, Mike Nowlin, Ron Henriquez, and Craig Larner, for their advice and support over the past few years. Brian Hosken helped me gain my footing in the group and provided a strong foundation from which I was able to expand into my dissertation project. I thank Leticia Espinosa, Richa Chandra, Mike Nowlin, and Craig Larner for the sharing of intellectual ideas regarding research in our group and for their general support during my graduate career.

I also greatly appreciate the collaborative efforts with Ron Henriquez in the latter stages of both of our dissertation projects. It has been invaluable being able to tackle the goals of our research projects when two different mindsets share ideas.

I also thank Dr. Catherine J. McNeal at Scott & White Hospital in Temple, Texas, for the opportunity to assist in ongoing clinical studies and to truly be able to observe what an impact that laboratory results can have outside of the scope of an individual research group.

I would also like to acknowledge Dr. Shane Tichy for his invaluable assistance with the MALDI-MS and LC-MS portions of my project and also Dr. Earle Stone for his guidance and support over the course of my graduate studies.

I would also like to acknowledge my committee members: Dr. David Russell, Dr. Gyula Vigh, and Dr. Stephen Smith for their support during my academic career.

LIST OF ABBREVIATIONS

1-D	One-dimensional
2-D	Two-dimensional
ACN	Acetonitrile
Apo	Apolipoprotein
BB	Borate buffer
bTRL	Buoyant triglyceride-rich lipoproteins
C_4	Carbon tail of four atoms
C_{18}	Carbon tail of 18 atoms
CE	Capillary electrophoresis
CETP	Cholesteryl ester transfer proteins
CHAPS	3-(3-choloamidopropyl)dimethyl ammonio-1-propane sulfonate
CM	Chylomicrons
CsBiY	Cesium bismuth ethylenediaminetetraacetic acid
Cs_2CdY	Dicesium cadmium ethylenediaminetetraacetic acid
CAD	Coronary artery disease
DGU	Density gradient ultracentrifugation
DMSO	Dimethyl sulfoxide
dTRL	Dense triglyceride-rich lipoproteins
EDTA	Ethylenediaminetetraacetic acid
HDL	High density lipoproteins

HAS	Human serum albumin
IEF	Isoelectric focusing
IPG	Immobilized pH gradient
IDL	Intermediate density lipoproteins
LCAT	Lecithin: cholesterol acyltransferase
LDL	Low density lipoproteins
LP	Lipoproteins
Lp(a)	Lipoprotein a
LPL	Lipoprotein lipase
MALDI-MS	Matrix-assisted laser desorption ionization mass spectrometry
NaBiY	Sodium bismuth ethylenediaminetetraacetic acid
NBD	7-nitro-2,1,3-benz-oxadiazol-4-yl
pI	Isoelectric point
SDS	Sodium dodecyl sulfate
TAG	Triglycerides or Triacylglycerol
TFA	Trifluoroacetic acid
TOF	Time of flight
TRL	Triglyceride-rich lipoproteins
UC	Ultracentrifugation
VLDL	Very low density lipoproteins

TABLE OF CONTENTS

CHAPTER Page

CHAPTER Page

LIST OF FIGURES

FIGURE Page

FIGURE Page

FIGURE Page

FIGURE Page

LIST OF TABLES

CHAPTER I

INTRODUCTION

1.1 Significance

In a sample of human serum there is a distribution of nanoparticles on the micromolar level known as lipoproteins that play key roles in the metabolism and transportation of lipids, triglycerides, cholesterols and their corresponding esters. In the diagnosis of coronary artery disease (CAD), it is important to evaluate the composition of serum for potential risk factors such as high concentration of low density lipoprotein (LDL), low concentration of high density lipoprotein (HDL), or the presence of potentially atherogenic proteins such as Apo C-I and Lp(a).[1]

One manner of separating and identifying lipoprotein particles is through the use of density gradient ultracentrifugation (DGU). In DGU, particles migrate to their isopycnic point during a spin at high speeds resulting in a lipoprotein density profile. Since different classifications of lipoprotein particles are defined by their hydrated densities, DGU is the primary tool of analysis in the field of lipoproteomics.[2] The different regions of the lipoprotein density profile can be enhanced by optimizing parameters such as the molecular weight of the density gradient-forming solute, its concentration, or the spin time.[3, 4] By utilizing these principles it becomes possible to isolate desired subclasses for further study.

Another analytical technique that yields information regarding the size/charge of the molecular system being studied is mass spectrometry. In this technique, the sample is ionized through a variety of means including electron ionization[5], chemical ionization[6], secondary ion mass spectrometry (SIMS)[7], electrospray ionization (ESI)[8], and matrix-assisted laser desorption ionization (MALDI).[9]

This dissertation follows the style of *Analytical Chemistry*.

The latter two are the most common in protein analysis since a soft ionization technique is desired to prevent excessive fragmentation of the molecules of interest.

Capillary electrophoresis (CE) is another useful analytical tool for the study of lipoproteins.[10, 11] By varying the properties of the buffer system to be used, lipoproteins can be analyzed in both their nascent and delipidated forms to give information regarding the size/charge of the intact molecule and their associated apolipoproteins.[12] The effective electrophoretic mobility for various subclasses can be determined for comparison between samples by analyzing the movement of lipoprotein particles in a buffer under the influence of an applied electric field. Molecules possessing different electrophoretic mobilities will travel at different rates, so this technique gives a second degree of separation after DGU.

Isoelectric focusing (IEF) is a very useful technique that utilizes differences in the inherent charge states of proteins in buffered solution. By introducing proteins into a gel matrix that contains a continuous pH gradient and then applying a potential, proteins can be separated based on mobility due to differences in their respective isoelectric points (pI).[13] Using this method, complex mixtures of macromolecules, such as the distribution of apolipoproteins inherent in HDL, can be separated with high resolution.[14]

This work utilizes the techniques of DGU, MS, CE, and IEF to develop a unified method for identifying new risk factors, particularly those regarding atherogenic HDL, for the early detection of CAD.

1.2 Structural and Functional Description of Lipoproteins

Lipoprotein particles are biochemical assemblies of lipids and proteins that are responsible for the transport of lipids in the bloodstream and are classified primarily based on their respective densities (Table 1).[15]

Table 1. Lipoprotein Characteristics

Class	Density (g/mL)	Size (nm)	Major Lipids	Major Apolipoproteins
Chylomicrons	< 0.93	100 - 500	Dietary TAGs	B-48, C-II, E
VLDL	0.93 -1.006	30 - 80	Endogenous TAGs	B-100, C-II, E
IDL	1.006 -1.019	25 - 50	CEs and TAGs	B-100, E
LDL	1.019 -1.063	18 - 28	CEs and TAGs	B-100
HDL	1.063 -1.210	5 - 15	PL	A, C-II, E
Lp(a)	1.040 -1.090	25 - 30	CEs	B-100, Glycoprotein

This classification is only relative to the condition of a lipoprotein in the lipid metabolic cycle since they are constantly in flux between identities and roles.[16] Lipoproteins are water-soluble macromolecules that contain a hydrophilic exterior surrounding a hydrophobic core and are very similar to micelles in structure (Figure 1).

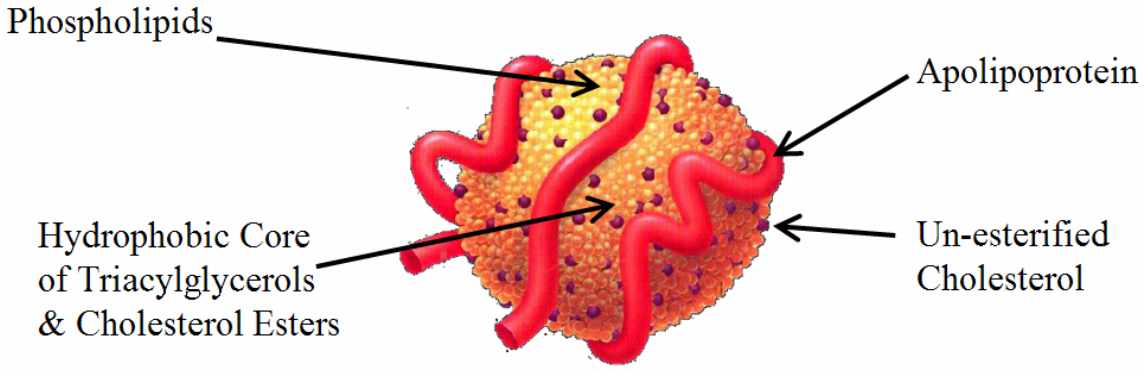

Figure 1. Basic Composition of a Lipoprotein

Encasing the lipid core is a shell of tightly packed phospholipids and cholesterol that is oriented in such a way that the polar groups extend outward and the hydrophobic tails point inward.

There is also a relationship between the density of lipoproteins and the biological role they play in lipid metabolism. Lipoprotein particles with lower densities have a higher lipid composition whereas denser lipoproteins have a higher protein composition. Chylomicrons, also known as buoyant triglyceride-rich lipoprotein (bTRL), are secreted by the small intestine and are responsible for the transport of exogenous lipids to the liver, adipose tissue, and muscle. In the case of the lipid transport lipoprotein, VLDL, also known as dense triglyceride-rich lipoprotein (dTRL), several exchanges of apolipoproteins with HDL and interactions with lipoprotein lipase (LPL) occur. This causes it to lose much of its lipid content and become IDL then eventually LDL, which are progressively denser molecules. Though their densities are similar, chylomicrons possess the apolipoprotein Apo B-48 which is a truncated form of Apo B-100 that VLDL contains. LDL is responsible for the transport of cholesterol and cholesteryl esters from the liver to tissues in the body while HDL is responsible for transporting these particles from tissues back to the liver in a process known as reverse cholesterol transport. The only apolipoprotein that is typically found on an LDL particle is Apo B-100, whereas HDL can contain an array of various apolipoproteins, though to be classified as HDL, a molecule of Apo A-1 must be present.

1.2.1 Lipoprotein Subclasses

In addition to the standard lipoprotein classes of VLDL, LDL, and HDL there are also subclasses of these groups that can serve as important markers of cardiovascular health, making it important to isolate these various molecules for further study. There are two subclasses of triglyceride-rich lipoproteins, five subclasses of LDL, and five subclasses of HDL that are assigned based on their respective densities as defined by sequential flotation (Table 2).[17]

Table 2. Densities of Lipoprotein Subclasses

Lipoprotein Subclass	Density (g/mL)
bTRL	< 1.000
dTRL	1.000 - 1.019
LDL-1	1.019 - 1.023
LDL-2	1.023 - 1.029
LDL-3	1.029 - 1.039
LDL-4	1.039 - 1.050
LDL-5	1.050 - 1.063
HDL-2b	1.063 - 1.091
HDL-2a	1.091 - 1.110
HDL-3a	1.110 - 1.133
HDL-3b	1.133 - 1.156
HDL-3c	1.156- 1.179

The triglyceride-rich lipoprotein subclasses are so named based upon their interaction with water following a density gradient separation; the buoyant fraction will float to the surface while the dense fraction will not. The buoyant fraction is composed primarily of chylomicrons and chylomicron remnants while the dense class is composed of VLDL and VLDL remnants, also known as intermediate density lipoprotein (IDL). Remnant lipoprotein particles are also important subclasses of lipoproteins that can play a significant role in impacting the cardiovascular health of an individual. Chylomicron remnants are essentially what are leftover after the triglyceride components from chylomicrons are unloaded by the activity of lipoprotein lipase. IDL is a remnant of VLDL hydrolysis and typically serves as a short-lived intermediate before being cleared by endocytosis or conversion into LDL.[2] These remnant particles tend to be smaller than their nascent structures and are mostly depleted of triglycerides, phospholipids, and Apo A and Apo C, and are enriched with cholesterol, cholesteryl esters, and apo E.[18] Their small size gives these types of particles an increased ability to penetrate into the arterial

wall for foam cell formation and should be considered an independent risk factor for the development of CAD.

The LDL subclasses are defined solely by their densities which reflect the relative amounts of cholesteryl ester and triacylglycerol present in each. Typically, two main phenotypes are recognized: phenotype A which is composed of predominately large, buoyant LDL, and phenotype B which is composed of predominately small, dense LDL.[19, 20] Particles of the most predominant LDL subclass in each phenotype have estimated diameters of greater or less than 25nm respectively for phenotypes A and B. Studies of family genetics have also linked the LDL distribution in phenotype B to the presence of a single major gene. [21, 22] Beyond these two main phenotypes, various degrees of further separation have been achieved, including the attainment of seven LDL subclasses by gradient gel electrophoresis (GGE)[23], and five LDL subclasses by DGU in our own laboratory. The principle difference between these different subclasses is lipid composition; as the LDL particles become smaller and denser, they carry with them an increased atherogenic risk due to their ability to more readily penetrate into the arterial wall.

The HDL subclasses are split into two functionally distinct categories: the buoyant HDL-2 group and the dense HDL-3 group, and then are further subdivided into density distinct subclasses. The lipid-deficient HDL-3 is typically converted into the more lipid-rich HDL-2 during the lipolysis of VLDL by hepatic lipoprotein lipase.[24] Another important distinction is that while both categories of HDL contain Apo A-I, only HDL-3 typically contains both Apo A-I and Apo A-II. While the general consensus seems to be that having a lipid profile containing a high concentration of HDL is desirable, there is currently a considerable amount of disagreement as to the true role of HDL in the development of CAD. There have been studies linking atherosclerosis[25] and myocardial infarction[26] with levels of HDL-2 cholesterol. There have also been clinical studies that show a strong relationship between HDL-3 cholesterol and cardiovascular risk.[27] Though these studies would imply that there are only two subclasses of HDL cholesterol, in actuality there are at least five by DGU and at least seventeen by IEF.[28, 29]

Ambiguity in this area lends itself to the importance of developing a method that is capable of thoroughly and accurately analyzing HDL to better understand its role in cardiovascular risk.

1.2.2 Major Apolipoprotein Components of HDL

Common risk factors for the development of CAD include: high levels of LDL cholesterol (greater than 160 mg/dL), high total cholesterol (greater than 200 mg/dL), low HDL cholesterol (less than 60 mg/dL), cigarette smoking, hypertension, family history, and age.[30] The objective of the study reported here is to examine serum samples for non-traditional risk factors with an emphasis on the apolipoprotein composition of HDL. It is currently suspected that there are atherogenic variants of HDL, usually known as the cardio-protective "good cholesterol," that may actually serve a role in the early development of CAD.

At any given time, a sample of serum contains a heterogeneous distribution of HDL molecules of various apolipoprotein compositions. The defining apolipoprotein of HDL is apo A-1, which serves as a the backbone of the HDL particle and has a high lipid binding capacity.[31] It exists as a 28,078.6 Da protein and serves in cholesterol transport through the activation of the enzyme lecithin:cholesterol acyltransferase (LCAT) which causes esterification of fatty acids from phosphatidylcholine to the 2-hydroxyl group of cholesterol.[32, 33]

In addition to apo A-I, the apolipoprotein A-II is another protein that is present in considerable abundance and helps to provide structure for the HDL molecule.[31] Apo A-II exists as a dimer of two 77 amino acid monomers that are linked together by a disulfide bridge and has a molecular weight of 17,379.8 Da.[34] It is synthesized in the liver and can act to displace apo A-I from HDL or even to form nascent HDL particles primarily containing only apo A-II.[35, 36] This apolipoprotein has also been determined to have a negative influence on reverse cholesterol transport and may contribute to the development of atherosclerosis when expressed in high abundance.[36-38]

Apo C-I is a much smaller apolipoprotein that is associated with HDL, composed of 57 amino acids and having a molecular weight of only 6630.6 Da.[31] Apo C-I can also be found in molecules of VLDL and even in chylomicrons though it is synthesized in the liver.[39, 40] It is mainly responsible for the activation of LCAT, but may also promote atherosclerosis due to its role in displacing apo E from the HDL molecule.[37, 41, 42] Apo E is required in the binding of β-VLDL to the LDL-receptor protein, but is hindered by apo C-I, thereby interfering with the clearance of triglyceride-rich lipoproteins (TRL) in the liver.[42] Apo C-I also inhibits cholesterol ester transfer protein (CETP), which is responsible for lipid transfer between lipoprotein particles, and lipoprotein lipase (LPL), which hydrolizes lipids in lipoproteins.[43-45] In normolipidemic individuals, the serum concentration is about 6 mg/mL.[46] However, an increased concentration of apo C-I may be a marker for the development of CAD.[47, 48]

Some other important apolipoprotein components of HDL that are present in low abundance include: apo C-II, apo C-III, and apo E, each with their own unique roles in lipid metabolism. Apo C-II is a 8914.2 Da protein that is responsible mainly for the activation of LPL and LCAT.[49, 50] A deficiency of this protein impairs plasma clearance of triglycerides and can cause hypertriglyceridemia.[51] Apo C-III is a 79 amino acid protein that exhibits three masses that are dependent on the degree of sialation at the 74th position and ranging in molecular weight from 8764.7 Da to 9712.6 Da.[31] Its main roles are in the modulation of the uptake of TRL remnants by the liver receptors, and in the inhibition of LPL and hepatic triglyceride lipase (HTGL).[45, 52-55] High concentrations of apo C-III have been shown to increase the progression of atherosclerosis and also recurrence of cardiac events.[56-58] Apo E is a 299 amino acid protein that also exhibits three masses that differ at the 112th and 158th positions and ranges in molecular weight from 34183.6 to 34928.8 Da.[31, 59, 60] It has many roles in lipoprotein metabolism, including: mediation of remnant TRL and cholesterol uptake in the liver through apo E receptor recognition, redistribution of lipids in tissue, formation of cholesterol ester-rich HDL particles, and binding of heparin.[31, 61-63] Elevated levels of apo E correlate with

hypertriglyceridemia while a deficiency correlates with increased levels of TRL remnants.[64, 65]

1.2.3 Markers of Cardiovascular Risk

In a healthy lipid profile, an individual traditionally expresses low total cholesterol with a low level of LDL cholesterol and a high level of HDL cholesterol. Conversely, an individual with an atherogenic lipoprotein phenotype expresses a high total cholesterol with elevated VLDL and LDL, particularly LDL-3 cholesterol, and a low level of HDL cholesterol. HDL is known to play a role in maintaining a healthy lipid metabolism, but recent evidence suggests that there are forms of HDL that can actually contribute to CAD risk in an individual.[66] Previous research also shows that there is a form of HDL that is rich in Apo C-I that was found in infants that were small for gestational age (SGA) who tend to prematurely develop CAD later in life.[67] Normally, Apo C-I is an apolipoprotein of HDL that is responsible for the inhibition of cholesterol ester transfer protein (CETP) and is important to the regulation of cholesterol transport, but it is currently a suspected independent risk marker for early onset of CAD.[47, 48, 67, 68]

1.3 Current Methods of Analysis

Several commercial methods of analyzing lipoproteins have been developed, such as: gradient gel electrophoresis (GGE), tube gel electrophoresis (TGE), ultracentrifugation-vertical auto profile (VAP), and nuclear magnetic resonance (NMR). Unfortunately, the low amount of agreement between the results of these techniques warrants more accurate and precise methods of analysis.[69]

In gel electrophoresis techniques, molecules are separated based on physical characteristics such as size, shape, or pI and can be used as a preparative tool for other techniques like mass spectrometry, sequencing, or blotting.[70] Krauss and coworkers have utilized GGE to investigate the small dense class of LDL that is associated with familial combined hyperlipidemia (FCHL). [71] This is a genetic disorder of lipid

metabolism usually associated with elevated cholesterol levels, high LDL concentration, and diminished HDL concentration. It was found that there is a bi-modal distribution of LDL size among patients that can be associated with two metabolically distinct phenotypes: pattern A consisting of large buoyant particles, and pattern B consisting of small dense particles. Under a similar separation principle to GGE, TGE permits separation of LDL into seven subfractions in a time span of sixty minutes, making it much more practical in a clinical setting.[72] Compared to slab gels, tube gels are advantageous because lateral movement of proteins is less prone to occur, thereby improving resolution.

The VAP method, utilized by Atherotech, is a centrifugation technique that employs dense solutions of KBr to isolate the various lipoprotein fractions followed by a scan of the absorbance of the solution over the length of the tube.[73, 74] This typically entails puncturing the bottom of the centrifuge tube using a continuous-flow chemistry analyzer to monitor the sample as it elutes. This method has allowed for the analysis of five subclasses of LDL as well as two subclasses of HDL and is similar to the DGU methods reported by Hosken and Johnson.[3, 4] The key differences are that the VAP method utilizes KBr salts as opposed to salts of heavy metal EDTA complexes and measures components based on UV absorbance instead of fluorescence. The VAP method also yields a crude separation of the lipoprotein classes, whereas the DGU method relies on the equilibration of lipoprotein particles as the gradient forms during a spin. The VAP method also utilizes a vertical orientation in the rotor as opposed to a fixed angle or swinging bucket configuration. A further disadvantage of this method is that some lipoprotein material may irrecoverably adhere to the sides of the elution tubing.

As an alternative to separatory techniques of analysis, NMR provides a spectroscopic means of both quantifying lipoprotein particles and also giving information regarding their respective sizes.[75, 76] This technique benefits from not requiring a pre-separation of the complex mixture of lipoprotein particles for analysis thereby offering a short analysis time, and has reportedly yielded results in good

agreement with both GGE and DGU. The basic concept involves three steps: measurement of the plasma NMR spectrum, computer deconvolution, and calculation of concentration. In particular, the methyl groups associated with the different types of lipid particles: phospholipids, cholesterol, cholesteryl esters, and triglycerides are measured. Though it is not possible to distinguish between the methyl groups between these particles, the intensity of the bulk signal allows a quantification of the concentration of the sample, while the size of the particles affects the frequency and shape of the signal.[77]

To date, the most widely cited and used method of measuring cholesterol has been the Friedewald method, dating back over three decades.[78] This method involves measuring the total cholesterol and total triglycerides by enzymatic methods, and measuring HDL cholesterol by rapid precipitation, then estimating the LDL cholesterol. (Eq. 1)

$$C_{LDL} = C_{Plasma} - C_{HDL} - \frac{TG}{5} \qquad (1)$$

Though this has been a useful approximation, a direct measurement of the LDL cholesterol is a more desirable method of analysis.

1.4 Density Gradient Ultracentrifugation

The lipid component of lipoprotein particles gives them a density that is substantially less than other constituents of plasma, allowing them to be isolated by ultracentrifugation (UC).[17] Traditionally, there are two primary techniques employed for lipoprotein separation: rate zonal UC and isopycnic UC. In rate zonal UC experiments, samples are layered beneath a preformed gradient comprised of different zones of particles of given flotation rates. When centrifugal force is applied, the sample particles float through the gradient in separate zones, and the experiment is stopped before these zones migrate to the top of the UC tube. Particles are therefore separated based on

which zone they migrate into. In isopycnic separations, the density gradient covers the entire range of densities expected in the sample to be measured. When centrifugal force is applied in this case, sample particles will migrate to the position in the tube at which its own density corresponds to the density of the gradient-forming solution, also known as the particle's isopycnic point. Particles in this case are separated based solely on differences in their respective densities. Though the isopycnic point of a particle is a fixed property of the molecule being studied, its relative position in a UC tube during an experiment can be modified by adjusting the density gradient-forming solute.

1.4.1 Sedimentation Theory

As a DGU experiment is being performed, there are two competitive forces that result in an equilibrium gradient solution: sedimentation and diffusion (buoyancy). If a particle with mass, m, is subject to a centrifugal field caused by a spinning rotor with angular velocity, ω, and radius, r, the particle will experience a centrifugal force as seen in the following formula: (Eq. 2)[79]

$$F_{centrif} = m\omega^2 r \qquad (2)$$

Displacement of solvent particles will occur as the solute particles are placed in motion, and will have a resistance to this displacement, otherwise known as the buoyant force (ν). This force will reduce the net force on the solute particles by a factor of (ω^2r) times the mass of the solvent being displaced. Since mass can be determined by multiplying the density (ρ) of a solution by its volume, written as mass (m) times the partial specific volume ($\bar{\upsilon}$), the resulting buoyant force is given by: (Eq. 3)[79]

$$F_{buoyant} = \omega^2 r m \bar{\upsilon} \rho \qquad (3)$$

The frictional force between the solvent and solute particles must also be accounted for since it opposes the motion of both the centrifugal and buoyant forces.

The frictional coefficient (f) is a function of the velocity (υ) of the moving particles, but when the net force on the particles is zero, as is seen in the case of equilibrium, the velocity of the particles is constant and the equation becomes: (Eq. 4)[79]:

$$\upsilon = \frac{\omega^2 m(1-\bar{\upsilon}\rho)}{f} \tag{4}$$

Equation 4 explains several key points about sedimentation theory. Massive particles, as well as dense particles, tend to move faster than smaller or more buoyant particles. Also, denser solutions will cause the particles to move more slowly due to a higher frictional coefficient between solute and solvent, thereby causing the particles to move more slowly as well.

When a gradient-forming solute system is spun in a DGU experiment beginning from a homogeneous solution, the density of the solution will increase exponentially as the solution depth proceeds away from the meniscus. (Eq. 5) In other words, the meniscus of the solution will have a low tube coordinate and the bottom of the UC tube will have a high tube coordinate. This density versus tube coordinate relationship can be fitted to an exponential curve function and will typically range from 1.00 g/mL, the density of pure water, to as high as approximately 1.40 g/mL.

$$\rho = Ae^{(x/B)} + y_0 \tag{5}$$

In this equation the density, ρ, is calculated as a function of the UC tube length, x, with coefficients A, B, and intercept y_0. By creating a calibration curve linking refractive index with the density of these solutions, the slope of the density curves can be obtained by spinning a solution of the desired density gradient-forming solute and measuring the refractive index as a function of tube depth. The resulting density curve is useful in equilibrium isopycnic DGU experiments because it becomes possible to determine the density of the components of a sample based on their position in the UC tube.

During a DGU experiment, it is seen that the molecular weight (M) of gradient-forming solute systems is an important factor in determining the slope of the density curve, resulting in various degrees of separation of components in a mixture.[4] The relationship between the molecular weight of the gradient-forming solute and the slope of the density curve can be derived by using the free energy concept. At equilibrium the concentration of molecules are not equal throughout the solution though the free energy must be the same throughout the solution. This means that free energy ($\Delta G_{centrif}$) decreases as work is done by centrifugal force to move a molecule of mass m' (corrected for buoyancy of the solute) from point r_1 to point r_2 as given by the following: (Eq. 6)[79]

$$\begin{aligned} \Delta G_{centrif} &= -\int_{r_1}^{r_2} m' r \omega^2 dr \\ &= -\frac{m'\omega^2}{2}(r_2^{\,2} - r_1^{\,2}) \end{aligned} \tag{6}$$

The variable m' is equivalent to the term $m(1-\bar{\upsilon}\rho)$, which, when substituted into Eq. 6 becomes: (Eq. 7)[79]

$$\Delta G_{centrif} = \tfrac{1}{2} m(1-\bar{\upsilon}\rho)\omega^2(r_2^{\,2} - r_1^{\,2}) \tag{7}$$

The free energy change is not zero, but does move in the direction of the centrifugal field and is balanced by the force of diffusion. This means that as a molecule moves from a coordinate of r_1 at a concentration of c_1 to a coordinate of r_2 with a concentration of c_2, the free energy change (ΔG_{diff}) is seen as: (Eq. 8)[79]

$$\Delta G_{diff} = kT \ln(c_2/c_1) \tag{8}$$

At equilibrium, $\Delta G_{centrif}$ is equal to ΔG_{diff}, therefore Eq. 7 and Eq. 8 can be reduced to: (Eq. 9)[79]

$$m = \frac{\ln(c_2/c_1)(2kT)}{(1-\bar{\upsilon}\rho)\omega^2(r_2^2 - r_1^2)} \tag{9}$$

Since m is in grams, the molecular weight can be determined by multiplying by Avogadro's number (N), and since N k = R, Eq. 9 becomes: (Eq. 10)[79, 80]

$$M = \frac{\ln(c_2/c_1)(2RT)}{(1-\bar{\upsilon}\rho)\omega^2(r_2^2 - r_1^2)} \tag{10}$$

1.4.2 Solute Systems

Common solute systems for the separation of lipoprotein particles in DGU include KBr,[81, 82] CsCl,[83] and sucrose.[84] These also exists less common, non-ionic solute systems such as the iodinated Nycodenz[85] and Iodixanol.[86] The evolution of these various solute systems over time has steadily led to better separations of lipoprotein particles.

Alkali halide salts such as KBr and CsCl require a discontinuous gradient system that is labor intensive to prepare and is more suitable for sequential flotation experiments. Since they require high salt concentrations, they also result in final solutions that have a high ionic strength. This can be detrimental to lipoprotein analysis because high salt concentration can potentially disrupt the hydrophobic domains of proteins, thereby affecting their native structure.

The non-ionic gradient-forming solutes circumvent the ionic strength problem, while still offering the ability to successfully separate lipoprotein particles. Sucrose has traditionally been utilized in such experiments due to its high solubility and low cost. However, sucrose is so viscous that DGU experiments are typically limited to rate-zonal spins. Furthermore, sucrose also interacts so strongly with lipoprotein particles that it

can be difficult to fully remove from lipoprotein samples. This poses considerable problems when attempting to study the intact structure of lipoprotein particles since the sucrose can affect their native state. Nycodenz and Iodixanol are two other non-ionic self-generating gradients that allows for a much shorter analysis time than the alkali halide salt methods. Due to the iodization found in their structures, they are a considerably higher molecular weight than sucrose, which allows them to form a density gradient more quickly. They also can be removed relatively easy from samples following a centrifugation experiment, making them useful for preparative work.

1.4.3 Fluorometric Imaging of Lipoproteins

Prior to DGU analysis, lipoprotein molecules are fluorescently labeled by a lipophilic molecule known as NBD (C_6-ceramide) (Figure 2).[3, 4, 10]

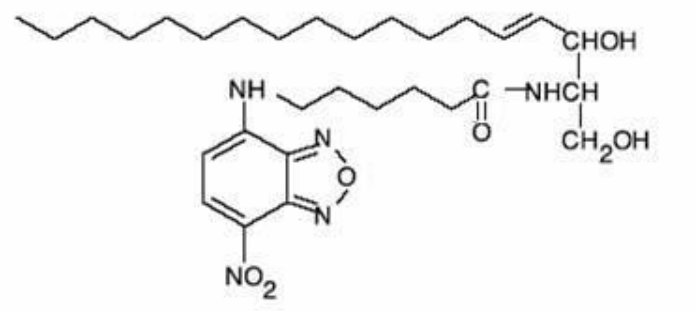

Figure 2. Structure of NBD (C_6-ceramide)

This fluorophore consists of a hydrophilic head and a hydrophobic tail and only fluoresces when the fluorescent head is incorporated into a hydrophobic environment, such as the lipid core of a lipoprotein particle. When it is in a favorable environment, the NBD-lipoprotein complex will exhibit characteristic excitation and emission spectra (Figure 3). Once the serum sample is incubated with this molecule, it is analyzed by DGU. Upon completion of the spin, the fluorescence of the NBD-lipoprotein complex allows for the generation of a lipoprotein density profile that enables a visualization of the distribution of lipoprotein particles.

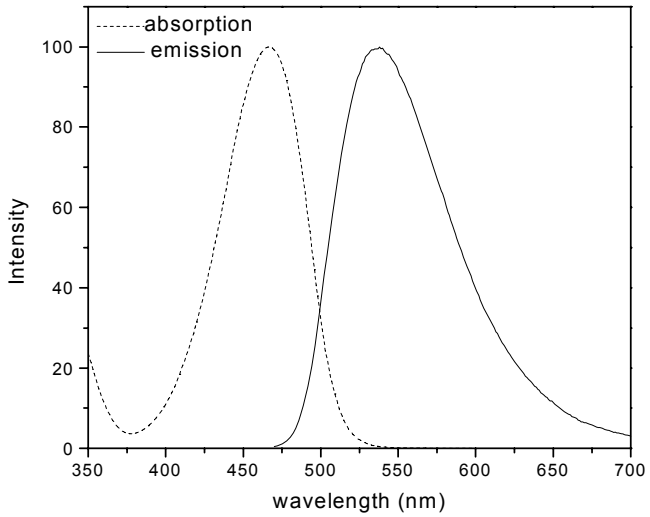

Figure 3. Excitation and Emission Spectra of NBD (C_6-ceramide)

1.4.4 Statistical Analysis

The utilization of NBD (C_6-ceramide) as a lipophilic stain for lipoprotein density profiling can be useful in generating data to describe the distribution of lipoproteins in a patient sample as a function of density and abundance. In addition, this data can be used to classify cardiovascular risk in subjects by way of modern statistical methods.[87] These statistical methods can be used to rank lipoprotein subclasses according to how strongly they influence this classification. One study utilized high performance liquid chromatography (HPLC) to study lipoprotein particle size as the defining parameter.[87] To classify two groups as belonging to a control group or at risk for developing CAD, a method of analysis known as linear discriminate analysis (LDA) can be applied.[88, 89] This method attempts to find a linear combination of variables that can best separate the two groups in terms of the mean of their linear combination. Newer statistical methods include sliced average variance estimation (SAVE)[90, 91] and sliced mean variance covariance (SMVCIR). These two approaches search for linear combinations of variables which yield the best separation of the two groups based on the mean, variance, and covariance of these linear combinations. It was shown that classification can

typically be greatly improved by including both the variance and covariance in addition to the mean.[90, 91] The combination of these statistical methods, results in a strong classification system that can be useful in screening samples prior to secondary analysis.

1.5 Mass Spectrometry

Methods of analyzing lipoproteins by mass spectrometry have become highly desirable due to the richness of information acquired in the data, the sensitivity of the technique, and the diversity in the types of mass spectral analysis that can be performed.[92-95] In particular, techniques employing matrix-assisted laser desorption ionization (MALDI) and electrospray ionization (ESI) have run a large portion of the gamut over the past decade because the softer method of ionization possesses a lower risk of fragmenting the ions of interest.

The goal of utilizing mass spectrometry in this study is to assist in generating a link between the composition of lipoprotein particles and the inherent risk of developing cardiovascular disease. In particular, the lipoprotein HDL when observed at any point in its biological cycle will typically contain a mixture of apolipoproteins of various molecular weights ranging from approximately 6-30 kDa. Even more interesting is that in a given serum sample, different HDL molecules may possess different quantities of these apolipoproteins, or even contain apolipoproteins that have undergone post-translational modification.

1.5.1 MALDI-MS

In the late 1980's, a novel ionization method known as MALDI mass spectrometry (MALDI-MS) was introduced that quickly became widely used in biological applications.[96] It was discovered that by mixing a biological sample with an organic matrix, that non-volatile analytes could be desorbed by the use of an ultraviolet laser resulting in a plume of desorbed matrix and analyte ions, otherwise known as the MALDI plume.[97] This phenomenon results in a soft-ionization of the biological sample which minimizes fractionation of large macromolecules and results primarily in a

mixture of singly and doubly charged intact molecular ions as well as some dimers.[96, 98, 99] Though it is still not currently fully understood how the ionization mechanism works, it is thought that the high UV absorbance of the matrix transfers energy to the analyte for ion formation.[96, 100]

It is very common to couple a time of flight (TOF) mass analyzer to a MALDI ionization source, generating the analytical technique known as MALDI-TOF.[101] In a typical MALDI-TOF experiment, analyte ions are accelerated by applying a fixed potential, known as the extraction potential, giving them a kinetic energy that is proportional to their mass-to-charge (m/z) ratio. The accelerated ions then progress through a flight tube until they impinge on a detector plate which produces a signal for the ions as a function of time. Since the time it takes the ions to reach the detector is a function of their kinetic energy, which is related to their m/z, a mass spectrum can be generated. This means that molecular ions with a higher m/z will achieve a slower final velocity than ions with a low m/z.

The resolution the instrument is capable of depends on factors such as the spatial orientation of molecules as they desorb from the matrix, the kinetic energy of the molecules, and the time required for acceleration of the analyte ions.[102] In other words, this depends on whether all of the molecules start at the same position and are accelerated towards the detector uniformly. There are two methods that can be utilized combat these setbacks: delayed extraction[103, 104], or use of a reflectron[105]. Delayed extraction involves delaying the extraction potential by a finite amount of time after the ionization event occurs as opposed to leaving the potential on continuously. This serves to prevent molecular ions that are quickly formed from being instantly accelerated towards the detector. As the MALDI plume forms, ions that are closer to the source of the extraction potential will experience less of an accelerating force as those that are further away because they will be exposed to it for a shorter duration of time. This method normalizes the initial momentum of molecular ions at the beginning of the experiment and helps to provide a higher mass resolution.[106] A reflectron, on the other hand, takes into account differences in kinetic energy and involves applying a fixed

potential gradient at a 180º angle to the direction of ion motion at a position where the detector would typically be placed in a linear TOF experiment. Ions with a higher kinetic energy will penetrate deeper into this potential gradient and will take longer to turn around than ions with lower kinetic energy. This adaptation to the TOF experiment has the advantage of refocusing the molecular ions, but also to give a flight path that is twice as long as an experiment performed in the linear mode.

Careful consideration must also be taken in the choice of the MALDI matrix to be used.[107] Common matrices include: sinapinic acid, ferulic acid, 2,5-dihydroxybenzoic acid (DHB), and α-cyano-4-hydroxycinnamic acid (CHCA).[108, 109] Typically, the matrix compound must absorb the laser radiation strongly and must also be soluble enough in the sample solvent to be present in excess relative to the sample analyte.[108] Additionally, the macromolecule being studied should not absorb the laser radiation to prevent fragmentation of the molecular ion. There are typically two methods for preparing a sample for MALDI analysis: the dried-droplet method[96] and the thin-layer[110] method. The dried-droplet method consists of mixing the analyte with the desired matrix, then applying a small volume to a MALDI plate and allowing crystals to form through evaporation. The thin-layer method involves first creating a layer of matrix only crystals, and then subsequently layering the matrix/sample mixture on the previous layer. The thin-layer method has become advantageous because it leads to more homogeneous spotting of sample analyte, while the dried-droplet method tends to lead to heterogeneous "hot spots". Additionally, the thin-layer method allows for washing of the dried spot with deionized water for removal of contaminants that would otherwise be trapped in the crystallized matrix.

The characterization of proteins and apolipoproteins by MALDI-TOF has been very successful over the past two decades, and has allowed for high mass accuracy of intact proteins and even identification of post-translational modifications.[100, 111] The technique is not without its faults however. Differences in ionization efficiencies of components of a mixture make quantification by MALDI difficult. This is further compounded by mass discrimination and suppression effects as well as possible

fragmentation of the molecular ions during ionization. Despite these setbacks, MALDI-TOF still remains a rugged and robust method for analyzing macromolecules.

1.5.2 LC-MS

By combining the physical separation capabilities of liquid chromatography with the mass analysis capabilities afforded by mass spectrometry, the analytical technique of liquid chromatography mass spectrometry (LC-MS) has evolved as a powerful method of analyzing complex mixtures. Akin to the technique of high performance liquid chromatography (HPLC), LC-MS functions on the same chromatographic principles, except on a much smaller scale, with typical column diameters of 4.6 mm for HPLC and 300 μm for LC-MS. For protein analysis, the liquid chromatography experiment is typically performed in the reversed phase by means of a hydrophobic c-4 or c-18 column and elution in a polar mobile phase consisting of a mixture of buffer and polar organic solvents. The most common detection systems for LC-MS include: atmospheric pressure chemical ionization (APCI), thermospray, and also electrospray ionization (ESI).[108, 112] Off-line MALDI deposition has even been used as a means of combining a liquid separation method with a gas phase ionization method.[113, 114]

APCI is a form of chemical ionization that takes place at atmospheric pressure. Ions are produced when the analyte collides with ions of a reagent gas that have been exposed to electrons in the ion source. The primary ions formed from the collision of electrons and the reagent gas will in turn collide with either other reagent gas molecules or analyte molecules. The possible combinations include: protonation, proton abstraction, adduct formation, or charge exchange, leading to a host of different product ions.[115] Thermospray is an adaptation of APCI in which the total effluent from a column is vaporized in a stainless steel capillary tube, forming an aerosol of solvent and analyte molecules This aerosol is then ionized through a charge exchange mechanism with a salt that is incorporated into the eluent.[116] In this manner, thermospray serves as both an interface to liquid chromatography and also as an ionization source.[115] However, the thermospray interface can only be applied to polar analyte molecules and the mobile

phase used in the liquid chromatography portion must be capable of dissolving the salt responsible for the charge exchange step.

Interfacing a liquid phase technique, which continuously flows liquid, and a gas phase technique carried out in a vacuum was still difficult for a long time, but the advent of ESI changed this. Electrospray ionization mass spectrometry (ESI-MS) was first described in 1984 and has become one of the most important analytical techniques for analyzing biomolecules with molecular weights above 100,000 Da.[117] This technique involves an ionization process that is extremely soft and results in little fragmentation of large and thermally fragile biomolecules.[108] The method of ionization involves pushing a solution of analyte dissolved in a volatile solvent, usually containing an acid or a base, through a small diameter capillary that is charged. Upon exiting the capillary the analyte particles will retain their charge state and will repel each other when a voltage is applied due to coulombic forces. As the potential is increased up to a point known as the threshold voltage, the coulombic repulsive force of the analytes will begin to overcome the surface tension holding them together in solution, forming what is known as a Taylor cone.[118] Two competing theories exist that explain how lone analyte ions are generated from the Taylor cone: the charged residue model (CRM), and the ion evaporation model (IEM).[119] In the CRM, the electrospray droplets undergo evaporation and disintegration cycles in which coulombic repulsion reaches a critical level and explodes, causing the droplet to form progressively smaller daughter droplets which contain on average one or less analyte molecules. The IEM however, suggests that as evaporation occurs, the field strength at the surface of the droplet becomes great enough to desorb lone analyte ions directly out of the droplet. It is thought that both models probably occur depending on the analyte/solvent system being studied. In either case, ESI serves to transfer analyte ions from a liquid to a gaseous state for entry into the mass analyzer.

1.6 Capillary Electrophoresis

Lipoprotein subclasses are largely considered to have heterogeneous physical properties such as composition, size, hydrated density, and even apolipoprotein composition.[120] As an example, all LDL molecules, regardless of density, should possess the apolipoprotein B-100. Similarly, all HDL molecules should possess the lipoprotein A-1. However, since HDL molecules possessing the same physical properties can also contain a host of other apolipoproteins in addition to A-1, it becomes important to utilize other techniques capable of separating them. One such technique is CE, which has evolved as a powerful separation technique for the study of these biomolecules.[10, 11]

1.6.1 Separation Theory

The main principle of CE involves the separation of components in a mixture based on their size-to-charge ratio when an electric field is applied to a capillary containing a conductive buffer, also known as the background electrolyte (BGE).[121] Smaller, more highly-charged species will be influenced by the electric field more, and will therefore have a higher rate of migration than molecules that have a lower size-to-charge ratio. This phenomenon is known as electrophoresis. In addition to electrophoresis, there is another force known as electroosmosis that occurs as a result of the interaction between the charge of the surface of the capillary wall and the BGE when an electric field is applied. A typical uncoated capillary wall is covered with deprotonated silanol groups, giving the capillary wall a net negative charge. As the pH of the BGE increases, the degree of deprotonation also increases. Cations from the BGE are attracted to the negatively charged capillary wall, forming an immobile wall of positive charge near the wall, known as the Stern layer. Beyond the Stern layer, a diffuse layer of mobile cations, known as the Helmholtz plane, also forms. Together, these layers are known as the electrical double layer. When a potential is applied to the capillary, the diffuse layer of cations migrates toward the cathode, dragging its hydrated layer of water molecules with it in a bulk flow known as the electroosmotic flow (EOF).

In CE, the measure of the rate of migration of molecules is known as the mobility (μ), and is a function of the total capillary length in cm (L_c), length to the detector in cm (L_d), the applied voltage in volts (V), and time for an ion to reach the detector in seconds (t). (Eq. 11)

$$\mu = \frac{L_c \times L_d}{V \times t} \tag{11}$$

The apparent mobility of the analyte of interest (μ_{app}) is the sum of the effective mobility of the analyte (μ_{eff}) and the mobility of the EOF (μ_{EOF}). (Eq. 12).

$$\mu_{app} = \mu_{eff} + \mu_{EOF} \tag{12}$$

The apparent mobility for the analyte of interest is found by calculating the mobility, as given by Eq. 11, with the time it takes for it to reach the detector. The mobility of the EOF is calculated in the same manner, but by using the time required for a neutral marker to reach the detector (t_{EOF}). By calculating these two mobilities, it becomes possible to solve for the effective mobility of the analyte of interest. Another way to express this is by combining Eq. 11 and Eq. 12 and solving in terms of the effective mobility. (Eq. 13)

$$\mu_{eff} = \frac{L_c \times L_d}{V} \times \left(\frac{1}{t} - \frac{1}{t_{EOF}} \right) \tag{13}$$

The choice of polarity also influences the separation. Under normal polarity, in which the anode is located at the inlet and the cathode is located at the outlet, the EOF will travel towards the detector. As a result, the mobility of the EOF versus the mobility of the analytes to be studied becomes important. If the analyte molecule is an anion, it must have a lower mobility than the EOF so that it can essentially be pulled to the

detector by the bulk flow; otherwise it will simply migrate to the anode and will never be detected. When analyzing biomolecules by CE, the pH of the BGE becomes important because it will dictate both the mobility of the EOF as well as the charge of the analyte molecule. Therefore, for protein studies, a pH above the pI of the protein will yield an anionic analyte ion, whereas a pH below the pI will yield a cationic analyte ion.

Electromigration dispersion (EMD) can also cause considerable distortions of peak shape that will affect the separation efficiency.[122-124] This phenomenon is characterized by peak tailing or fronting, and occurs as a result of a difference in mobilities between the buffer ions and sample ions in a given separation experiment. Through careful selection of BGE to match the mobility of buffer ions with the mobility of sample ions, this deleterious effect can be minimized.

It is also important to note that significant analyte/wall interactions can occur when the net charge of the biomolecules is opposite to that of the capillary wall, thereby hindering the separation. Methods of solving this include: using a high pH BGE to minimize protein adsorption through coulombic repulsion, adding surfactants to the buffer to dynamically coat the capillary wall, or shielding the capillary wall by coating it with a neutral hydrophilic compound.[125-127] The addition of surfactants may also serve a role in denaturing proteins, which can serve to alter their hydrodynamic volume, thereby causing deviations in mobility from their native structure. Furthermore, modifications to the BGE that include adding charged surfactants can change the surface charge of proteins which can also affect their mobility. For example, the addition of the anionic detergent sodium dodecyl sulfate (SDS) will cause a significant increase in the charge of the protein to be analyzed, therefore increasing its electrophoretic mobility.[128] SDS also has the added benefit of reducing protein-protein interactions and helps to eliminate aggregation of biomolecules.[129]

1.7 *Isoelectric Focusing with an Immobilized pH Gradient*

Immobilized pH Gradients (IPG) were developed in the early 1980's to overcome setbacks with existing IEF methods.[13] In this technique, ampholytic molecules are immobilized by chemical bonds to a gel matrix composed of polyacrylamide, forming a continuous pH gradient. Typically these molecules are derivatives of acrylamide of the form: CH_2=CH-CO-NH-R, where R can be either a carboxyl group or a tertiary amino group.[14] When a protein sample is loaded onto the gel, the protein will be charged relative to the environment it is in and will migrate under the influence of an applied electric field. Migration of the protein will stop once the protein migrates to a region of the IPG gel in which the pH matches the pI of the protein. This indicates that the protein will have a neutral charge and its mobility will be zero. In this manner, a complex mixture of macromolecules can be separated if the various components possess unique pI values, with a resolution as high as $\Delta pI = 0.001$.[14] An equation for the resolving power of IEF can be expressed as a function of electrical and diffusional mass transport. (Eq. 14)[14]

$$\Delta pI = \sqrt[3]{\frac{D[d(pH)/dx]}{E[-du/d(pH)]}} \qquad (14)$$

In this equation, D is the protein diffusion coefficient at the pI, d(pH)/dx describes the slope of the pH gradient of the IPG gel, E is the electric field strength, du/d(pH) is the mobility gradient of the analyte at the pI, and ΔpI is the difference in pI between analytes. This equation demonstrates that the highest resolution can be obtained when the analyte has a low diffusion coefficient and a high mobility slope. Since proteins have high molecular weights with low charge states, this condition is met. Shallow pH gradients and high electric field strengths also contribute to higher resolutions.

Experimental pI values can be predicted for proteins by examining amino acids that contain residues capable of ionization.[130] However, ampholytes in the IPG gel are sensitive to temperature, urea concentration, and presence of detergents, all of which can

alter their pI values. Urea is typically used as a chaotropic agent to disrupt hydrogen bonding in a protein, essentially eliminating secondary and tertiary structures, and resulting in a protein with only primary structure.[131, 132] Detergents are used to bind to non-polar domains of a protein in order to reduce hydrophobic interactions.[133, 134] While the presence of urea and detergents are helpful in IEF separations, the presence of salts are detrimental. Salt contamination can deplete water from the gel prior to protein entry, and can allow for precipitation of proteins from solution, or slow migration of the protein in the gel.[135] Protein identification can be accomplished by either comparing predicted pI values with experimental values, or through the use of reference standards.[130] Other advantages include: sharp protein bands, high reproducibility, and low background staining. The method however is capped at a maximum mass limit on the order of 750,000 Da.

1.8 *Application of Methods*

Ultimately, the goal of this research is to generate information-rich methods for analyzing clinical samples to determine a patient's risk of developing CAD. Since the information acquired from many of these methods overlaps, it becomes possible to investigate many aspects of an individual's lipoprotein composition to give an improved overview of their CAD risk assessment. With this goal in mind, the term lipoproteomics was coined by our research laboratory to describe the combination of techniques utilized to paint the picture of an individual's cardiovascular risk profile. Traditionally, the predominant risk factors associated with CAD risk have focused on the concentrations of LDL cholesterol (LDL-C) and HDL cholesterol (HDL-C). Specifically, people with elevated levels of LDL-C are at greater risk for developing CAD and are deemed pro-atherogenic, while those with elevated HDL-C are deemed anti-atherogenic.[136] However, cholesterol levels are only a small piece of a much larger puzzle, and investigations into the protein content of lipoproteins will aid in unveiling the direction in which cardiovascular research should progress. The largest bottleneck in proteomics has been identification. Relatively high amounts of protein are required, and

cumbersome sequencing techniques greatly limits throughput.[137] Although two-dimensional polyacrylamide gel electrophoresis (2D-PAGE) coupled with mass spectrometry has long been the go-to method for identification of new proteins, the throughput simply is not high enough. The research described here presents an approach in combining various analytical techniques in order to not only more thoroughly analyze the complex distribution of apolipoproteins present in a sample of human serum, but to help increase sample throughput as well.

MALDI-MS has been widely used for the characterization of complex protein mixtures because it yields many singly-charged ions with high mass accuracy, making individual protein identification possible.[100, 111] Post-translational modifications such as glycosylation, phosphorylation, and acetylation can also easily be detected.[94, 95] MALDI-MS experiments following an isolation of lipoprotein types by DGU has allowed for considerably more selective examination of subclasses of major lipoprotein types. Mixtures of apolipoproteins, particularly those from different fractions of HDL, have been analyzed and multiple isoforms have been reported.[138-141] Novel isoforms of the inflammatory response protein, serum amyloid A (SAA), have also been successfully analyzed by DGU-MALDI experiments.[142] Fractions of VLDL have also been analyzed in this fashion, and novel isoforms of apo C-III were detected as well as different polymorphisms of the apolipoproteins.[139, 143] Several cases of suspected methionine residue oxidation have also been detected in the apolipoproteins of both VLDL and HDL.[139, 144-147] MALDI-MS can serve as an invaluable qualitative analysis tool with a very high sensitivity, but it is not typically used in experiments requiring quantitation.

LC-MS is advantageous over MALDI because of its ability to separate complex mixtures prior to mass spectrometric analysis, thereby enabling researchers to study complex mixtures of the lipids or proteins associated with lipoprotein particles. It has been particularly useful in the qualitative and quantitative analysis of lipid and phospholipid content of human lipoproteins, especially HDL.[148-151] This technique has even been utilized in studies aimed at tracking the hydrolytic activity of various phospholipases towards phosphatidylcholine contained in human LDL and HDL.[152] For

nutritional studies, LC-MS has also been useful in identifying and quantifying circulating phenolic compounds and their metabolites.[153, 154] These compounds can be obtained from meals containing olive oil or red wine and are considered to act as in vivo antioxidants. In regards to protein analysis, LC-MS has been useful in determining post-translational modifications of single proteins, as is the case when analyzing the oxidation of apoB-100 in samples of human LDL.[155] It has also been used considerably in studies aimed at identifying and quantifying the apolipoproteins of VLDL, LDL, and HDL.[156, 157] While these experiments report the absolute quantities of the various apolipoproteins studied, tryptic digestion is required, thereby eliminating the nascent structure of the proteins. The results reported in this dissertation describe methods to begin filling in this vital missing information.

Considerable efforts are being made to push CE towards more commercial use to be utilized alongside techniques such as high performance liquid chromatography (HPLC), mass spectrometry and gel electrophoresis.[158] Electrophoretic methods that have been utilized to study lipoprotein particles for the last two decades include techniques such as capillary isotachophoresis (CITP)[159], capillary zone electrophoresis (CZE)[160], capillary sds gel electrophoresis[161], and microchip CE[11]. In its simplest form, CZE involves analyzing a heterogeneous mixture of samples in a low viscosity buffer which is subjected to an electric field, with separation occurring as a result of differences in mobility.[162] Additional advantages include the relatively low sample volume required for the measurement, as well as higher sample throughput. For lipoprotein analysis, CE experiments exist in two primary branches: intact lipoprotein analysis, and delipidated analysis of apolipoproteins. Lipoprotein particles in their nascent state are negatively charged when at physiological pH. In studies involving intact lipoproteins, a slightly basic buffer is typically utilized to ensure that lipoprotein molecules will remain near their physiological pH and ensure their negative charge. In this manner, information regarding the size/charge of the lipoprotein particles can be acquired. This information can be used to help determine the inherent differences between both the apolipoprotein content, and the lipid content in a variety of samples, particularly in oxidation studies.[163]

Oxidation can affect the size/charge of a lipoprotein particle, thereby affecting its electrophoretic mobility. CITP experiments of intact LDL particles have been used to study its various subfractions.[10, 159, 164-166] Since the primary apolipoprotein associated with LDL particles is apo B-100, it then becomes possible to look at changes to the lipid structure. For the analysis of the apolipoproteins, the intact particles can be delipidated by various techniques, such as addition of detergent to the CE buffer, or solid phase extraction (SPE), prior to the electrophoresis experiment.[12, 128] This provides a means of analyzing the apolipoproteins of LDL and HDL for quantitative purposes by CZE.[12, 167] The effective electrophoretic mobility of the various apolipoproteins allows a second degree of separation over DGU because molecules possessing different electrophoretic mobilities will travel at different rates.

Experimental data from apolipoprotein studies also suggests that there are multiple isoforms of the major apolipoprotein classes. The distribution and quantity of these isoforms could potentially yield information that would benefit the diagnosis of cardiovascular health. Coupling immunoaffinity with traditional CE experiments has opened up a large avenue of possibilities for proteomics studies as well.[137] Immunoaffinity CE (IACE) experiments involve capturing an analyte of interest with an affinity ligand, washing non-specifically bound material, followed by elution of the desired analyte in a desorption buffer. This would offer the researcher additional selectivity since the majority of apolipoproteins have very similar electrophoretic mobilities.

IEF can be used as either a standalone method to analyze the distribution of pI values of a sample mixture or it can be used as a preparatory step for 2D-PAGE experiments. Due to its high inherent resolution, IEF is a very suitable technique for resolving complex mixtures of apolipoproteins. Several staining methods, including visible organic stains, fluorescent stains, and silver staining are available for imaging of proteins.[14] Typically, colloidal solutions of the dyes in acidic solutions are utilized for proteins separated on an IPG strip in order to minimize background staining of the gel support.[168] At low pH the protein molecules are protonated, giving nucleation centers

which are capable of binding molecules of the dye through electrostatic attraction while the gel support cannot be penetrated as well by the colloidal dye molecules. Acid Violet 17 was found to be a very reproducible stain for protein samples, with a sensitivity as low as 5-10 ng of protein per zone and a linear range of 1-100 ug.[169] As the first dimension of a 2D-PAGE experiment, IEF has been used to identify several post-translational modifications of human plasma apolipoproteins.[170] IPG gels have also been useful in detecting differences in isoforms of Apo C contained in VLDL in studies involving hypertriglyceridemic indviduals.[171] The phenotyping of apolipoprotein E from samples of VLDL and serum has been accomplished by combining IEF with immunodetection.[172, 173] Isoforms of apolipoprotein A-I from HDL samples have also been separated by IPG gels and detected by a combination of staining with Coomassie Blue and immunoblotting.[174, 175] Genetic polymorphisms have also been analyzed from a mixture of lipoprotein fractions that were analyzed through use of pre-cast IPG gels and stained by colloidal Acid Violet 17.[169, 176, 177] Tryptic digest of protein spots from gels has also been utilized as a preparative step for analysis by MALDI-MS.[178]

By working in conjunction with clinicians at Scott & White Hospital, we are developing a library of patients that do not possess traditional risk factors for development of CAD, yet have severe levels of atherosclerosis. Our goal is to apply this array of methods to a sample population consisting of subjects with a known history of cardiovascular events and subjects considered to be at low risk for development of CAD. The final aim is the potential discovery of new risk factors to provide insight as to how and why CAD develops. Combining DGU, both as a standalone analysis method and as a preparative tool, with techniques capable of secondary separation and analysis, such as MS, CE, and IEF, enables a much more focused ability to observe distributions of the subclasses of lipoproteins. In addition, this combination of methods also yields important information regarding the quantity and distribution of apolipoproteins. Pooled together, this information will become part of an ongoing effort to better understand features of lipoproteins, and how CAD develops. The following table summarizes the

relative abundances, CE mobilities, mass averages, and pI values expected for the A and C apolipoproteins in a typical sample of HDL (Table 3).[31, 143, 167, 179-181]

Table 3. Summary of Apolipoprotein A and C Properties

Apolipoprotein	Serum Conc. (mg/dL)	Mobility (x 10^{-5} cm^2/Vs)	Avg. Mass (m/z)	pI
A-I	100-150	-24.8	28,078.60	5.34 - 5.75
A-II	30-40	-22.8	17,379.80	4.20 - 5.17
C-I	6	-26.8	6,630.60	6.50
C-II	4	-24.1	8,914.20	4.50 – 4.82
C-III	12	-24.6	9,429.98	4.80 - 4.95

CHAPTER II

MATERIALS AND METHODS

2.1 Materials

2.1.1 Chemicals and Supplies

NBD (C_6-ceramide) was purchased from Molecular Probes (Eugene, OR). Sodium bismuth ethylenediaminetetraacetic acid (NaBiY) was purchased from TCI America (Portland, OR). Cesium hydroxide, cesium carbonate, cadmium carbonate, ethylenediaminetetraacetic acid (H_4EDTA), sodium carbonate, lead carbonate, disodium copper ethylenediaminetetraacetic acid (Na_2CuY), sodium iron ethylenediaminetetracacetic acid (NaFeY), trichloroacetic acid, trifluoroacetic acid (TFA), ferulic acid, sinapinic acid, sodium borate, sodium dodecyl sulfate (SDS), Dextralip® 50, and magnesium chloride hexahydrate were purchased from Sigma Aldrich (St. Louis, MO). Acetonitrile (ACN), dimethyl sulfoxide (DMSO), glycerol, phosphoric acid, and methanol were purchased from EM Science (Gibbstown, NJ). Bismuth oxycarbonate was purchased from Alfa Aeser Co. (Ward Hill, MA). Immobiline™ DryStrips and DeStreak™ rehydration solution were purchased from GE Healthcare (Piscataway, NJ). Acid Violet 17 was purchased from Serva Electrophoresis (Heidelberg, Germany). Strata C18-E solid phase extraction cartridges and syringe adapters caps were purchased from Phenomenex (Torrance, CA). Fused-silica capillary columns were purchased from Polymicro Technologies (Phoenix, AZ). ApoA-I and ApoC-I standards were purchased from Academy Biomedical (Houston, TX).

2.1.2 Synthesis of EDTA Complexes

In all EDTA complexes that are synthesized, the term "Y" represents a molecule of "EDTA" when complexed with a metal ion. Complexes of CsBiY, Na_2PbY, Cs_2PbY, Na_2CdY, and Cs_2CdY were synthesized by stoichiometric combination of H_4EDTA, the

appropriate alkali carbonate or alkali hydroxide, and the appropriate heavy metal carbonate in 100mL of deionized water (DI H_2O), followed by a 2-h reflux, yielding a clear solution. (Eq. 15)

$$H_4EDTA + X\text{-}CO_3 + M(Z) \rightarrow X\text{-}M\text{-}EDTA + H_2O(l) + CO_2(g) \quad (15)$$

In this equation, the general scheme of the reaction involves combining the fully protonated variant of EDTA with the desired alkali metal (X) carbonate, and with various forms of a heavy metal (M) such as its carbonate, oxide, oxycarbonate, or hydroxide, designated as (Z). For example, the synthesis of CsBiY would involve reacting EDTA with cesium carbonate and bismuth oxycarbonate. (Eq. 16)

$$2H_4EDTA + Cs_2CO_3 + Bi_2O_2CO_3 \rightarrow 2CsBiEDTA + 4H_2O(l) + 2CO_2(g) \quad (16)$$

After reaction, the resulting solution was then titrated with the appropriate alkali hydroxide to a pH ranging from 6.75-7.25, then reconstituted to a final volume of 100mL to account for evaporation during reflux. As long as the stoichiometry of the reaction is preserved, it can be scaled to give a higher concentration or volume of the desired EDTA complex.

2.2 Analytical Methods

2.2.1 Serum Collection

Serum samples were collected by a blood draw into a 9mL Vacutainer tube treated with a polymer gel and silica activator from Beckton Dickinson Systems (Franklin Lakes, NJ). The serum was then separated from red blood cells by centrifugation at 3,200 rpm for 20 minutes at 4ºC, followed by aspiration of the supernatant into 500uL Eppendorf tubes for storage at -80ºC prior to analysis. Informed consent was obtained from all donors.

2.2.2 Calibration of EDTA Complexes

Stock 0.4000M solutions of the EDTA complexes of NaBiY, CsBiY, Na_2PbY, Cs_2PbY, Na_2CdY, Cs_2CdY, NaFeY, and Na_2CuY were prepared, and were used to prepare subsequent dilutions down to a final concentration of 0.0133M. Gravimetry and refractometry were used to determine the relationships between concentration, density, and refractive index for each of the eight EDTA complexes. A calibrated 10mL glass pipet was utilized to gravimetrically determine the density of the solutions at each concentration. The refractive index was measured at 20ºC using an Abbe 60/DR refractometer from Bellingham + Stanley (Lawrenceville, GA).

2.2.3 Measurement of Gradient Formation

Density gradients were formed in an Optima TLX UC with a TLA 120.2 fixed-angle rotor and in 1.5mL thick-walled, polycarbonate UC tubes from Beckman-Coulter (Palo Alto, CA). Tubes contained 1,000uL of the appropriate EDTA metal complex and were centrifuged at a rotor speed of 120,000 rpm for 6 hours at 5ºC. When the experiment is performed with a TLA 120.2 fixed-angle rotor, this rotor speed corresponds to a relative centrifugal force of 510,000g. Once centrifugation was complete, 20uL aliquots were removed from sequentially lower positions within the UC tube (determined by imaging the location of the pipette tip during each removal step).

The refractive index was measured from each of these aliquots and was compared to the position from which they were removed. From this series of refractive indices, the relative densities can be calculated, thereby linking the tube coordinate with the density of the EDTA metal complex solution. This was repeated for each of the eight solute systems and yielded unique density curves for each EDTA metal complex.

2.2.4 Ultracentrifugation of Serum Samples

There are two modes of operation for UC experiments: serum density profiling, and preparative UC. For serum density profiling, 6uL of serum and 84uL of DI H_2O were added to a 1100uL solution of the desired density gradient-forming solute, followed by addition of 10uL of a 1mg/mL solution of NBD (C_6-ceramide) dissolved in DMSO. From this mixture, a 1,000uL aliquot was added to a UC tube and spun according to the conditions described above. Following the spin, 200uL of DI H_2O was layered atop the solution to assist in separating the buoyant and dense TRL classes.

For preparative UC in studies involving VLDL or LDL, 50-200uL of serum was added to a 1100uL solution of a 0.3000M solution of Cs_2CdY, followed by addition of 10uL of a 1mg/mL solution of NBD (C_6-ceramide) dissolved in DMSO. From this mixture, a 1,000uL aliquot was added to a UC tube and spun according to the conditions described above. Studies involving HDL were first subjected to treatment with dextran sulfate (DS) and magnesium chloride in order to precipitate out lipoproteins containing apoB such as VLDL, LDL, and Lp(a) as follows.[182] The 50,000 MW variant of DS is commercially available as Dextralip® 50. 1.0g of DS was combined with 10.15g of the dried salt of magnesium chloride hexahydrate in 100mL of DI H_2O. The final solution should have a concentration of 10 g/L of DS and 0.5M magnesium chloride. This working solution was added to a sample of serum at a volume of 10% of the serum volume. For example, a 100uL sample of serum should have 10uL of this working reagent added. This solution was mixed briefly by vortexing and left to stand at room temperature for 10 minutes. Centrifugation in a tabletop centrifuge at 12,000g for 5

minutes was then performed to sediment out the apo-B containing particles. The supernatant was then prepared for UC as previously described.

2.2.5 Fluorescent Imaging Analysis

Following a UC experiment, an image of the UC tube was obtained and analyzed by using a digital color microscope camera, Microfire S99808, purchased from Optronics (Goleta, CA) with a Fiber-Lite MH100A Illuminator from Edmund Industrial Optics (Barrington, NJ). The camera and light source were positioned orthogonally to each other on an optical bench to illuminate the sample. Filters matching the excitation and emission properties of the fluorophore, NBD (C_6-ceramide), were purchased from Schott Glass (Elmsford, NY). The respective filters for excitation and emission were a blue-violet filter (BG-12) with a bandwidth centered about 407nm and a yellow filter (OG-515) with a bandwidth centered about 570nm. Specific settings for the Microfire camera software included an exposure time of 15.8ms for serum density profiling and 29.0ms for preparative UC. A gain of 1.000 and a target intensity of 30% were also applied.

From the image capture of the UC tube, a density profile was generated as described by a published method.[4] Using Origin 7.0 software, the image was first converted into grayscale intensity values as a function of pixels in two dimensions, then the grayscale intensity from a small strip of 10 pixels oriented in the center of the UC tube was averaged. This average grayscale intensity was then plotted as a function of tube coordinate (0-34mm) to give the final lipoprotein density profile.

2.2.6 Lipoprotein Fraction Collection

Lipoprotein fractions were collected by using a novel freeze/slice method. After preparative UC and imaging, the UC tubes were slowly frozen in liquid nitrogen. This was accomplished by placing the UC tubes into a custom 10-slot holder and slowly lowering the holder into a Dewar of liquid nitrogen, causing the liquid in the tubes to

freeze from the bottom to the top. In this manner, the expansion of water to ice can be accounted for by the following equation: (Eq. 17)

$$mm_s = \frac{\rho_l}{\rho_s} \times mm_l - 10.405 \quad (17)$$

In this equation, mm_s corresponds to the tube coordinate in solid state, while mm_l corresponds to the tube coordinate in the liquid state, the state in which the image of the UC tube is captured. The term ρ_l/ρ_s corresponds to the ratio of the density of water at its liquid state ρ_l to its density at its solid state ρ_s. Since water is denser in its liquid state, this ratio gives a correction factor greater than unity and the equation can be simplified to: (Eq. 18)

$$mm_s = 1.058 \times mm_l - 10.405 \quad (18)$$

Also, 10.405mm was subtracted from the solid state tube coordinate to correct for the calibration of the micrometer/tube holder assembly that was used to dial in the correct cut points. This micrometer/tube holder assembly contains a micrometer head that was used to dial in the desired cut point, which functions to advance the position of the UC tube relative to the location of the notch for the saw blade. A Dremel® scroll saw (Racine, WI) was fitted with 0.25mm blades for the cutting of the tubes. The freeze/slice method is depicted below (Figure 4).

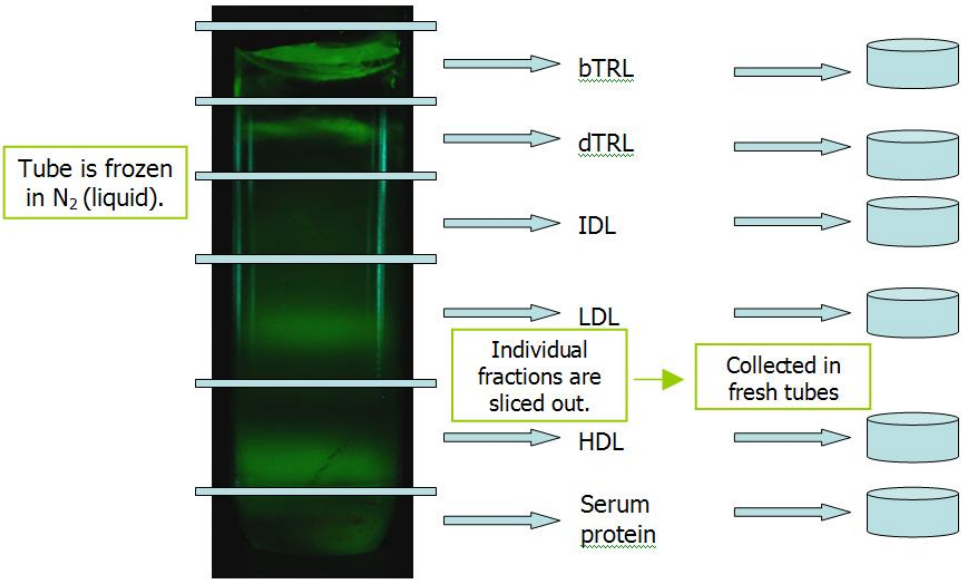

Figure 4. Freeze/Slice Method for Excising Lipoprotein Fractions

2.2.6.1 Solid Phase Extraction

After sample excision and thawing, apolipoproteins were separated from lipids by means of a solid-phase extraction (SPE) cartridge from Phenomenex, Strata C18-E (Torrance, CA). Delipidation of samples was accomplished based on a published method.[181]

1. The cartridge was conditioned dropwise with three 1mL rinses of 0.1% (v/v) TFA in ACN, allowing no air to enter the cartridge.
2. The cartridge was then conditioned dropwise with three 1mL rinses of 0.1% (v/v) TFA in DI H_2O, allowing no air to enter the cartridge.
3. The sample to be delipidated was first mixed with an equivalent-volume of 0.1% (v/v) TFA in DI H_2O, then slowly added to the cartridge, allowing no air to enter the cartridge.
4. The cartridge was washed with three 1mL rinses of 0.1% (v/v) TFA in DI H_2O in order to remove salts and non-specifically bound apolipoproteins. Air was then pushed through the cartridge to remove any remaining liquid.

5. The apolipoproteins were then eluted in 100uL aliquots of 0.1% TFA in ACN. The first four aliquots contained the majority of the apolipoproteins (verified by MALDI-MS) and were combined.

Following the SPE procedure, the samples were evaporated to dryness through use of a SVC-100H Speed-Vac concentrator with a refrigerated condensation trap from Savant Instruments (Farmingdale, NY) which was connected to a 5KC36PN435AX vacuum pump from General Electric (Fort Wayne, IN). Dried apolipoprotein fractions were then reconstituted in suitable solvents for the method of investigation: 0.1% TFA in DI H_2O for MS experiments, buffer for CE experiments, DeStreak™ for IEF experiments, and DI H_2O for cell culture studies.

2.2.6.2 Bicinchoninic Acid Assay (BCA)

For the determination of total protein concentration, a BCA protein assay reagent kit from Pierce Biotechnology was used (Rockford, IL). Standard working reagent for the kit was prepared as follows: (Eq. 19)

$$WR = (\#Stds + \#Unk) \times (\#Reps) \times (Vol\ per\ Sample) \tag{19}$$

In this equation, the volume of the working reagent (WR) is calculated by multiplying the total number of standards and unknowns (#Stds + #Unk) by the number of replicate measurements (#Reps) desired and by the volume required per sample. For typical analyses, 150uL of sample is required, so if there were 5 standards and 5 unknowns, and triplicate measurement was required, 4,500uL of working reagent would be required. In order to prepare the working reagent, three reagents need to be mixed in the proper ratio (Eq. 20).

$$MA : MB : MC = 25 : 24 : 1 \tag{20}$$

MA: = Sodium carbonate, sodium bicarbonate, and sodium tartarate in 0.2N NaOH

MB: = 4% (v/v) Bicinchoninic acid in water

MC: = 4% (v/v) Cupric sulfate pentahydrate in water

Using the above example, if 4,500uL of working reagent are required, then the ratios would calculate to 2,250uL, 2,160uL, and 90uL of MA, MB, and MC respectively. Once the standard working reagent was properly prepared, 150uL was pipetted into 96 well microtitre plates, followed by 150uL of the desired sample or standard to be analyzed. The microtitre plate was then placed in an oven and incubated at 37ºC for 2 hours, then cooled to room temperature for 10 minutes. The absorbance was then recorded at 562nm on a μQuant spectrophotometer from Bio-Tek Instruments (Winooski, VT).

In the BCA test for total proteins, Cu^{+2} is reduced to Cu^{+1} when it interacts with protein in an alkaline environment, with the amount of reduction being proportional to the concentration of protein present. In the second step of the reaction, the newly formed Cu^{+1} ions are chelated by two molecules of bicinchoninic acid (Figure 5).[183] The BCA/Copper complex is water-soluble and exhibits a strong linear absorbance at 562nm.

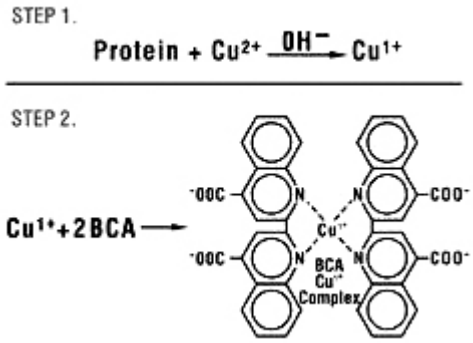

Figure 5. Reaction of Bicinchoninic Acid with Protein

2.2.6.3 MALDI-MS Analysis of Apolipoproteins

A commercial, Voyager-DE STR, MALDI-TOF mass spectrometer equipped with a 2m flight tube from Applied Biosystems (Foster City, CA, USA) was used for the

analysis of proteins (Figure 6).[184] MALDI matrices consisted of solutions of either sinapic acid or ferulic acid at a concentration of 15mg/mL dissolved in methanol. Apolipoprotein samples were prepared for MALDI analysis by de-salting and pre-concentrating with a C_4 ZipTip™ from Millipore (Billerica, MA). Samples then underwent a thin-layer sample preparation method in which a MALDI plate is first spotted with the desired MALDI matrix and allowed to dry, and then a mixture of the sample and matrix is deposited atop the original spot. Myoglobin was used as an external mass calibration standard. For MALDI analysis, the acceleration potential was held at 25kV, the grid potential was at 93%, and delay time was 550ns.

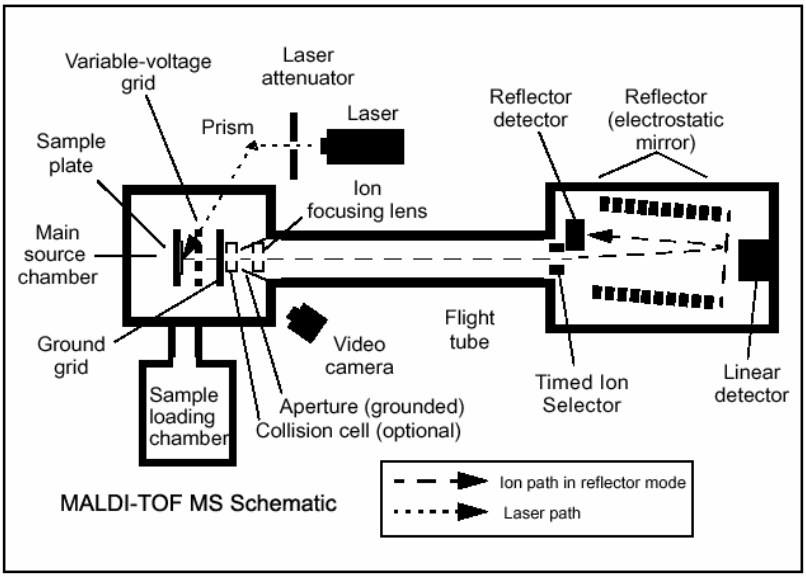

Figure 6. Voyager-DE STR MALDI-TOF Mass Spectrometer

2.2.6.4 LC-MS Analysis of Apolipoproteins

Dried protein samples were first reconstituted in 100uL of 0.1% TFA in DI H_2O. HPLC was then performed using an Agilent 1200 Capillary Pump and Microwell Plate (Santa Clara, CA) with an injection volume of 8μL onto a Jupiter C4 capillary column (150 x 0.5mm) from Phenomenex (Torrance, CA). The mobile phase for the HPLC experiment consisted of a gradient mixture of two solvents with a flow rate of 10μL per

second: (A) 0.1% (v/v) formic acid in DI H_2O, and (B) 0.1% (v/v) formic acid in ACN. The separation scheme involved a mixture of 95% of solvent (A), and 5% of solvent (B) held for 10 minutes and ramped to 100% of solvent (B) over 100 minutes, followed by holding 100% of solvent (B) for 20 minutes. The column was then re-equilibrated at the initial mixture of 95% of solvent (A) and 5% of solvent (B) for 10 minutes prior to the next sample injection.

Mass spectrometry was performed on an Applied Biosystems Qstar Pulsar (I) (Foster City, CA), which contains a hybrid quadrupole-TOF detector (Figure 7).[185] The electrospray source was operated in positive-ion mode at a voltage of 4.5 kV with scanning from 500 to 1,700 Da. Instrument parameters were optimized with myoglobin.

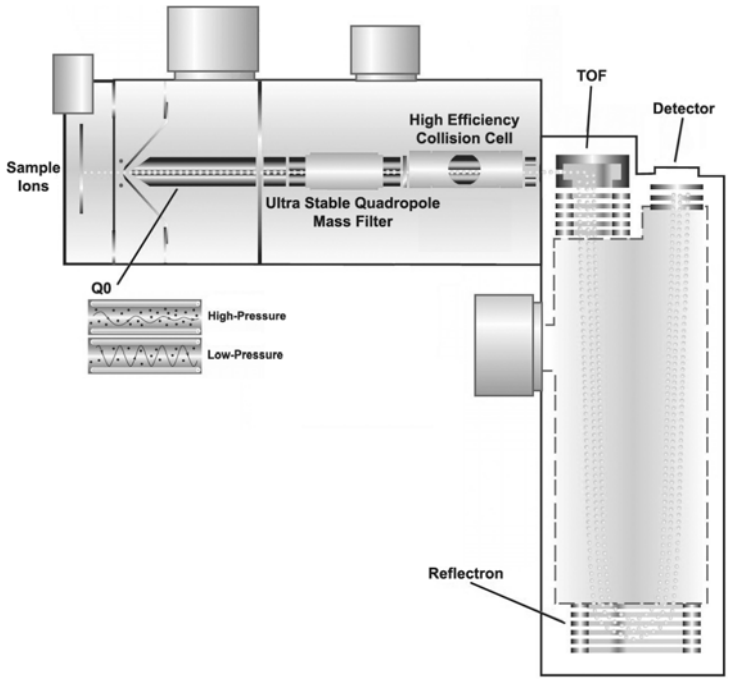

Figure 7. Schematic of a Typical Quadrupole-TOF System

2.2.6.5 CE Analysis of Apolipoproteins

Dried protein samples were reconstituted in 100uL of a buffer solution consisting of 12.5mM sodium borate, 3.5mM SDS (70%), and 20% (v/v) ACN prior to CE analysis. A fused-silica capillary column with dimensions of 75µm i.d., 375µm o.d.,

length to detector (L_d)of 50.6cm, and total length (L_c) of 60.7cm was used for the analysis. On initial use, the capillary was rinsed with 1N NaOH for 10 minutes, 0.1N NaOH for 10 minutes, and DI H_2O for 10 minutes. Between all subsequent sample analyses, the column was rinsed with 1N NaOH for 2 minutes, followed by a rinse with buffer for 2 minutes. The neutral marker consisted of a 0.5% (v/v) solution of DMSO in DI H_2O. CE analysis was performed on a Beckman P/ACE™ MDQ system (Fullerton, CA) that was equipped with a diode array detector. Run parameters for a typical apolipoprotein separation were as follows:

1. Rinse with buffer for 2 minutes
2. Inject neutral marker at 0.5 psi for 5 seconds
3. Inject sample at 0.5 psi for 5 seconds
4. Apply voltage of 17.5kV for 30 minutes

The resulting electropherograms were analyzed by 24 Karat software from Beckman (Fullerton, CA). Quantification was performed at a wavelength of 214nm. Calibration curves for apoA-I and apoC-I were created by serial dilution from 1.0mg/mL standards from Academy Biomedical (Houston, TX). Identification of other apolipoprotein peaks was possible by comparison to previously published results.[167, 180]

2.2.6.6 IEF Analysis of Apolipoproteins

Dried protein samples were reconstituted in 255uL of DeStreak™ rehydration solution and shaken for one hour at room temperature with a M71700 Slow Speed Rotomix® Variable Speed Rotator from Barnstead/Thermolyne (Dubuque, IA) prior to IPG gel application. A 250uL aliquot of the sample mixture was then applied to a 13cm aluminum oxide strip holder and a 13cm, pH 4-7 Immobline™ DryStrip was placed gel-side down into the holder. Mineral oil was then layered on top of the strip and the cover strip was set atop the sample holder. IEF IPG experiments were performed on an IPGPhor IEF Unit from Amersham Pharmacia Biotech (Piscataway, NJ) with a built-in

8,000V power supply and a Peltier solid state temperature control. IEF parameters included a current of 50μA per strip at 20ºC and a run protocol consisting of a 12 hour rehydration step, followed by steps of 500V for 1 hour, 1,000V for 1 hour, and 8,000V for 4 hours.

Upon completion of the IEF experiment, a published method for staining with colloidal acid violet 17 was followed.[169] Gels were removed from the strip holders and fixed for 30 minutes in a 20% (w/v) trichloroacetic acid solution, then de-fixed for 1 minute in a 3% (v/v) solution of phosphoric acid. The gels were then stained for 10 minutes with a colloidal acid violet 17 solution consisting of 100mg of acid violet 17 dissolved in 50mL of DI H_2O and 50mL of 20% (v/v) phosphoric acid. Gels were then de-stained during three 10 minute periods in 3% (v/v) phosphoric acid followed by three 5 minute periods in DI H_2O. Images were acquired by placing the gels face down on a digital scanner and using Origin 7.0 software to visualize the negative image of the gel (akin to visualization of the bands in an UC tube). The grayscale intensity of the IPG gels were plotted along the length of the strips, and pI values were determined by comparison to the pH gradient of the gel (Figure 8).

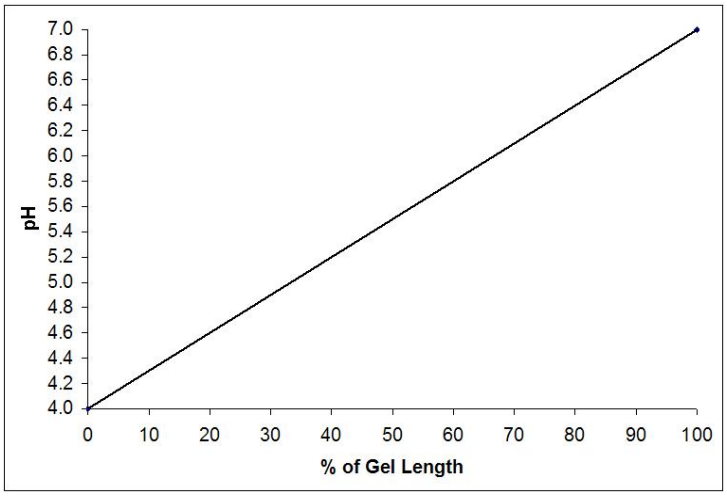

Figure 8. Gradient for Commercial IPG Strips, 13cm, pH 4-7

2.3 Clinical Studies

2.3.1 Patient Selection

Two patient groups were selected: control samples, and a CAD risk group. The control group consisted of donors with normal to elevated HDL cholesterol, normal LDL cholesterol, and a clear angiogram. The CAD risk group consisted of donors exhibiting normal to elevated HDL cholesterol and normal LDL cholesterol, but possessed documented CAD events.

2.3.2 Smooth Muscle Cell Apoptosis

Selected samples of intact HDL-2 and HDL-3 were isolated using the freeze/slice method following preparative UC. Samples were subjected to micro-concentration using filter units from Millipore (Billerica, MA) with a 10,000 molecular weight cutoff in order to remove the EDTA solute which would otherwise interfere with the apoptosis analysis. Samples were then sterilized by means of a 0.2μm sterile filter unit from Millipore (Billerica, MA). Following purification, samples were submitted to Johns Hopkins University to determine whether they induced apoptosis. It was previously seen that samples of HDL from infants enriched with apoC-I, as well as pure human apoC-I markedly induced apoptosis in aortic smooth muscle cells (ASMC) via the N-SMase pathway.[186] Studies were also performed to analyze apoptotic effects on human arterial endothelial cells (HAEC). Submitted HDL fractions were analyzed for apoptotic effects on both cell types in order to gain understanding of the functionality of HDL subclasses between control patients, and those with recorded CAD events.

2.3.3 Statistical Classification

In total, 15 control samples and 15 CAD samples were analyzed by lipoprotein density profiling followed by statistical analysis. Lipoprotein density profiles were generated for each sample by using 0.2000M solutions of both NaBiY and Cs_2CdY. Following lipoprotein density profiling, the area under the curve of various lipoprotein subclasses were obtained with the peak integration software native to Origin software.

In the NaBiY solute system 12 subclasses were identified: b-TRL, d-TRL, LDL-1, LDL-2, LDL-3, LDL-4, LDL-5, HDL-2a, HDL-2b, HDL-3a, HDL-3b, and HDL-3c. In the Cs_2CdY solute system, the buoyant subclasses of LDL-1 and LDL-2 were not resolved from the TRL fractions, and only 10 subclasses were used in classification. The integrated intensities were then analyzed by LDA and SAVE using SPSS statistics software (Chicago, IL).

CHAPTER III

RESULTS AND DISCUSSION*

The overall objective of this study was to develop a combination of information-rich methods for the analysis of clinical samples in order to determine an individual's risk of developing CAD. To meet this objective, several developmental studies were conducted and methods were eventually combined into a clinically viable protocol once they were established. The first steps toward this goal involved more thoroughly understanding how parameters in DGU can be altered in order to achieve an optimal separation of lipoprotein classes. After a successful initial study with the cesium salt of bismuth EDTA (CsBiY), it was decided that research should focus on understanding how other heavy-metal complexes of EDTA can be utilized to manipulate the shape of a density gradient following a UC experiment.

Results of this experiment revealed novel properties of the di-cesium cadmium salt of EDTA, Cs_2CdY, such as a low UV absorbance, high electrophoretic mobility, and high solubility. These properties made Cs_2CdY an ideal complex for applications that followed preparative UC. Additional studies were then initiated to establish optimal conditions utilizing this EDTA complex as a preparatory step for electrophoresis, mass spectrometry, and isoelectric focusing experiments.

---

*Reprinted with permission from "Metal Ion Complexes of EDTA for Density Gradient Ultracentrifugation: Influence of Metal Ions" by Johnson, J.D.; Bell, N.J.; Donahoe, E.L.; Macfarlane, R.D.; *Anal. Chem.,* **2005,** *77,* 7054-7061, Copyright 2005 (ACS Publications) and from "UC/MALDI-MS Analysis of HDL: Evidence for Density-Dependent Post-Translational Modifications" by Johnson, J.D.; Henriquez, R.R.; Tichy, S.E.; Russell, D.H.; McNeal, C.J.; Macfarlane, R.D.; *IJMS,* **2007,** *268,* 227-233, Copyright 2007 (Elsevier)

As the research project evolved, strong evidence began to emerge that could potentially link cardiovascular risk with atherogenic HDL. Conditions for isolating lipoprotein classes by DGU were established, and the project then focused on isolation of HDL subclasses for further study. A protocol was developed to isolate these fractions, and then delipidate them for study of the apolipoproteins contained in the HDL-2 and HDL-3 subclasses by other methods. A study utilizing serum samples from a library of patients containing samples from healthy volunteers, i.e. the controls, and those from patients with diagnosed cardiovascular events was then initiated in order to compare information from this combination of methods between the two cohorts.

The research described here presents an approach in combining various analytical techniques to not only more thoroughly analyze the complex distribution of apolipoproteins present in a sample of human serum, but to help increase sample throughput in a clinical setting as well.

3.1 Analytical Methods

3.1.1 Development of EDTA Complexes

The objective of this study was to develop a library of aqueous metal-ion complexes of EDTA that can be used to generate a family of density gradients in the UC for highlighting features of the serum lipoprotein particle density profile for clinical studies. This study investigated the properties of the metal ion-EDTA solute systems in more detail, focusing on the influences resulting from changing both the complexing ion and the counter-ion of the EDTA complex. In particular, emphasis was placed on complexing metal ions ranging from 55 to 209 Da, and counter-ions containing sodium or cesium. A synthesis scheme was developed to synthesize various EDTA complexes while eliminating undesirable by-products. The properties examined included density, refractive index, solubility, absorptivity, interaction with the fluorophore NBD (C_6-ceramide), and ability to generate a self-forming density gradient when spun in a UC for lipoprotein density profiling.

3.1.1.1 Synthesis of EDTA Complexes

The various EDTA complexes were synthesized by combining the fully protonated H_4EDTA, alkali carbonate, and the heavy metal oxide, hydroxide, carbonate, or oxycarbonate in DI H_2O. The rather insoluble H_4EDTA and heavy metal compounds are stirred and heated to reflux for two hours, yielding a clear solution. It was discovered that better control of the final solution could be attained by adding a half-equivalent of the alkali carbonate during the reflux step, and titrating the final solution to a pH between 6.75 and 7.25 with the remaining alkali carbonate. Once neutrality was achieved, the solution was added to a volumetric flask and reconstituted to the desired volume.

3.1.1.2 Properties of EDTA Complexes

A stock solution of 0.4000M ± 0.0040M of each EDTA complex was used to create serial dilutions that would cover the dynamic range of concentrations expected in a UC experiment. The density of each solution was determined gravimetrically by recording the weight of a 1,000µL aliquot from a 1,000µL micropipette. A 20µL aliquot was used to determine the refractive index at room temperature as seen in the example data table and calibration plots for the solute Cs_2CdY (Table 4) (Figure 9). By using the same method values for these measurements were used to generate a calibration curve linking the density and refractive index for each solution (Table 5). This relationship was given by the following equation, where ρ is the solution density, m is the slope of the curve, η is the refractive index of the solution, and y_o is the y-intercept. (Eq. 21) In each case, this relationship was found to be linear over the density range of interest (1.00 to 1.30 g/mL). The slopes of the density/refractive index relationship correlated linearly with the molecular weight of the solutes.

$$\rho = m\eta + y_o \tag{21}$$

Table 4. Calibration of Density vs. Refractive Index for Cs_2CdY

Concentration (M)	Density (g/mL)	η
0.3994	1.1899	1.3600
0.3728	1.1787	1.3582
0.3462	1.1674	1.3566
0.3195	1.1491	1.3543
0.2929	1.1447	1.3530
0.2663	1.1237	1.3509
0.2396	1.1187	1.3490
0.2130	1.1050	1.3471
0.1864	1.0949	1.3452
0.1598	1.0842	1.3436
0.1331	1.0708	1.3419
0.1065	1.0599	1.3378
0.0799	1.0473	1.3400
0.0533	1.0296	1.3360
0.0266	1.0229	1.3340
0.0000	0.9955	1.3320

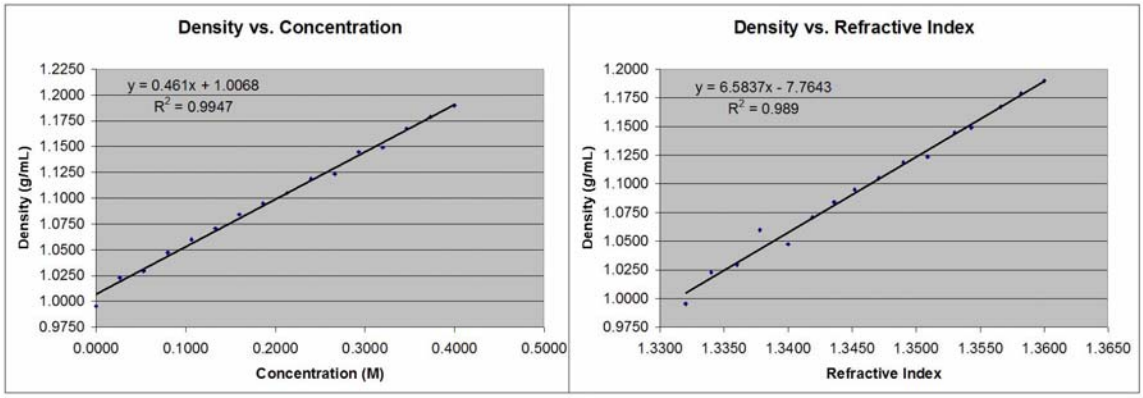

Figure 9. The Linear Relationship of Concentration, Density and, Refractive Index for Cs_2CdY

Table 5. Equation Values for Density vs. Refractive Index Formula

Salt	MW (g/mole)	Slope (m)	Y-Intercept (y_0)	R^2
CsBiEDTA	630.0938	5.4548	-6.2502	0.9954
NaBiEDTA	520.1782	4.7647	-5.3525	0.9896
Cs_2PbEDTA	761.2093	6.7665	-8.0089	0.9956
Na_2PbEDTA	541.3780	5.016	-5.6811	0.993
Cs_2CdEDTA	666.4193	6.612	-7.8024	0.9961
Na_2CdEDTA	446.5880	4.4776	-4.9596	0.9904
Na_2CuEDTA	397.7280	4.0663	-4.4191	0.9901
NaFeEDTA	367.0452	3.3795	-3.5019	0.9885

Solutions of each of the EDTA complexes at a concentration of 0.2000M were then spun in a UC for 6 hours at 120,000 RPM and 5ºC in order to determine their gradient-forming capabilities. The density profiles generated during UC were measured by sampling the resulting solution at specific depths and measuring the refractive indices. The depths were determined by capturing an image of the pipette inside the UC tube with the camera used for lipoprotein density profiling. These values were then used to calculate the density of the solution at specific tube coordinates in order to determine the shape of the gradient. The density profile data was fitted to an exponential function where ρ is the solution density in g/mL, x is the tube coordinate in mm, A and B are constants generated by Origin's peak fitting module, and y_o is the y-intercept (Eq. 22) (Table 6).

$$\rho = Ae^{(x/B)} + y_o \tag{22}$$

Table 6. Density Profile Equations for Each Solute System

Salt	A	B	Y-Intercept (y_0)	R^2
CsBiEDTA	0.0004	4.4632	1.0284	0.9864
NaBiEDTA	0.0004	4.8752	1.0177	0.9918
Cs_2PbEDTA	0.0158	10.2158	0.9846	0.9895
Na_2PbEDTA	0.0122	12.0084	1.0061	0.9875
Cs_2CdEDTA	0.01937	12.2364	0.9860	0.9827
Na_2CdEDTA	0.0172	17.5396	1.0051	0.9918
Na_2CuEDTA	0.0106	16.3193	1.0114	0.9919
NaFeEDTA	0.0038	11.0600	1.0114	0.9935

It was observed that solutes with a higher molecular weight yielded a steeper density gradient. The previous discussion of sedimentation theory in the materials and methods sections dictated that the molecular weight of the chosen solute system affected the slope of the density gradient during a UC experiment (Eq. 10). A linear relationship between molecular weight and steepness of the density profile was expressed by plotting the natural logarithm of the concentration ratios (c_2/c_1) of the solute versus the square of the difference in their tube coordinates (r_2^2-r_1^2).

$$M = \frac{\ln(c_2/c_1)(2RT)}{(1-\bar{\upsilon}\rho)\omega^2(r_2^{\,2} - r_1^2)} \qquad (10)$$

By substituting the density of the solution for the the (c_2/c_1) term and replacing the solution coordinate term (r_2^2-r_1^2) with the tube coordinate of a UC tube squared (x^2), then solving the equation for the natural log of the density, the equation becomes: (Eq. 22)

$$\ln(\rho) = \frac{(M)(x^2)(1-\bar{\upsilon}\rho)(\omega^2)}{(2RT)} \qquad (22)$$

By plotting the natural log of the density against the square of the tube coordinate, an equation of the form (y = mx + b) can be generated, thereby allowing comparisons to be made between different EDTA complexes (Figure 10).[4]

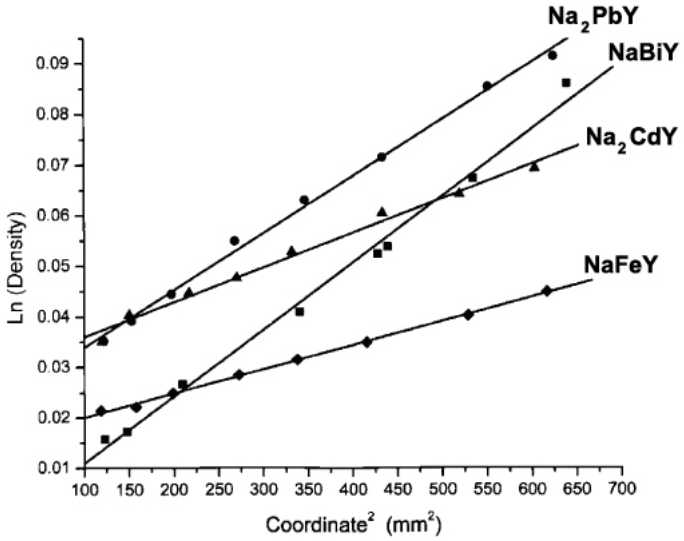

Figure 10. Plot of ln(Density) vs. Coordinate^2 for 0.2000M Solutions of NaBiY -■-, Na_2PbY -●-, Na_2CdY -▲-, and NaFeY -♦-.

The partial specific volume of the solute, $\bar{\upsilon}$, its density, ρ, the angular velocity of the UC rotor, ω, and the temperature, T, influenced the slope of this linear function. For sodium salts of the various EDTA complexes, it was observed that complexing metal ions with higher molecular weights yielded steeper slopes, as was the case with NaBiY and Na_2PbY (Table 7).

Table 7. Equation Values for ln(Density) vs. $(Coord)^2$ Formula

Salt	MW	Slope	Intercept	R^2
NaBiY	520.2	1.300×10^{-4}	1.012×10^{-2}	0.9930
Na_2PbY	541.4	1.100×10^{-4}	3.048×10^{-2}	0.9963
Na_2CdY	446.6	7.000×10^{-5}	3.059×10^{-2}	0.9889
NaFeY	367.0	5.000×10^{-5}	2.005×10^{-2}	0.9981

It was also observed that the complexes containing divalent metals, Na_2PbY and Na_2CdY also shared a higher intercept than complexes with trivalent metals, NaFeY and NaBiY. The combination of slope and intercept showed that both the complexing metal ion and counter ion are important to determining the effect of molecular weight on the shape of the density curve. Furthermore, by plotting the slope obtained from these linear functions against the molecular weight of the solute being used, it was seen that there was a good correlation between several different solute systems with an R^2 of 0.9556 (Figure 11).

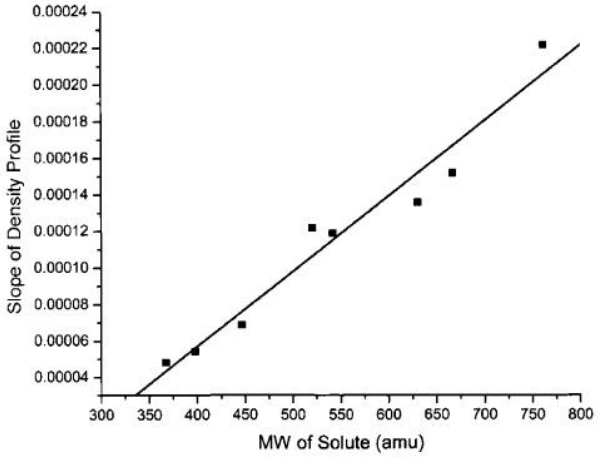

Figure 11. Slope of Density Equation vs. MW of Solute System Used

The use of the UC served a dual role of providing a useful lipoprotein density profile and a means of pre-separating the lipoprotein subclasses prior to secondary analysis. Since UV absorbance was a critical part of CE experiments, it was necessary

to gain understanding about how the absorbance properties of different solute systems could potentially interfere with this analysis. It was previously shown by our laboratory that bismuth complexes of EDTA displayed a very high UV absorbance. This resulted in such a high level of interference that CE experiments were not possible without labor intensive removal of the salt. With the exception of the copper and iron complexes, the various solutions were transparent in the visible region but absorbed in the ultraviolet region. Interestingly, the maximum absorbance wavelength of each solution was strongly dependent on the metal ion that is chelated to the EDTA ligand (Figure 12).

The bismuth complexes displayed very high absorbance maximums at 241nm and 264nm, while the lead complexes displayed equally high absorbances at 210nm and 241nm. The complexes containing cadmium had a much lower absorbance at a wavelength of 206nm. The complexes containing iron and copper displayed a very broad absorbance that covered most of the ultraviolet region and also a strong visible absorbance. The absorbance of the copper complex was very intense between 400-500nm, which overlapped with the absorbance maximum of the NBD (C_6-ceramide) fluorophore at 460nm. The absorbance of the iron complex was very intense between 500-700nm, which overlapped with the emission spectra of NBD (C_6-ceramide). The overlap of the absorbance and emission spectra of the fluorophore with these two EDTA complexes contributed to interference with imaging, as is discussed in the lipoprotein density profiling section.

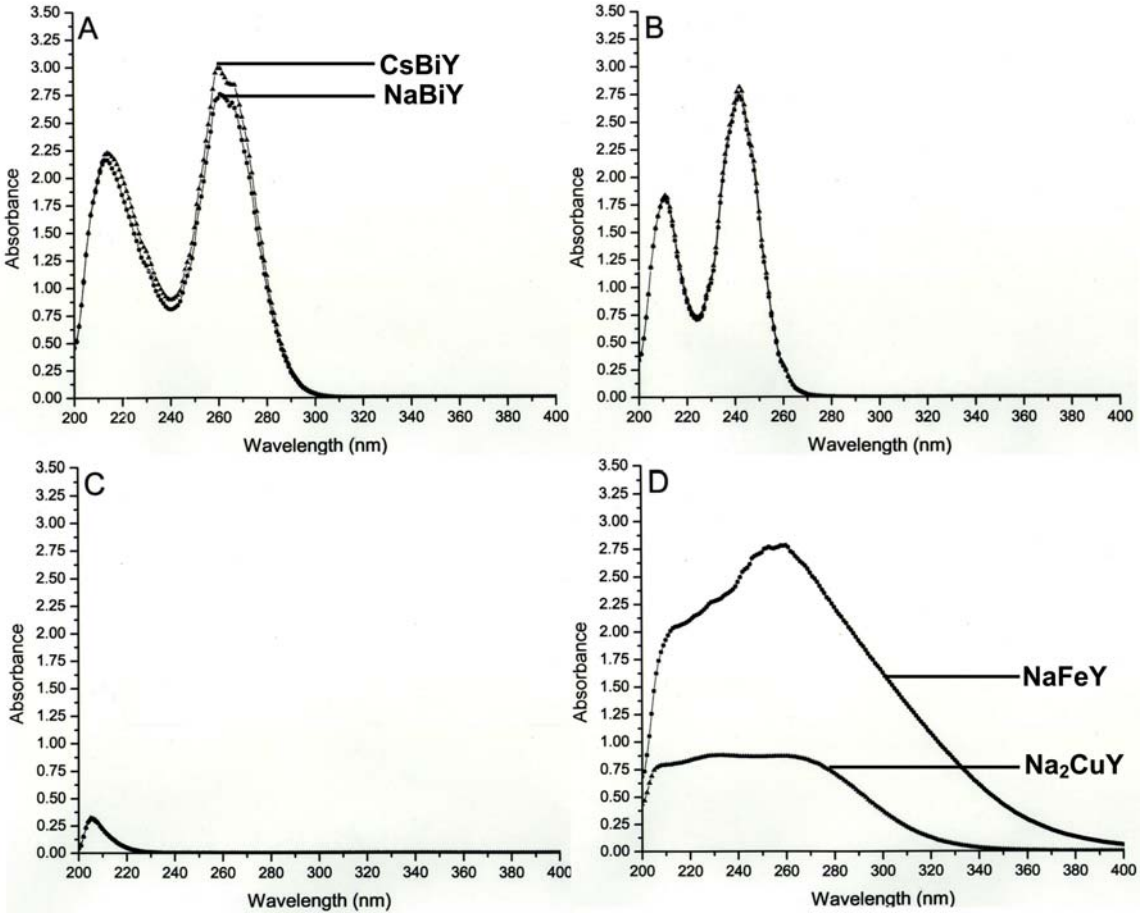

Figure 12. UV Absorbance Spectra of the Solute Systems: (A) CsBiY -▲-, NaBiY -●-, (B) Cs_2PbY -▲-, Na_2PbY -●-, (C) Cs_2CdY-▲- , Na_2CdY -●-, (D) Na_2CuY -▲-, and NaFeY -●- at a Concentration of 0.4000M.

Looking at the absorbance spectra for each complex, it was seen that altering the counter-ion of the complexes of Bi^{+3}, Pb^{+2}, and Cd^{+2} between Na^+ and Cs^+ had no discernible effect on the UV absorbance. The absorbance maxims are the same for both counter-ions, and even the absorbance intensity remained unchanged when comparing the two. A set of dilutions in the linear range for each stock solution was made to determine the molar absorptivity of each EDTA complex by Beer's Law (Table 8).

Table 8. Molar Absorptivity at the Maximum Absorbance Wavelength

Salt	Wavelength (nm)	ε (L $cm^{-1}mole^{-1}$)
CsBiEDTA	264	7,889
NaBiEDTA	264	7,855
Cs_2PbEDTA	241	7,527
Na_2PbEDTA	241	7,517
Cs_2CdEDTA	206	780
Na_2CdEDTA	204	717
Na_2CuEDTA	250	2,219
NaFeEDTA	256	7,029

It was shown that complexes containing the same complexing ion but different counter-ions had very similar absorption properties. Complexes containing cadmium had an approximately ten-fold reduction in molar absorptivity from the others. The absorptivity of complexes containing the Bi^{3+}, Pb^{2+}, and Cd^{2+} ions occurred as a result of ligand to metal charge transfer (LMCT) and were examined elsewhere.[187-190] This effect was seen because the Bi^{3+} and Pb^{2+} ions are capable of undergoing charge transfer between the ligand and metal, whereas this process is presumably less favorable for the Cd^{2+} ion due to its filled d-shell and empty p-shell. Since EDTA is a hexadentate ligand, considerable charge transfer was possible due to the number of coordination sites from which the ligand can chelate to the metal ion. The strong interaction between the complexing metal ion and the EDTA ligand was also reflected by their high formation constants.[191]

3.1.1.3 Counter-ion Effect

It was observed by refractometry that solutions of complexes containing the Cs^+ counter-ion yielded a steeper density profile than those containing the Na^+ counter-ion in each case due to the inherently higher molecular weight of these complexes. It was also

noticed that when a serum sample is spun in a solute containing Cs^+, the corresponding density of the lipoprotein subclasses were higher than those spun in a solute containing the Na^+ ion (Table 9). Lipoproteins are macromolecular anions at a pH of 7, so the Na^+ and Cs^+ ions will form an ionic atmosphere around them and increase their density relative to their natural state. Since the Cs^+ ion is heaver than the Na^+ ion, the density of the lipoprotein was greatly altered by substituting the counter-ion of the EDTA complex. These findings suggested that the ionic atmosphere configuration is retained under the influence of the forces operating during UC as the lipoproteins migrated to their isopycnic positions. When comparing densities obtained from solutes containing either Na^+ or Cs^+, the densities differed by as much as 0.0192 g/mL for LDL and 0.0294 g/mL for HDL. This result was verified by the relatively low RSD% of 0.0083, indicating that the difference in densities was not due to a lack of precision in the measurement of refractive index, which was precise up to four decimal places.

Table 9. Effect of Counter-ion on Density of Lipoproteins

Solute	LDL Density (g/mL)	HDL Density (g/mL)
CsBiEDTA	1.0588	1.1473
NaBiEDTA	1.0396	1.1179
Cs_2PbEDTA	1.0571	1.1296
Na_2PbEDTA	1.0480	1.1204
Cs_2CdEDTA	1.0574	1.1378
Na_2CdEDTA	1.0491	1.1002

3.1.1.4 Lipoprotein Density Profiling

During developmental work, various UC rotor speeds and times were studied to determine the optimal conditions for separating lipoprotein subclasses. The maximum rotor speed of 120,000 rpm was chosen to optimize the equilibration process between sedimentation and diffusion of the particles contained in the UC tube and yielded a

sufficient separation of the lipoprotein molecules.[3] Solutions containing complexes of CsBiY, NaBiY, Cs_2PbY, Na_2PbY, Cs_2CdY, and Na_2CdY were each observed to give unique separations of the different lipoprotein subclasses (Figure 13). In the six lipoprotein density profiles below, a distinct difference in separation was achieved by using equi-molar concentrations of the various EDTA solutes.

The two primary methods of modifying the lipoprotein density profiles discussed here involve altering the concentration of the gradient-generating solute or by changing the solute system altogether. In the case of the latter, it becomes possible to tailor the lipoprotein profiles to enhance specific areas, such as the region between VLDL and LDL or the region between LDL and HDL. An example of this application would be in the study of Lp(a) that is located between the LDL and HDL regions of the lipoprotein profile. Solutions of Na_2PbY and Na_2CdY at a concentration of 0.2000M, panels D and F, respectively, would give the best separation for this region of interest.

In EDTA complexes containing Bi^{+3}, a near-baseline separation was achieved among all five regions as seen in panels A and B although the separation between VLDL and LDL was greater when using CsBiY, while the separation between LDL and HDL was greater when using NaBiY. Looking at the separation achieved by CsBiY in panel A and NaBiY in panel B, the slope of the density curve was very steep, which explains the good separation of different lipoprotein classes. In addition, since the density profile was not as steep for the NaBiY solution, the resulting LDL and HDL subclasses tended to be expanded more than when using CsBiY as the density gradient generating medium. This verified that simply changing the counter-ion from cesium to sodium can have a large impact on the resulting density gradient.

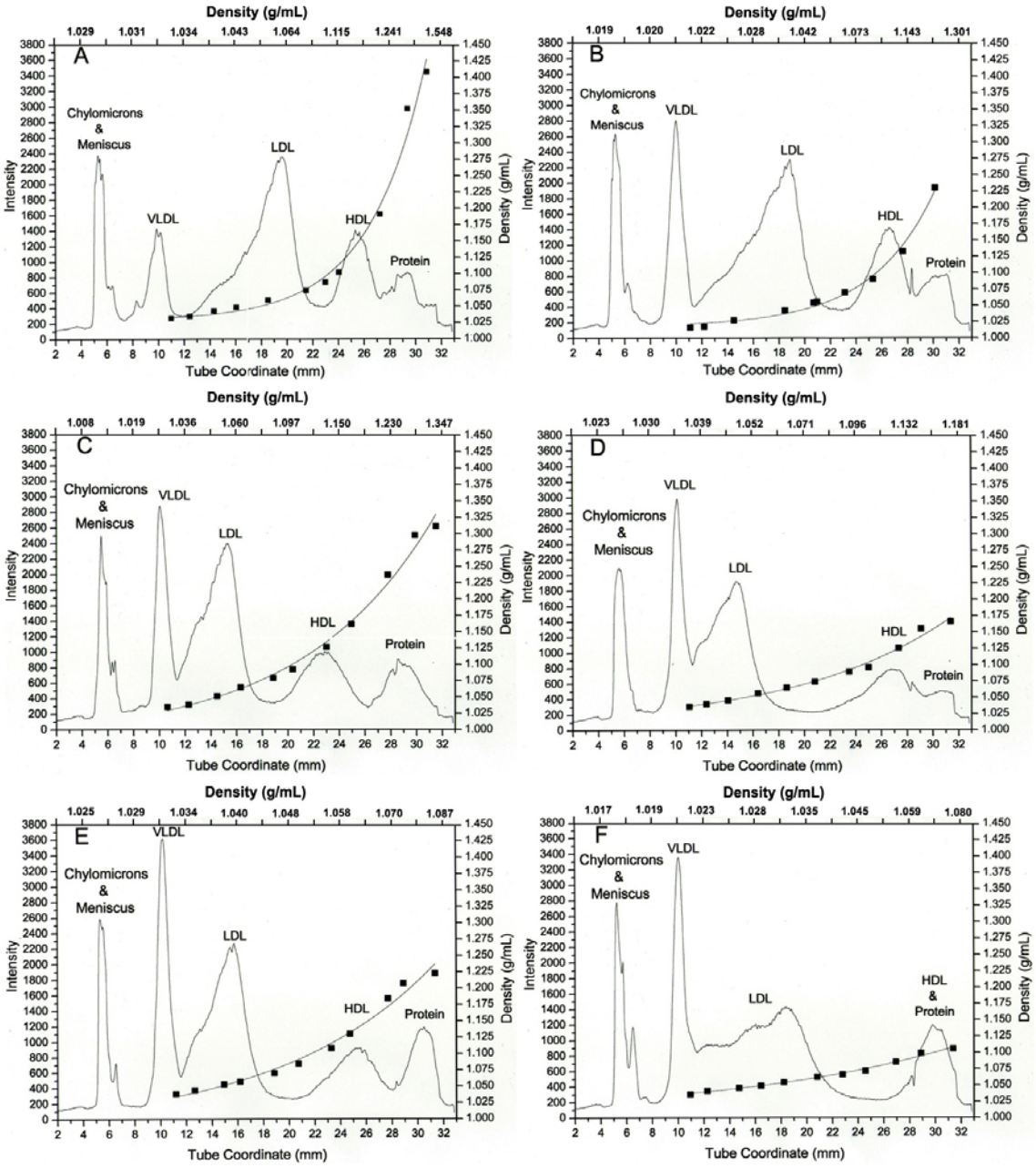

Figure 13. Lipoprotein Density Profiles Obtained with 60µL of Serum and Spun in 0.2000 M Solutions of (A), CsBiY, (B) NaBiY, (C) Cs_2PbY, (D) Na_2PbY, (E) Cs_2CdY and (F) Na_2CdY for 6 Hours at 120,000 RPM and 5°C.

When Pb^{2+} was used as the complexing metal ion, as opposed to Bi^{3+}, two counterions of Cs^{+} or Na^{+} will be associated with the EDTA complex, resulting in compounds of Cs_2PbY and Na_2PbY that have a higher molecular weight than the corresponding bismuth complexes. In the cases seen in panels C and D, the shape of the density gradient resulted in an expansion of the HDL region relative to that seen in panels A and B, and the LDL region was forced to a lower position on the tube coordinate scale (i.e., closer to the meniscus). Because the gradient is more linear and shallow in the Pb^{+2} complexes than the Bi^{+3} complexes, the separation between LDL and HDL was not as good.

As in the case of the Pb^{+2} systems, when Cd^{+2} was used as the complexing metal ion, two counterions will associate with the EDTA complex. The result was that the Cd^{+2} complexes had a molecular weight between the Bi^{+3} and Pb^{+2} complexes. In the Cs_2CdY solute system seen in panel E, the slope of the density gradient was less steep than the Cs_2PbY system seen in panel C, causing the HDL and protein regions of the lipoprotein profile to shift to a higher position on the tube coordinate scale for the Pb^{+2} system. There was essentially no difference in the LDL region of the lipoprotein profiles between these two solute systems. The density gradient formed by Na_2CdY in panel F, however, was relatively linear, resulting in two noticeable alterations to the lipoprotein profile. Since the density of this complex did not exceed 1.10 g/mL, the HDL contained in the sample was not separated from the higher density protein region. Additionally, the LDL region of the profile was elongated to such an extent that three discernible subclasses were seen for this particular sample.

The low molecular weight complexes of Na_2CuY and $NaFeY$ yielded density gradients that were shallower than the solution of Na_2CdY, thereby making them impractical for separating the different lipoprotein subclasses. In addition, the NBD (C_6-ceramide) intensities for the lipoprotein subclasses are considerably smaller than for the other solute systems mainly due to the overlap of the absorbance and emission spectra between the fluorophore and the copper and iron complexes (Figure 14). The only regions of the lipoprotein profiles that were visible were the chylomicron/meniscus and

VLDL regions, where the concentrations of these EDTA complexes were significantly lower in the region at a low tube coordinate. Fluorescence quenching also occured as a result of binding of the NBD (C_6-ceramide) fluorophore to Fe^{3+} ions.[192] Binding of Fe^{3+} to fluorophore competes with binding of Fe^{+3} to the EDTA ligand and can only be reversed at low pH with an excess of EDTA present.[193] The combination of absorbance/emission interference between Fe^{+3} and Cu^{+2} ions and NBD (C_6-ceramide) along with fluorescence quenching makes these solute systems impractical for lipoprotein density profiling. Since Cu^{2+} is also a transition metal with an empty d-orbital, quenching occured here as well, although to a lesser extent, since the copper ion is more tightly bound to the EDTA ligand.[194-196] This result was particularly interesting because it indicated that these paramagnetic ions must be in close proximity to the NBD (C_6-ceramide) fluorophores that were imbedded in the hydrophobic domains of the lipoproteins.

The EDTA solute systems allowed for isopycnic separation of lipoproteins beginning with a homogenous solution. The use of EDTA solutes also offered the advantage of having a flexible molecular weight due to the ability to substitute both the counter-ion and complexing ion. By simply altering these ions, varying degrees of separation were achieved in order to tailor a separation for a specific class of lipoproteins if so desired.

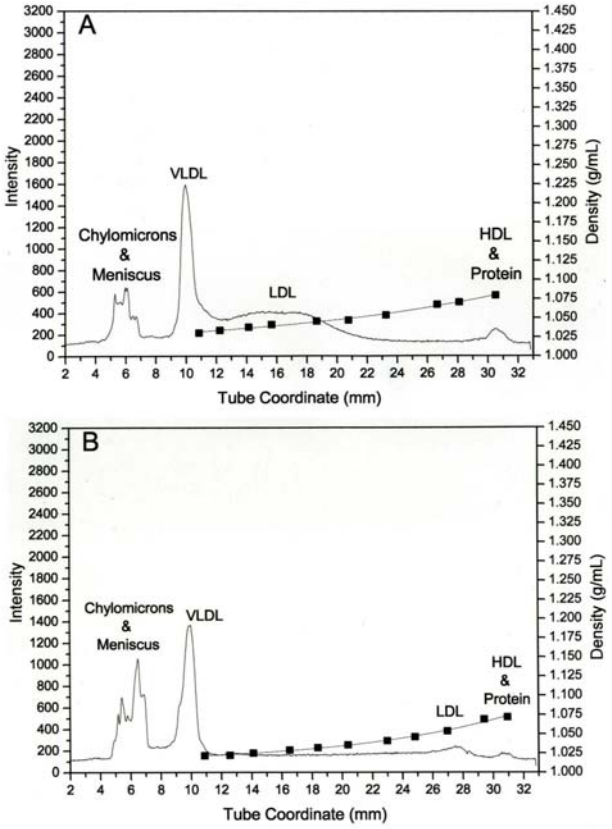

Figure 14. Fluorescence Quenching of NBD (C_6-ceramide) in the Lipoprotein Density Profiles Obtained from 60µL of Serum Spun in 0.2000M Solutions of (A) Na_2CuY and (B) NaFeY, for 6 Hours at 120,000 RPM and 5ºC.

The true benefit of the ability to tailor the DGU separation with the various EDTA solutes was shown when the method was used in a preparative mode for further analyses. With full control over the complexing metal ion and counter-ion, as well as the concentration of the solution, it became possible to isolate specific regions of the lipoprotein profile for subsequent experimentation. Since the Cd^{+2} complexes are doubly-charged (i.e. CdY^{-2}) and had a relatively low absorptivity as opposed to the much higher absorptivity of the singly charged Bi^{+3} complexes (i.e. BiY^{-1}), it was determined that they are a better choice of solute for preparative UC. Their ability to separate lipoprotein subclasses effectively coupled with their favorable absorbance and

electrophoretic properties made them ideal solutes for preparation of CE and MS experiments.

3.1.1.5 Preparative Ultracentrifugation

The goal of preparative UC experiments was to cleanly isolate the region of interest in a lipoprotein profile in order to extract it for secondary analysis. Since the aim of this research was to study atherogenic particles of HDL, this approach involved two further developmental steps once Cs_2CdY was determined to be the density gradient solute of choice. First, the required concentration of Cs_2CdY to isolate the HDL region was determined by UC of the solute at various concentrations ranging from 0.2000M to 0.4000M. It was found that a solute concentration of 0.3000M gave the optimal isolation of the HDL region. Secondly, it was desirable to remove all apo-B containing lipoproteins from solution prior to UC in order to minimize interference from LDL and Lp(a). The standard method for HDL quantification involved precipitation of Apo-B containing lipoproteins by addition of a DS reagent to whole serum prior to UC.[182] This reagent was generated as described in the materials and methods section. This mixture was then added to whole serum in a 1:10 ratio (v/v) and allowed to incubate for 10 minutes at room temperature, followed by centrifugation at 12,000 rpm on a tabletop centrifuge. The supernatant was recovered and was prepared for lipoprotein density profiling as if it were a normal whole serum sample. A comparison between the lipoprotein density profiles of a normo-lipidemic patient spun in 0.2000M NaBiY with and without the DS precipitation step showed that this procedure very cleanly removed all apo-B containing lipoproteins from the serum profile (Figure 15). By combining the DS precipitation steps with a UC spin using 0.3000M Cs_2CdY, it became possible to freeze the sample and excise out fractions of the buoyant HDL-2 fraction and the dense HDL-3 fraction for clinical studies (Figures 16-17).

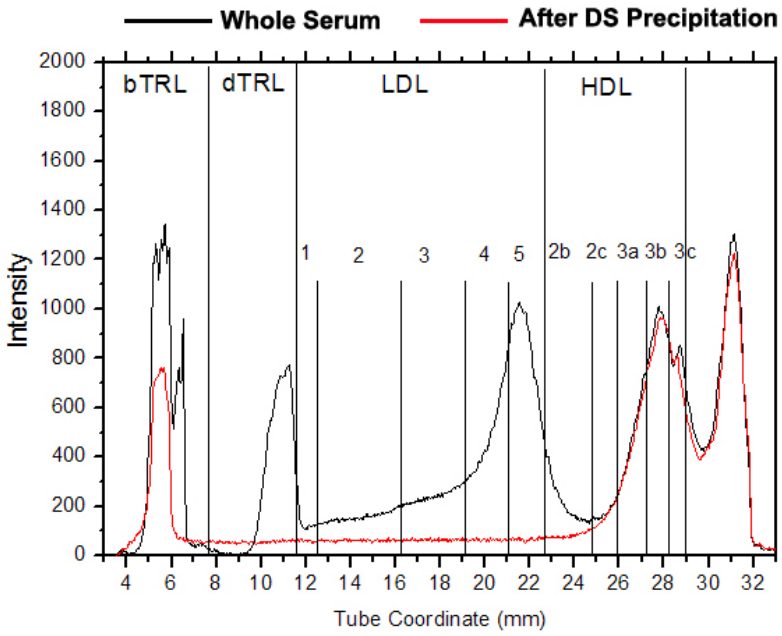

Figure 15. Comparison of Lipoprotein Density Profiles for Whole Serum to Supernatant of DS Precipitation in a 0.2000M Solution of NaBiY, Spun for 6 Hours at 120,000 RPM and 5ºC.

In the density profiles of the patient samples it was observed that there was baseline separation of the entire HDL zone from other lipoproteins. In total, there were 12 samples analyzed in this study, 6 controls, and 6 with a pre-existing condition of CAD. For the duration of this dissertation, the focus will remain with one control, sample #47, and one CAD patient, sample #10, with data for the other 10 samples contained in the appendix. Of interest was that in samples designated as controls, there appeared to be a higher distribution of HDL towards the denser HDL-3 subclass, while in CAD samples, the shift favored the buoyant HDL-2 subclass. In none of the samples analyzed was there baseline separation between the two HDL subclasses.

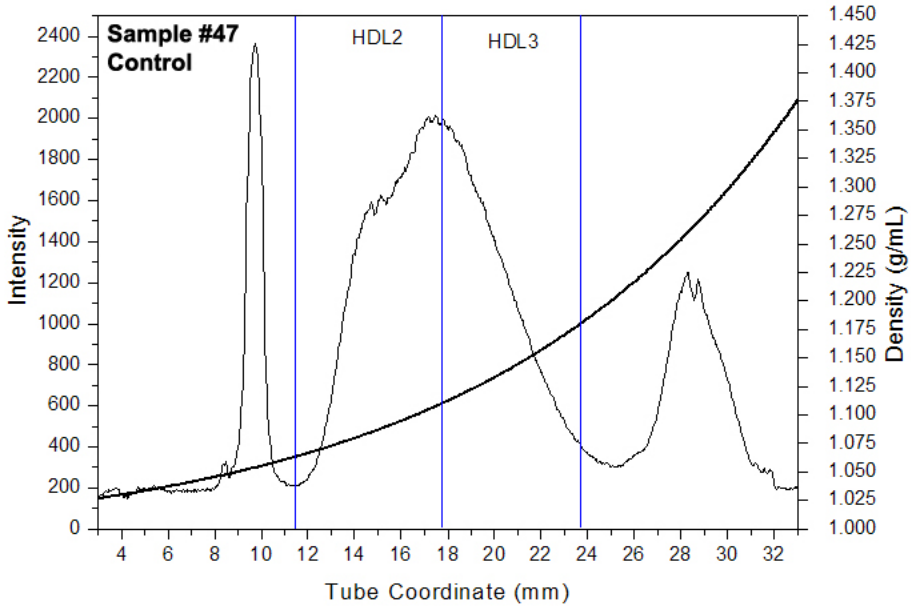

Figure 16. Lipoprotein Density Profile of Sample #47 in a 0.3000M Solution of Cs_2CdY, Spun for 6 Hours at 120,000 RPM and 5ºC after DS Precipitation.

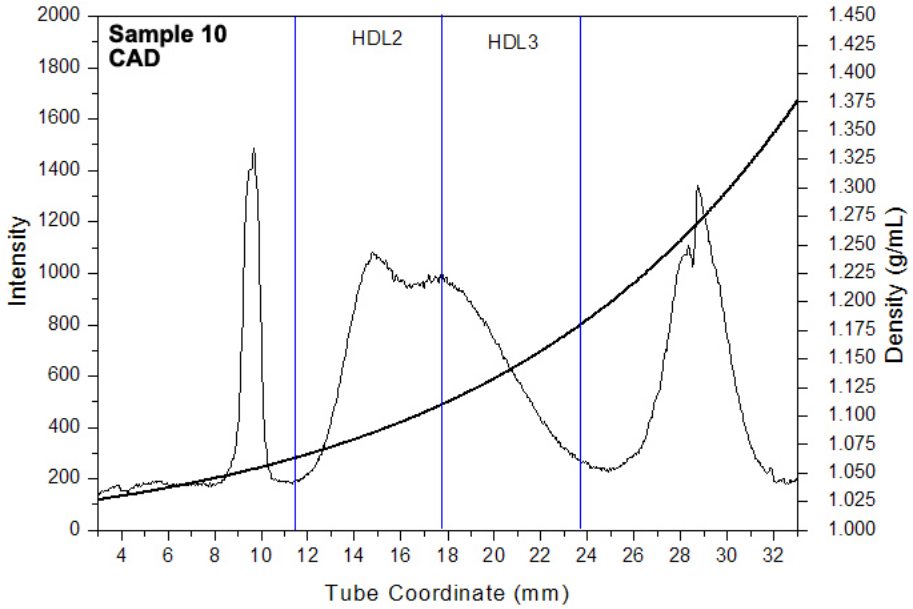

Figure 17. Lipoprotein Density Profile of Sample #10 in a 0.2000M Solution of Cs_2CdY, Spun for 6 Hours at 120,000 RPM and 5ºC after DS Precipitation.

3.1.2 Delipidation and Purification of Apolipoproteins

For apolipoprotein analysis of HDL, the excised fraction must be subjected to a delipidation step prior to secondary analysis. This involved the use of a solid phase extraction (SPE) cartridge which served to both de-salt, and to remove the lipid content of the sample, operating much like a reverse-phase liquid chromatography experiment. SPE experiments were performed as described in the materials and methods section, and served to elute the polar components of a sample fraction, while retaining the most non-polar lipid components. MALDI-MS was utilized to determine the elution profile from the SPE cartridge. Four aliquots of 50µL eluents were obtained, and each was prepared for MALDI-MS analysis by use of a C_4 ZipTip, which behaved like a very small scale reverse-phase column. A 5µL aliquot of each sample was concentrated in the ZipTip, and then eluted with a solution consisting of 60% ACN, 0.1% TFA, and 40% DI H_2O by volume. The effluent was then mixed with a 5µL volume of a solution containing 15mg/mL of ferulic acid in 60% ACN, 40% DI H_2O, and 0.1% TFA by volume and then evaporated to dryness. It was found that any HSA remaining after the wash steps primarily eluted from the SPE cartridge in the first 50µL aliquot, while the remaining apolipoproteins of HDL eluted in the first through fourth aliquots (Figure 18). In this particular case, however, no HSA was detected in the MALDI mass spectrum. Typically the wash step was enough to fully remove all of the HSA, but it was observed in the first aliquot if it was not completely removed. It was seen in panels A, B, and C that the expected apolipoproteins were eluted from the SPE column. It was also observed that the majority of the apolipoproteins eluted during the first and second 50µL aliquots, and that nothing above baseline could be seen in the fourth 50µL aliquot in panel D. It is also important to note that apo A-II was not fully eluted until after the third aliquot, while apo A-I appeared to be fully eluted by the second aliquot. This result gave evidence that even though apo A-I is a larger apolipoprotein, apo A-II as a dimer is more hydrophobic. As a result, the first four aliquots from samples delipidated by SPE were pooled together for all HDL fractions to be analyzed to ensure maximum recovery.

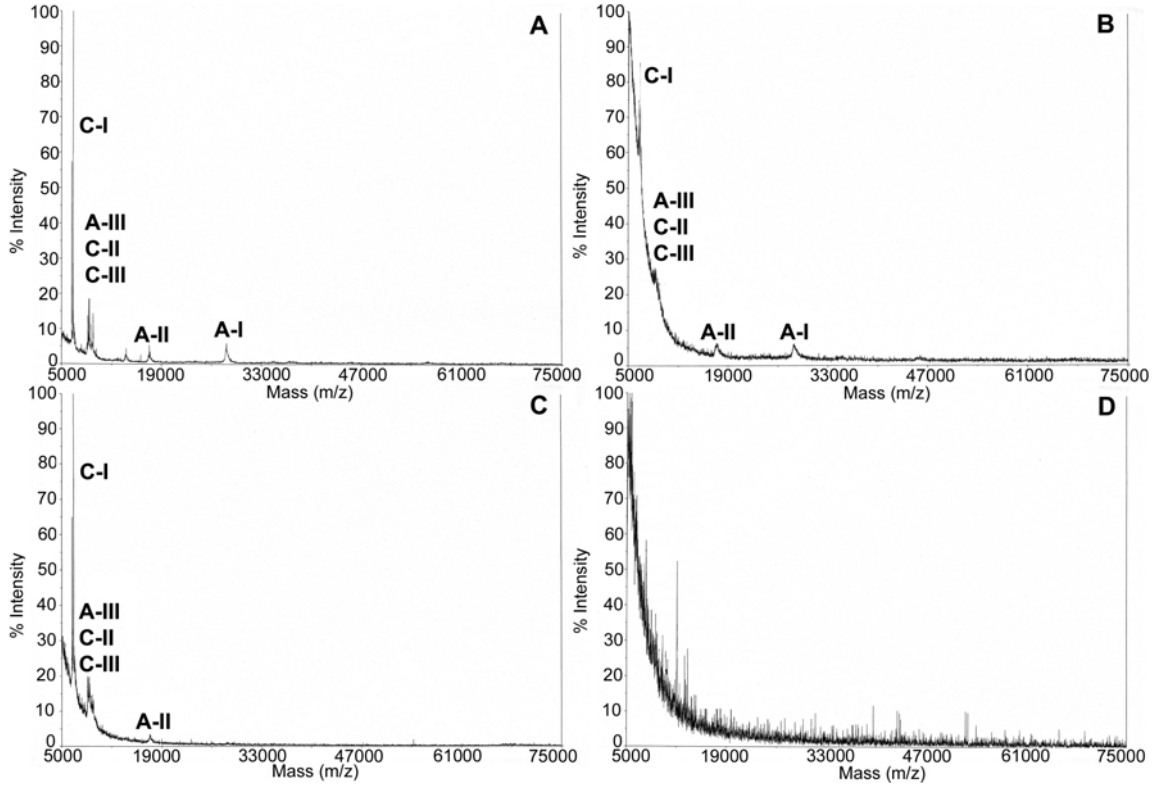

Figure 18. Elution Profile for SPE of HDL Apolipoproteins for the 1st (A), 2nd (B), 3rd (C), and 4th (D) 50µL Effluents

3.1.3 Desalting and Purification of Intact Lipoproteins

For analysis of intact lipoproteins,the sample must be de-salted without removing the lipid content of the apolipoprotein. Because of this stipulation, de-salting must be performed by way of micro-concentration of the excised fraction. Micro-concentration of excised samples allowed for replacement of the EDTA solute with a suitable solution for apoptosis studies, such as DI H_2O. Samples were typically micro-concentrated from a volume of 500µL down to 50µL, and then reconstituted back to 500µL for each cycle. It was seen that five reconstitution cycles gave adequate removal of the undesired EDTA solutes. Following micro-concentration, samples were then sterilized by means of a 0.22µm syringe filter unit. For studies involving apoptosis, it was important to both desalt and sterilize the HDL samples to limit the amount of background apoptosis that would interfere with the analysis.

3.1.4 MALDI-MS Analysis of HDL Fractions

The objective of this study was to determine whether the nature of the post-translational modifications of the major apolipoproteins of HDL was different for density-distinct subclasses. The serum of two subjects, a control with a normo-lipidemic profile, and a subject with diagnosed cardiovascular disease, were studied. Aliquots of three HDL subclasses were analyzed by MALDI and considerable differences were seen when comparing density-distinct subclasses and also when comparing the two subjects. A detailed analysis of the post-translational modification pattern of apoA-1 showed evidence of considerable protease activity, particularly in the more dense fractions. It was hypothesized that part of the heterogeneity of the population of HDL particles is due to density-dependent protease activity.

This study was aimed at understanding density-distinct differences between HDL subfractions. It was discovered that the 0.3000M Cs_2CdY solution could be utilized to isolate three regions in the HDL profile. There regions were labeled "buoyant", "middle", and "dense" HDL during this study. After UC, samples were frozen and excised as previously described, then desalted and purified for MALDI-MS (Figure 19).

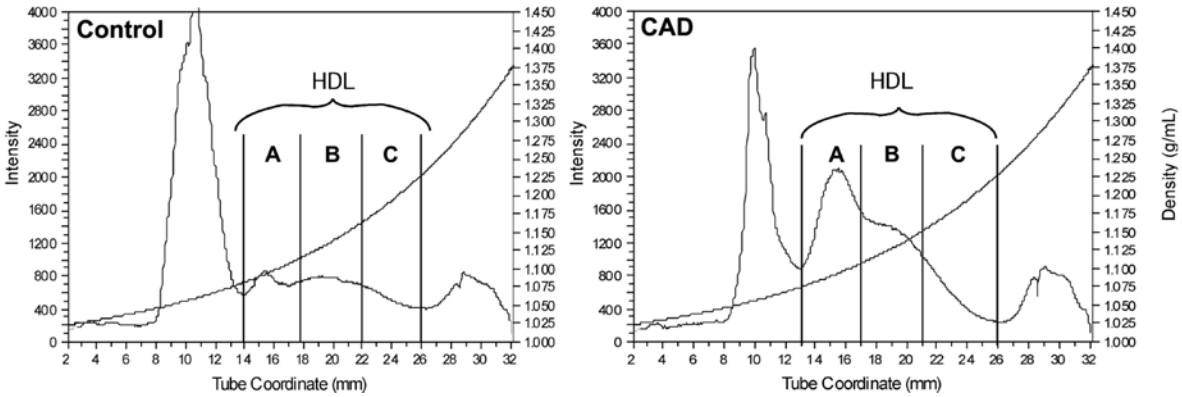

Figure 19. Preparative UC Profiles of Control and CAD Samples for Buoyant (A), Middle (B), and Dense (C) HDL Fractions

A 5μL aliquot of each HDL fraction was concentrated by using a C_4 ZipTip and eluted with a solution consisting of 60% ACN, 0.1% TFA, and 40% water (v/v) The

effluent was then mixed with a 5μL volume of a solution consisting of ferulic acid (15 mg/mL) in 40% H_2O, 60% ACN, 0.1% TFA (v/v) and evaporated to dryness on a MALDI plate.

3.1.4.1 Post-Translational Modifications in MALDI-MS

Three suspected differences that could be seen in MALDI-MS include: oxidative processes that could modify the HDL apolipoproteins, presence or absence of inflammatory response markers, and the possibility of post-translational modifications of the major apolipoproteins. Oxidation and post-translational modifications would be revealed in MALDI-MS by shifts in m/z distributions for the various apolipoproteins. The presence or absence of specific proteins, such as SAA, could indicate an inflammatory response. It was uncertain as to whether these conditions would appear across the entire density range of HDL, so MALDI spectra were recorded for the three HDL subfractions for a normo-lipidemic patient and a patient with diagnosed cardiovascular events (Figure 20). This experiment reports the results of a feasibility study in determining what differences, if any, can be observed by analyzing both density-distinct, and patient specific sample fractions. At first glance, the spectra were qualitatively similar to what was observed in previous studies, with the dominant peaks coming from: apoA-I,II, and apoC-I,II,III.[141] The m/z peaks due to apo C-I dominated the spectra despite the low abundance of this apolipoprotein compared to A-I. This occurred due to a high concentration of lysine residues, which makes apo C-I more basic than the other apolipoproteins, and therefore gives it a higher proton affinity.

What was remarkable about these spectra was that the pattern of post-translational modifications showed significant differences for all three density regions of both a control sample and a CAD sample. The accuracy of the mass measurements was not sufficient to identify every observed peak, but the majority of post-translational modifications could be accounted for (Table 10).

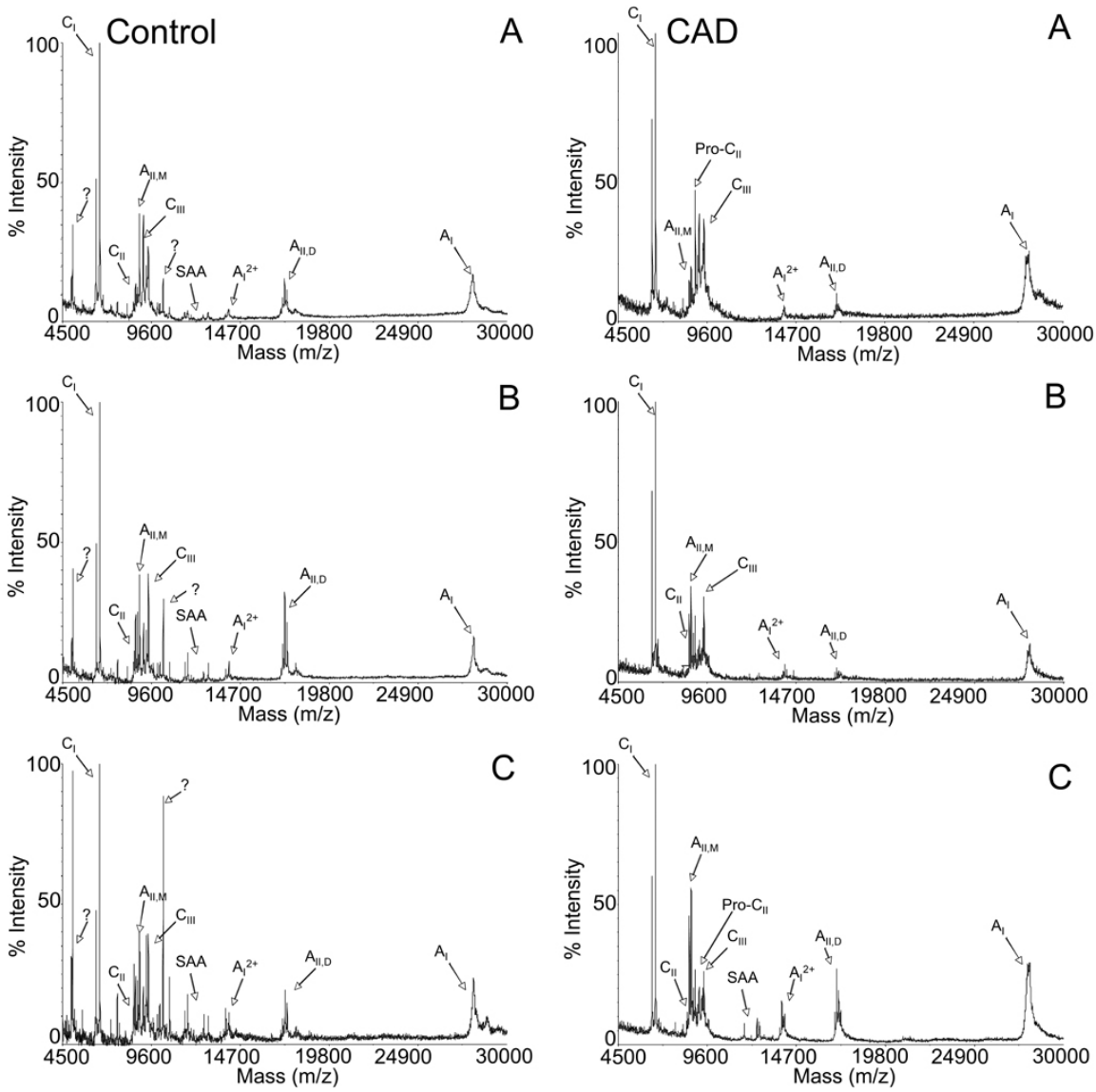

Figure 20. MALDI Spectra of Control and CAD Samples for Buoyant (A), Middle (B), and Dense (C) HDL Fractions

Table 10. Identification of Apolipoproteins in MALDI Spectra

Identification	Code	Avg. Mass
Apo C-I minus N-Thr-Pro	C-I'	6,440.25
Apo C-I	C-I'	6,639.30
C-I plus 206 Da Adduct	$C\text{-}I_{add}$	6,845.72
Apo C-II	C-II	8,217.89
Apo A-II minus C-Gln-Gln, z = 2	$A\text{-}II'^{2+}$	8,634.09
Apo A-II Monomer minus C-Gln	$A\text{-}II'_{m}$	8,692.80
Apo $C\text{-}III_0$	$C\text{-}III_0$	8,778.00
Apo A-II Monomer	$A\text{-}II_m$	8,819.47
Pro Apo C-II	pro C-II	8,924.90
Galβ, 3GalNAc-O-$C\text{-}III_0$	$C\text{-}III_{0,Glyc}$	9,140.78
Apo $C\text{-}III_1$ minus C-Ala-Ala	$C\text{-}III_1$"	9,301.33
Apo $C\text{-}III_1$ minus C-Ala	$C\text{-}III_1$'	9,363.79
Apo $C\text{-}III_1$	$C\text{-}III_1$	9,429.98
Apo $C\text{-}III_2$ minus C-Ala-Ala	$C\text{-}III_2$"	9,574.07
Apo $C\text{-}III_2$ minus C-Ala	$C\text{-}III_2$'	9,645.03
Apo $C\text{-}III_2$	$C\text{-}III_2$	9,721.06
SAA_1 minus N-Arg	SAA_1'	11,536.64
SAA_1	SAA_1	11,695.05
SAA_1 plus 189 Da Adduct	$SAA_{1,add}$	11,884.05
SAA_4 minus C-Lys-Lys-Tyr	SAA_4'"	12,464.63
SAA_4 minus C-Lys-Tyr	SAA_4"	12,582.71
SAA_4 minus N-Glu-Ser	SAA_{4n}"	12,674.19
SAA_4	SAA_4	12,873.51
Prealbumin	Prealb	13,781.97
Apo A-I minus C-Thr-Gln, z = 2	$A\text{-}I''^{2+}$	13,934.21
Apo A-I minus C-Gln, z = 2	$A\text{-}I'^{2+}$	13,983.24
Apo A-I, z = 2	$A\text{-}I^{2+}$	14,049.10
Apo A-I plus 294 Da Adduct, z = 2	$A\text{-}I^{2+}{}_{add}$	14,343.10
Apo A-II Dimer minus C-Thr-Gln and C-Gln	$A\text{-}II_t$"	17,042.71
Apo A-II Dimer minus C-Gln-Thr-Ala	A-II'"	17,085.79

Table 10. (Continued)

Identification	Code	Avg. Mass
Apo A-II Dimer minus 2x C-Gln	A-II"	17,146.45
Apo A-II Dimer minus C-Gln	A-II'	17,267.74
Apo A-II Dimer	A-II	17,396.94
Apo A-II Dimer plus 322 Da Adduct	$A\text{-}II_{add}$	17,718.94
Apo A-I minus C-Gln	A-I'	27,974.84
Apo A-I	A-I	28,111.50
Apo A-I plus 554 Da Adduct	$A\text{-}I_{add}$	28,665.50

Examining these spectra in greater detail revealed some significant differences. There appeared to be a marked change in the shape and intensity of the apo A-I peak as a function of density for both the control sample and the CAD sample. This phenomenon was seen in greater detail when looking at expanded views of the doubly-charged ions of Apo A-I, as opposed to the singly-charged ions. This observation was due to the higher resolution that was obtained in the lower m/z range where the doubly-charged ion was located (Figures 21-26). We can only postulate that different proteases are resident on the HDL particles dependent on the density of the particle. There appeared to be more protease activity in the dense HDL component for the CAD subject. It was clear from these results that the nature of post-translational modifications was linked somehow to the density of the HDL particle.

Apo C-I and its truncated form Apo C-I' were consistently observed for all six sample fractions and alterations in structure were not as prevalent as that which was seen for apo A-I. Apo C-I' differed in mass from Apo C-I by approximately 200 mass units as the result of truncation of two amino acid residues, threonine and proline, from the N-terminus.[143] Interestingly, the ratio of apo C-I' to apo C-I appeared to be enhanced in all 3 fractions of the CAD sample, with the greatest amount of enhancement seen in the buoyant fraction. This result suggests that there may be a link between the relative amounts of the two isoforms of apo C-I that could assist in assessing an individual's cardiovascular risk.

Significant differences were also seen in the serum amyloid A (SAA) region of the MALDI spectrum for the two patients. The isoform designated as SAA_1 is indicative of an acute-phase response to inflammation while the isoform SAA_4 is typically seen in normal serum.[197, 198] A peculiar result was that both the control sample and the CAD sample contained each of these isoforms, but SAA_1 was observed in every density fraction for the control patient and only in the dense fraction for the CAD patient.

There were two regions of the MALDI spectra that contained results that were largely the same throughout the various density ranges for both patients. The apo A-II dimer was observed to contain the same distribution of isoforms regardless of which density region or patient from which it was obtained. The intensity of the peaks in this portion of the spectra also tended to scale with the intensity of the rest of the mass spectra. At the high molecular weight end of the mass spectra, the singly-charged apo A-I did not display well-resolved peaks as was seen in lower molecular weight regions of the spectra, and consisted primarily of the main apo A-I peak, a truncated apo A-I', and an apo A-I' containing a suspected adduct that added approximately 554 Da to its native mass. As previously mentioned, the resolution of the doubly-charged ions of apo A-I were much improved and allowed for a more thorough analysis.

The busiest region of the mass spectra resided with the other apo C apolipoproteins and appeared as a "fingerprint" that was seemingly density dependent. In buoyant sample fractions, the apolipoproteins, and their modifications, C-III_0, pro C-II, and C-III_1 appeared to be the most intense. For dense sample fractions, the apolipoproteins, and their modifications, A-II, and C-III_2 appeared to be the most intense. The HDL fraction in between these two densities displayed an intermediate intensity for each apolipoprotein. Substantial differences between the control and CAD samples were not observed in this region.

By coupling mass analysis by MALDI-MS with the sample preparation developed with DGU, these results demonstrated feasibility in a new approach to better understanding the apolipoprotein distribution for patient samples as a function of density.

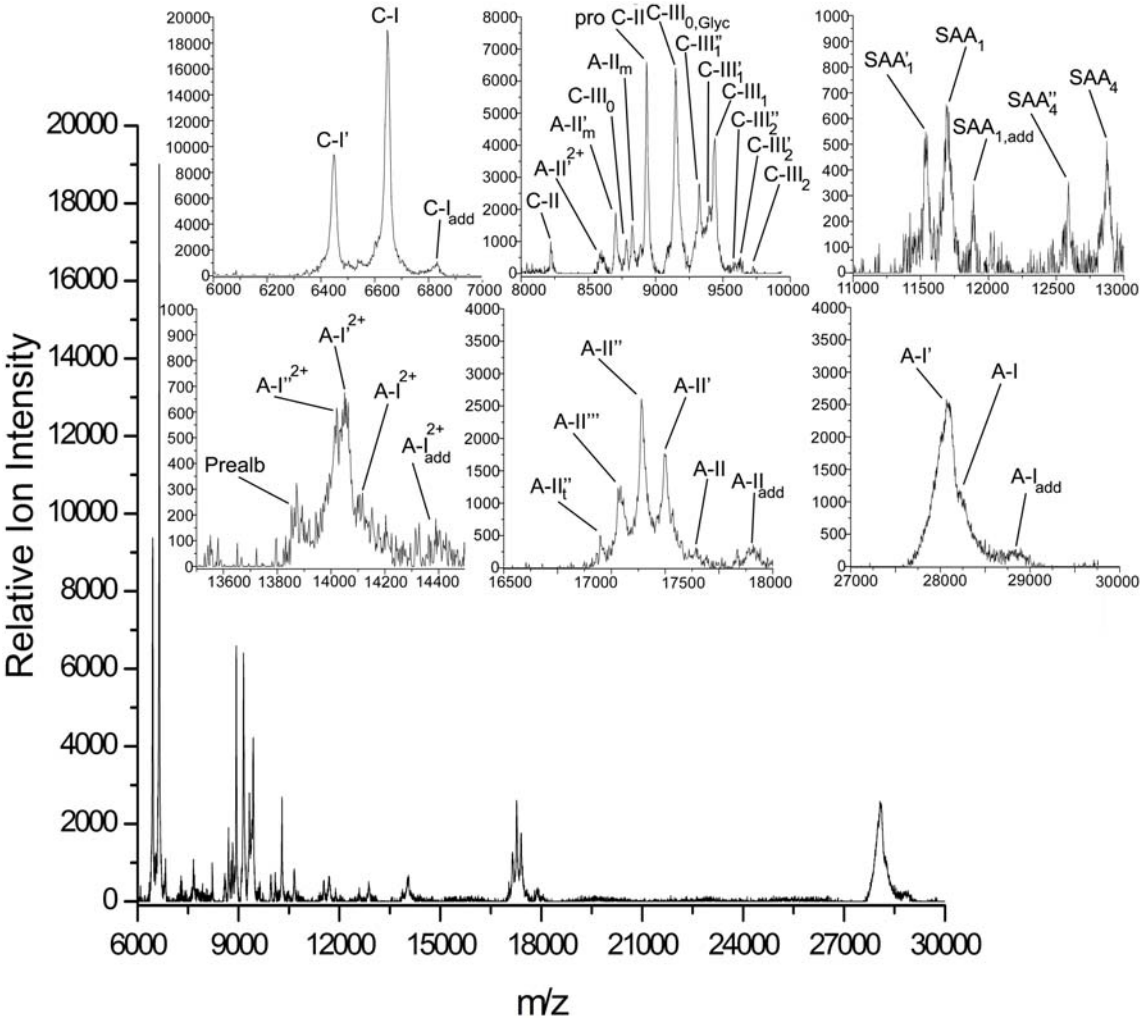

Figure 21. MALDI-MS Spectrum for Buoyant Fraction of Control Sample

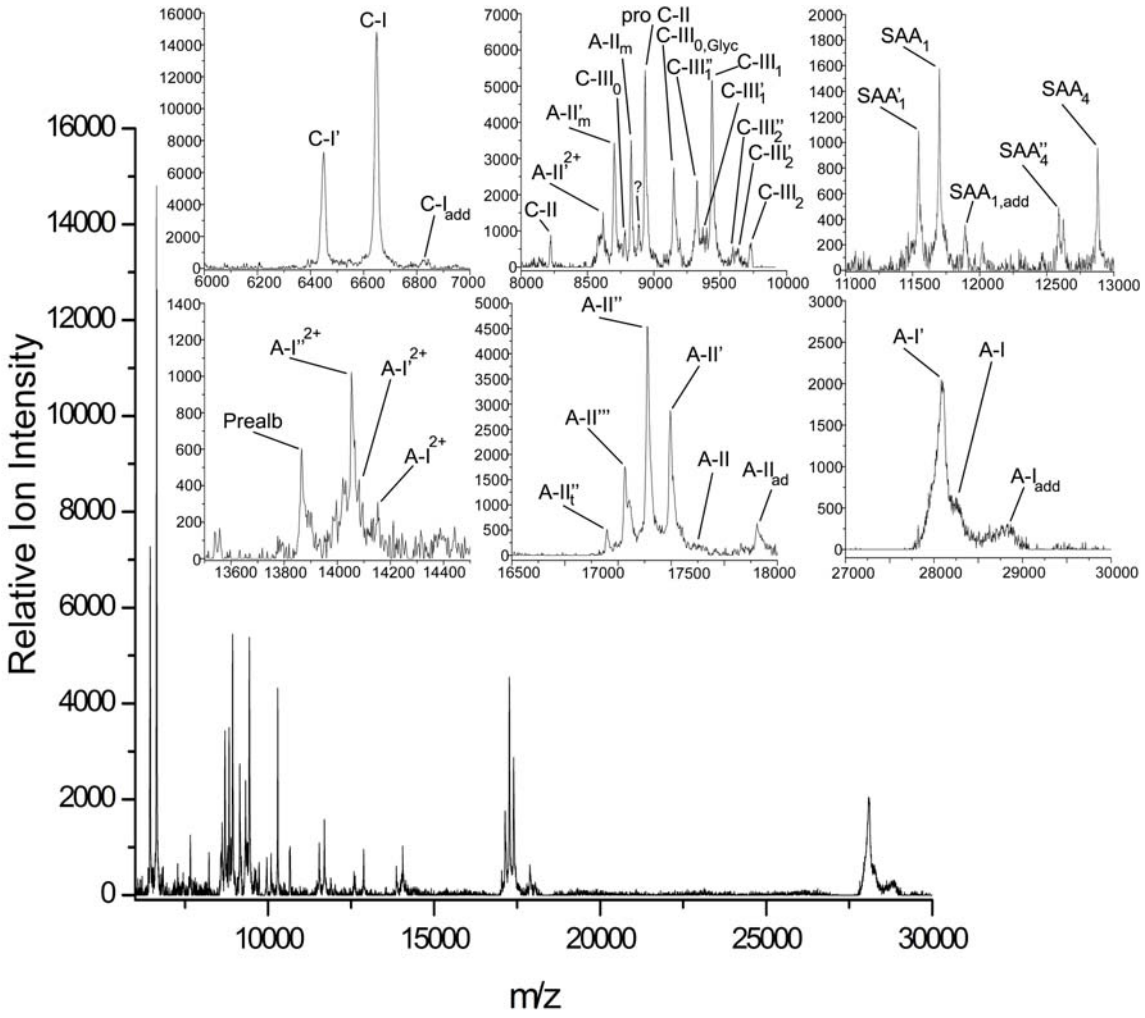

Figure 22. MALDI-MS Spectrum for Middle Fraction of Control Sample

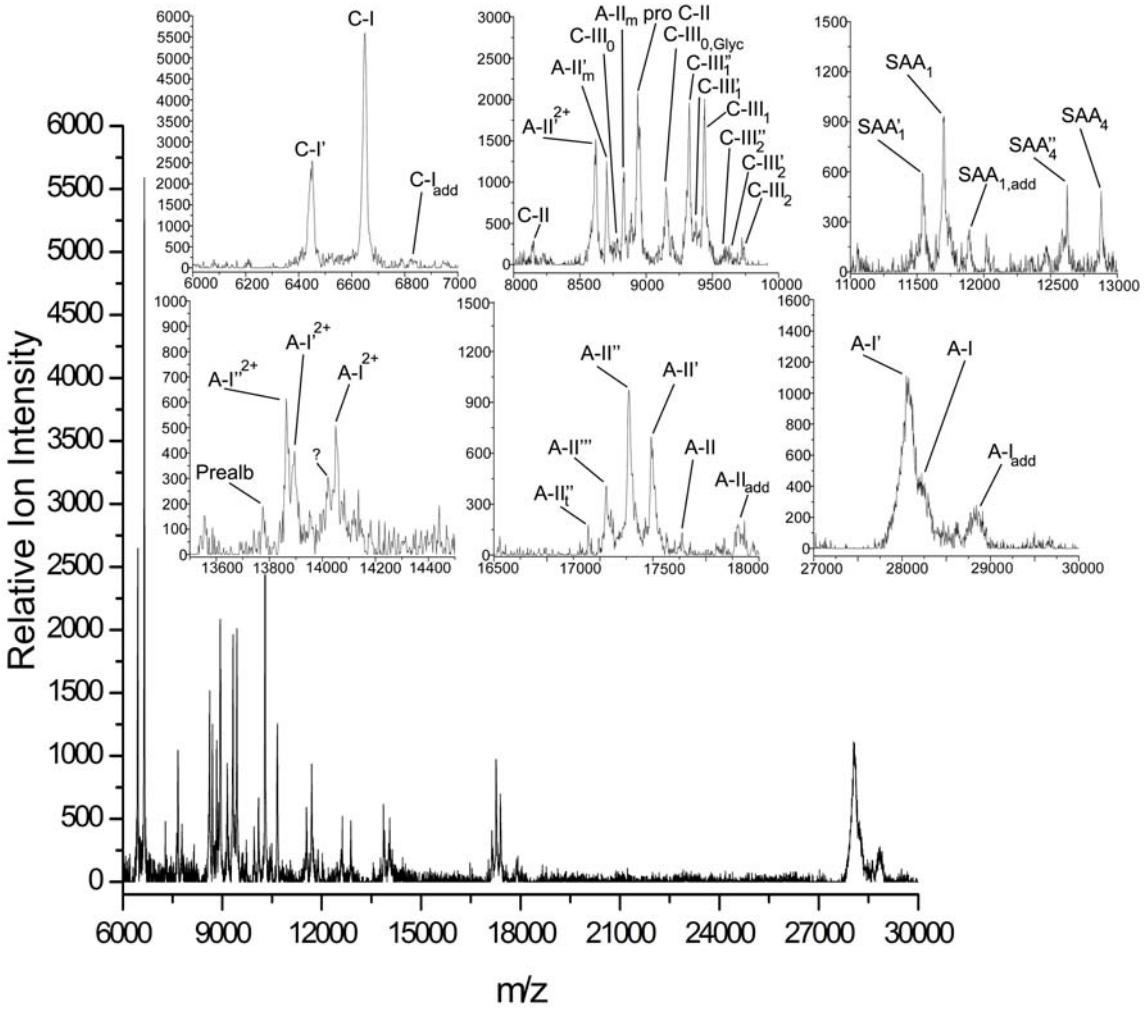

Figure 23. MALDI-MS Spectrum for Dense Fraction of Control Sample

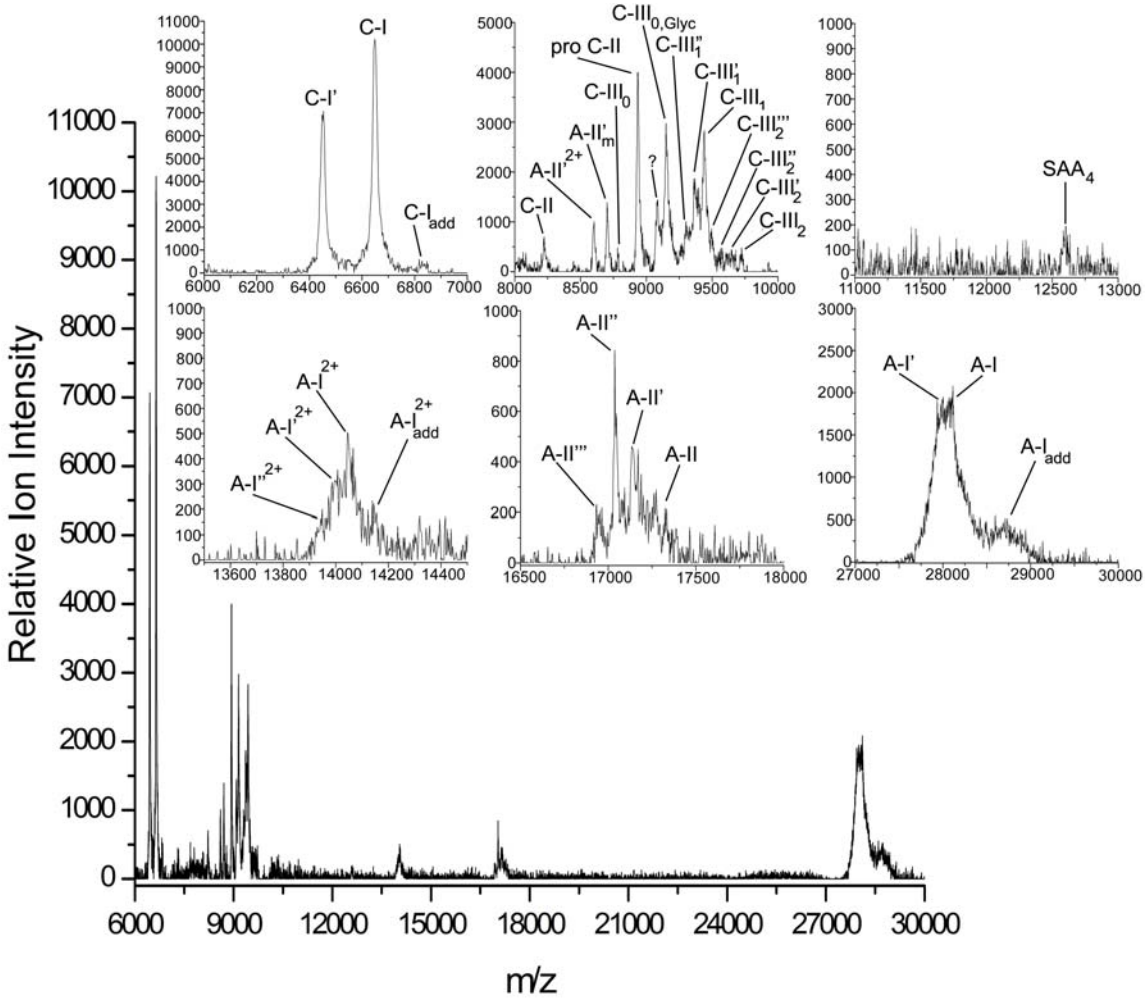

Figure 24. MALDI-MS Spectrum for Buoyant Fraction of CAD Sample

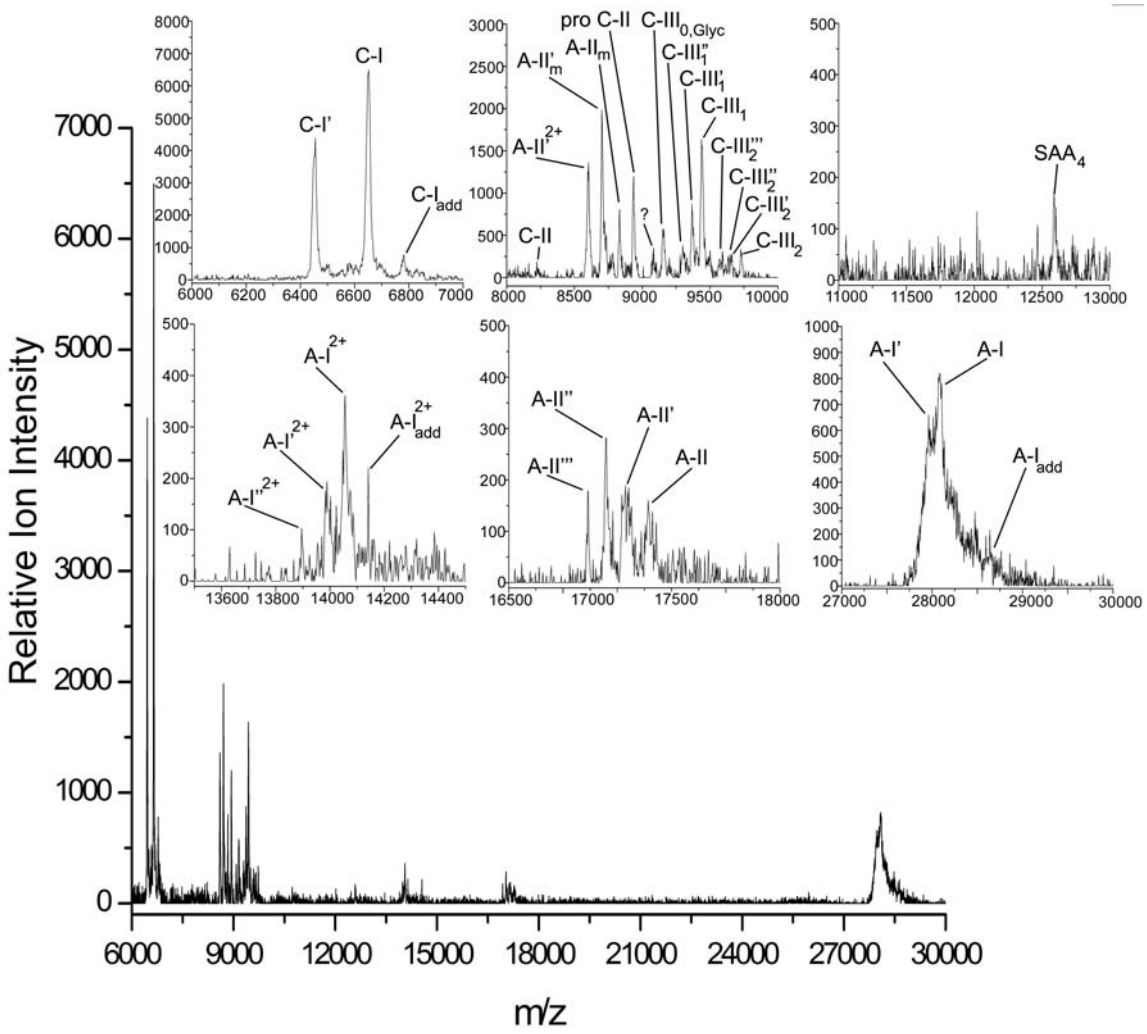

Figure 25. MALDI-MS Spectrum for Middle Fraction of CAD Sample

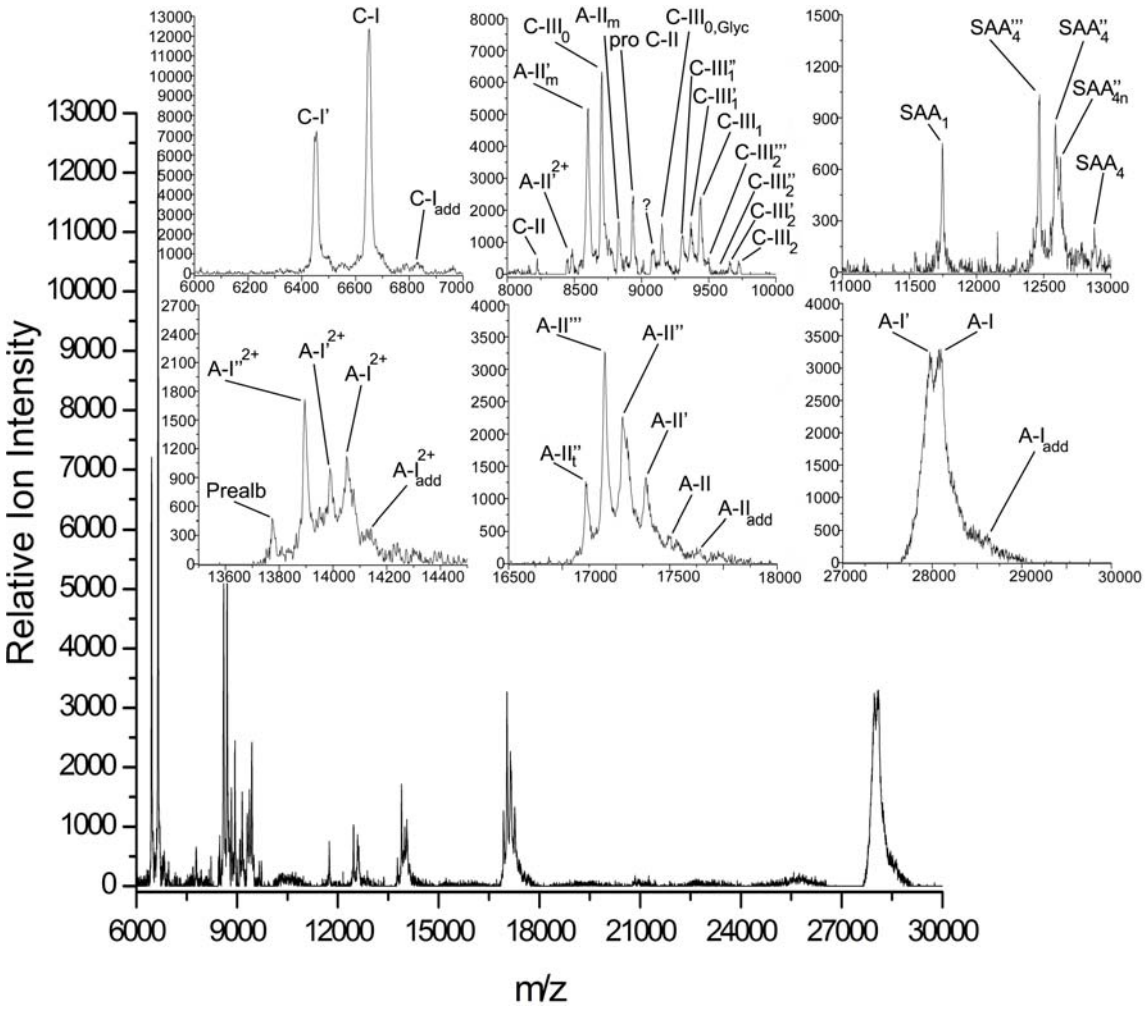

Figure 26. MALDI-MS Spectrum for Dense Fraction of CAD Sample

3.1.5 LC-MS Analysis of HDL Fractions

LC-MS was utilized as a means of looking at inherent differences in apolipoprotein structure and abundance for density-distinct fractions of HDL in both control and CAD samples. To achieve these goals, an external standard calibration curve was generated for the apolipoproteins apo A-I and apo C-I in order to determine whether the concentration of the suspected atherogenic apo C-I played a role in cardiovascular risk. The mass distributions of the major apolipoproteins of HDL were also studied from the electrospray ionization (ESI) mass spectra.

3.1.5.1 Identification and Quantification of HDL Apolipoproteins by LC Trace

Serial dilutions were performed on stock 1.000mg/mL standard solutions of apo A-1 and apo C-1 in order to generate a concentration range that would include the dynamic range of each apolipoprotein expected in a serum sample. The average concentration of apo C-I is a factor of twenty times less than that of apo A-I in normo-lipidemic serum, which was reflected in the establishment of these calibration curves. The instrumental parameters for the LC-MS experiment were as described in the materials and methods section. Integration of the LC trace was performed with Origin software in order to link the concentration of the apolipoprotein with the response of the instrument (total ion current). The LC traces of both apolipoprotein standards indicated that there was a considerably large polar component that eluted earlier than the apolipoproteins themselves (Figures 27-33). Electrospray data revealed that these large peaks were low-molecular weight impurities in the standards. It was seen that peaks centered about a retention time of 65min were indicative of apo A-I, and peaks that were centered about 57min were indicative of apo C-I. The lowest concentration of apo A-I that was visible in the LC-trace was 62.5μg/mL, while the lowest concentration of apo C-I was 25.0μg/mL. The expected dynamic range in a serum sample for apo A-I and apo C-I was 100-150mg/dL (1,000-1500μg/mL) and 3-6mg/dL (30-60μg/mL) respectively. Since HDL was split into two fractions, expected concentrations in a given sample should be roughly half of these values.

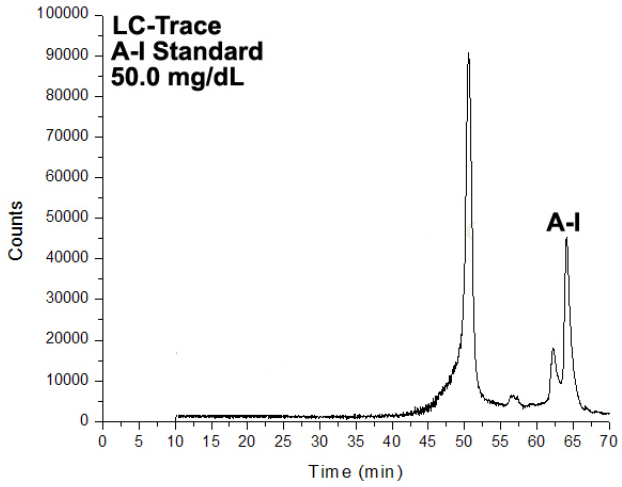

Figure 27. LC Trace of Apo A-I Standard at a Concentration of 50.0mg/dL

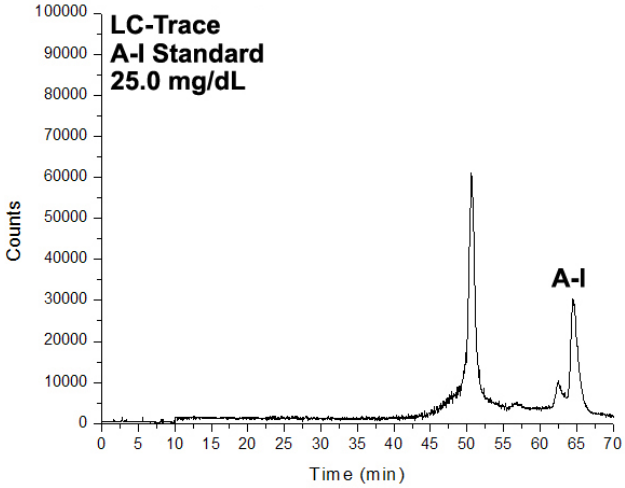

Figure 28. LC Trace of Apo A-I Standard at a Concentration of 25.0mg/dL

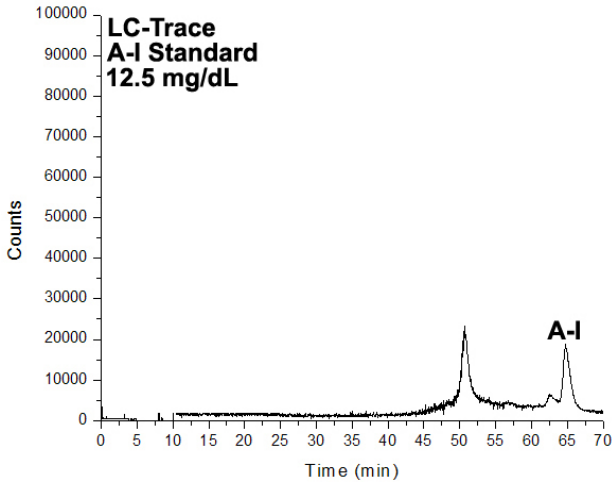

Figure 29. LC Trace of Apo A-I Standard at a Concentration of 12.5mg/dL

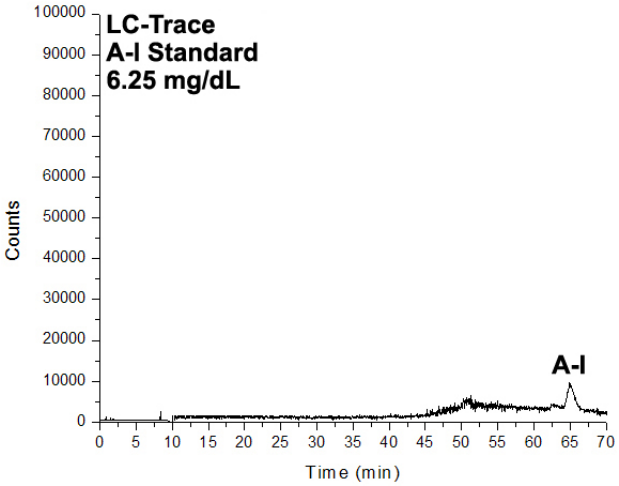

Figure 30. LC Trace of Apo A-I Standard at a Concentration of 6.25mg/dL

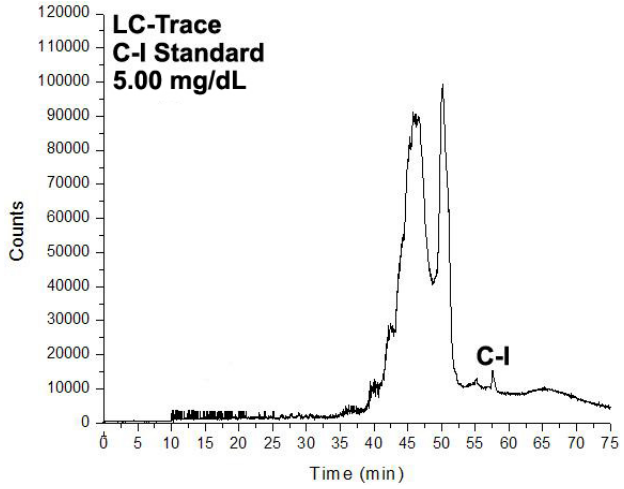

Figure 31. LC Trace of Apo C-I Standard at a Concentration of 5.00mg/dL

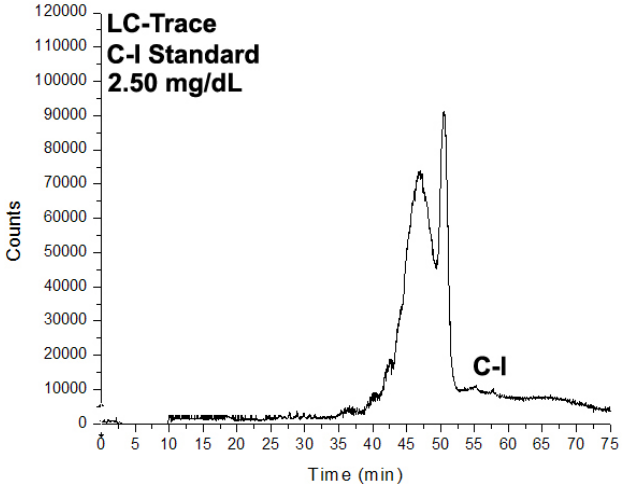

Figure 32. LC Trace of Apo C-I Standard at a Concentration of 2.50mg/dL

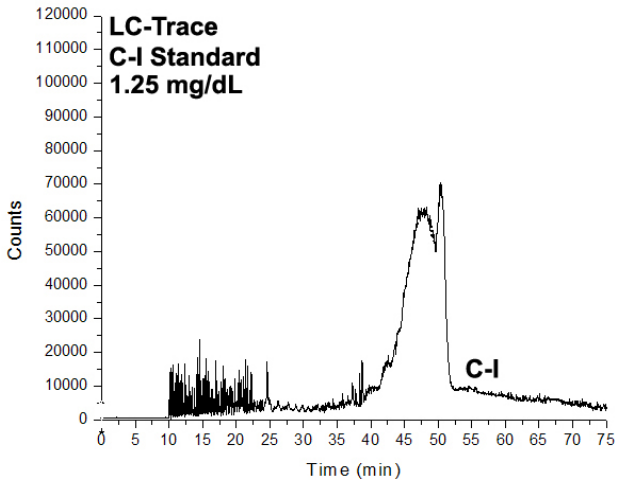

Figure 33. LC Trace of Apo C-I Standard at a Concentration of 1.25mg/dL

3.1.5.2 Analysis of ESI Spectra

The mass spectral signature of each apolipoprotein in ESI was also measured to look for patterns between control and CAD samples. The ESI spectra for the apo A-I standard revealed that multiple charge states between +21 and +39 were generated, with the most prominent charge state residing at +32 (Figure 34). These charge states were assigned based on the following formula:

$$z_1 = \frac{(J-1)\times(m_2 - m_p)}{(m_2 - m_1)} \qquad (23)$$

where z_1 is the calculated charge state of the unknown ion, J is the number of ions selected, m_2 is the mass of the peak with the highest m/z in the range selected, m_1 is the mass of the peak with the lowest m/z in the range selected, and m_p is the mass of a proton. (Eq. 23)[199] This formula was useful in determining the charge state of an unknown peak when the protein content of a sample was not known. However, when the protein content of a sample was already known, the charge state of a particular peak could more easily be determined. (Eq. 24)[199]

$$M = (z_1) \times (m_1 - m_p) \tag{24}$$

In this equation, M is the mass of the protein peak, z_1 is the charge state of a particular peak, m_1 is the m/z of a particular peak, and m_p is the mass of a proton. Once the charge states of all peaks were determined for a given protein, the average mass of the peak could be calculated. The mass of the molecular ion was determined by multiplying the m/z for the ion by its charge state. The mass of the molecular ion from each of the charge states was then added together, and an average mass was then calculated. (Eq. 25)

$$M_{avg} = \frac{\sum (z_i) \times (m_i - m_p)}{J} = \frac{\sum M}{J} \tag{25}$$

In this equation, the average mass of the molecular ion M_{avg} was calculated by dividing the mass of the protein peak (M) at each charge state and then dividing by the total number of charge states observed (J). For the dominant ion of apo A-I, the m/z of 19 different charge states were observed, and the average m/z calculated to 28081.72 Da with a RSD% of 0.01. This mass was higher than the literature value for apo A-I by 3.12 mass units.

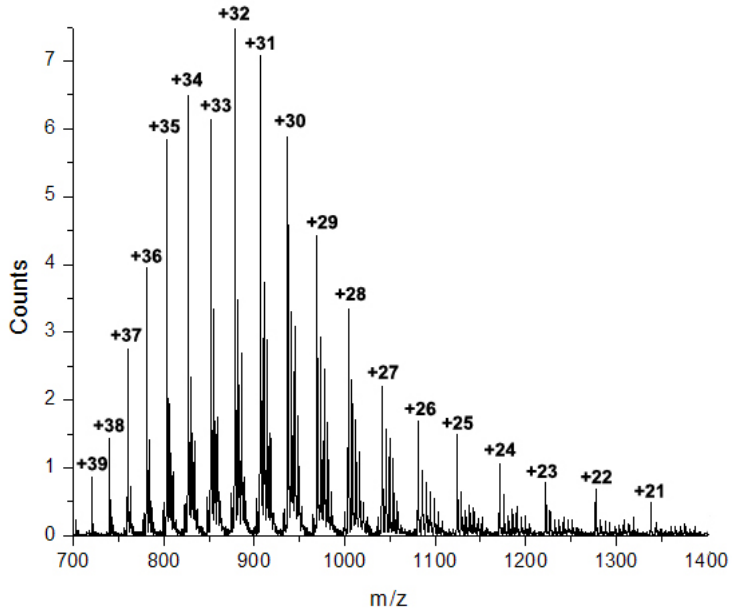

Figure 34. ESI Spectra for a Standard of Apo A-I at a Concentration of 50.0mg/dL

It was seen that there were several modifications of apo A-I in the standard sample due to the distribution of peaks at each charge state. The complexity of the spectra warranted further inspection, so three separate zones were focused upon in order to look at the finer structure of the distribution of peaks in the apo A-I standard. At a high charge state, the distribution of the apo A-I peak pattern appeared as four masses, with the dominant peak corresponding to the literature mass of apo A-I (Figure 35). The presence of a lower molecular weight ion suggested that a truncated form of apo A-I existed in the standard. There were also two peaks at a higher m/z than the most abundant mass, suggesting that either adduct formation occurred or that there were post-translational modifications of apo A-I that added mass to its structure.

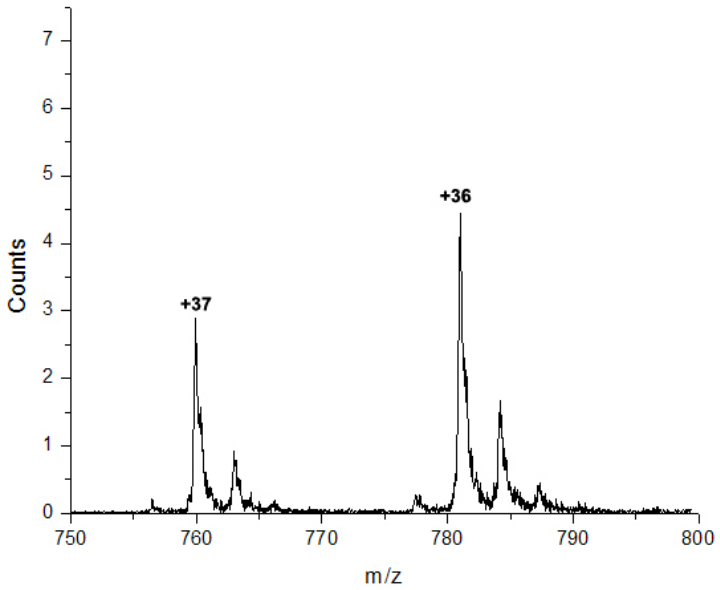

Figure 35. High ESI Charge States for a Standard of Apo A-I at a Concentration of 50.0mg/dL

For the zone centered about the most prominent ion of apo A-I, +32, five peaks were seen, with one below the dominant ion, and three above (Figure 36). The high charge state region also displayed a complicated spectrum, with as many as eight peaks, all of which were higher than the m/z of the dominant ion (Figure 37). The ion having a lower molecular weight than the dominant ion did not appear in the low charge state region of the spectrum.

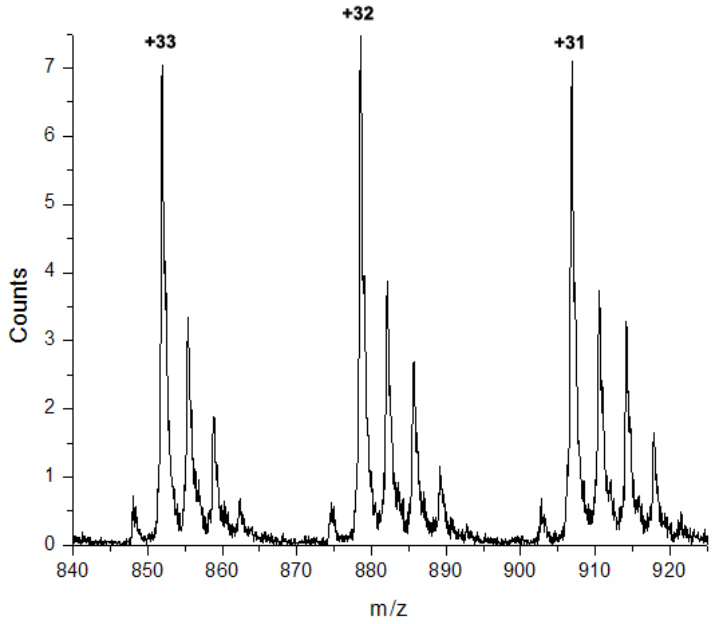

Figure 36. Most Prominent ESI Charge States for a Standard of Apo A-I at a Concentration of 50.0mg/dL

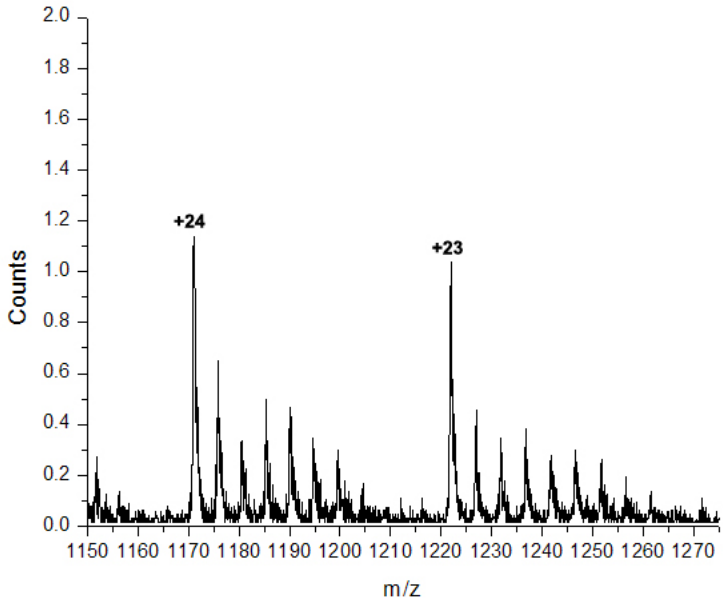

Figure 37. Low ESI Charge States for a Standard of Apo A-I at a Concentration of 50.0mg/dL

Over the entire range of the ESI spectra, there were 11 charge states observed in total observed for the dominant ion of apo A-I, and increasingly higher numbers of peaks of apo A-I as the number of charge states decreased (Table 11). The dominant ion is in bold font, ions that are smaller than the dominant ion have a negative Δ m/z, and ions that are larger have a positive Δ m/z value. For the ions with a higher m/z than the dominant peak, the mass difference for each subsequent peak increased by approximately 112-114 Da. Trifluoroacetic acid (TFA) has a molecular weight of 114.03 g/mol and was used in the solid phase extraction steps for the desalting and delipidating of the apolipoprotein samples, as well as in serial dilutions of the standard samples. From this observation, it was ascertained that adducts between apo A-I and TFA must have formed. It was also intriguing that more peaks were observed in the low charge state region of the spectrum. Ions of apo A-I in the low charge state region of the spectrum have a higher proton affinity than those with higher charge states, so adduct formation should more readily occur in the low charge state region. As the mass of the ions increased, subsequently more TFA adducts were observed to cause the increase in mass. Mass accuracy appeared to be very good up to a m/z ratio of 28678.02 Da, wherein the calculated number of TFA adducts began to deviate from whole number values. This was likely due to a lower precision at the higher mass range. The ion with a mass smaller than the dominant ion was likely a truncated form of apo A-I.

Table 11. Summary of Apo A-I ESI Calculations

Ion Number	Ion (m/z)	Δ m/z of Dominant Ion	(Δ m/z) / (MW of TFA)
1	**28,081.72**	**0.00**	**0.00**
2	27,960.23	-121.49	--
3	28,196.47	114.75	1.01
4	28,310.13	228.41	2.00
5	28,424.19	342.48	3.00
6	28,538.20	456.49	4.00
7	28,678.02	596.31	5.23
8	28,789.74	708.02	6.21
9	28,903.00	821.28	7.20
10	29,014.08	932.36	8.18
11	29,126.16	1044.44	9.16

The ESI spectra for apo A-II revealed that multiple charge states between +11 and +20 were generated, with the most prominent charge state residing at +14 (Figure 38). Looking at differences in the ESI spectra between apo A-II and apo A-I, the first major difference was that that were much fewer ions formed than in the apo A-II spectra. The number of charge states was roughly half of that seen with apo A-I, and the degree of charge in apo A-II ions ranged from +11 to +20 as opposed to the much higher values seen with apo A-I. This was a surprising result considering apo A-II exists as both a dimer and a monomer. It was originally expected that apo A-II would have a more complicated ESI spectra because it existed in both forms, but its spectra contained a total of only five peaks. Two peaks had an average m/z lower than the dominant ion, and two peaks had average m/z that were higher. The distribution of ions for apo A-II also appeared to favor higher charge states over lower ones. The average mass was determined for apo A-II in the same manner as for apo A-I and was found to be 17,253.58 Da, with a RSD% less than 0.01. This mass was lower than the literature value for apo A-II by 126.22 mass units.

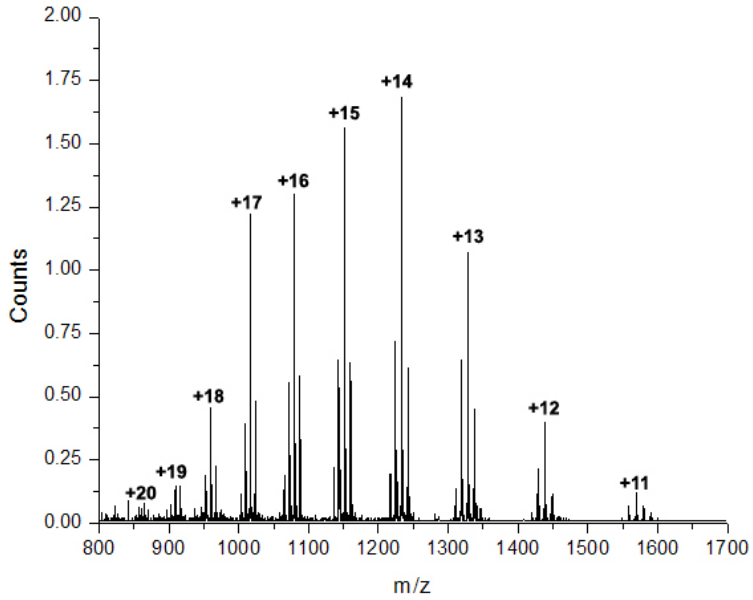

Figure 38. ESI Spectra for a Sample of Apo A-II

In the ESI spectra focused on the high charge state, prominent charge state, and low charge state regions, apo A-II appeared to be distributed more symmetrically around the most abundant mass than was seen with apo A-I (Figures 39-41).

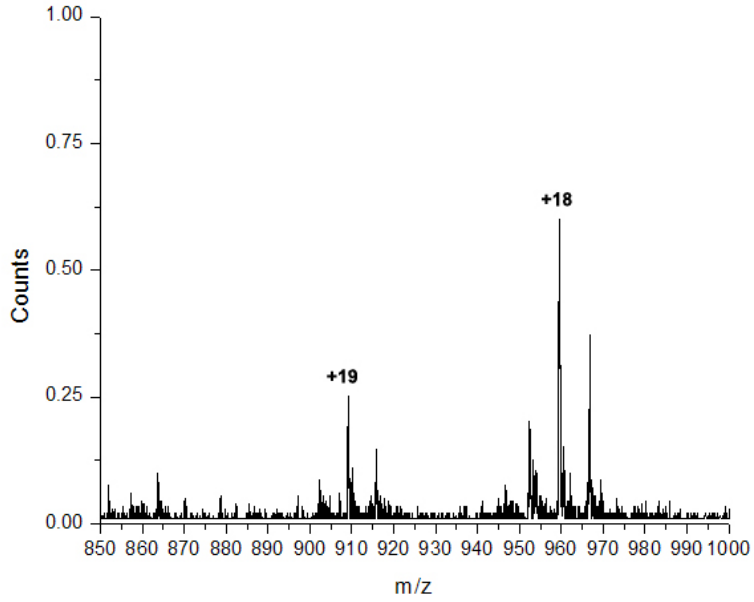

Figure 39. High ESI Charge States for a Sample of Apo A-II

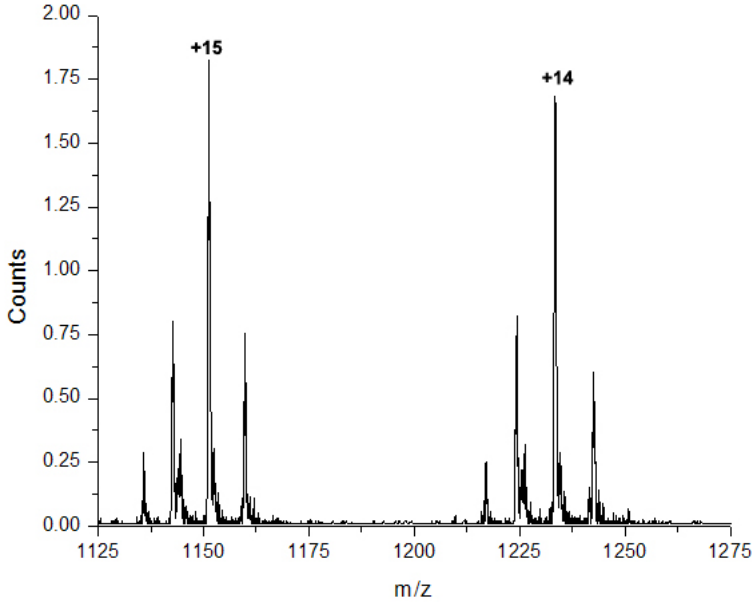

Figure 40. Most Prominent ESI Charge States for a Sample of Apo A-II

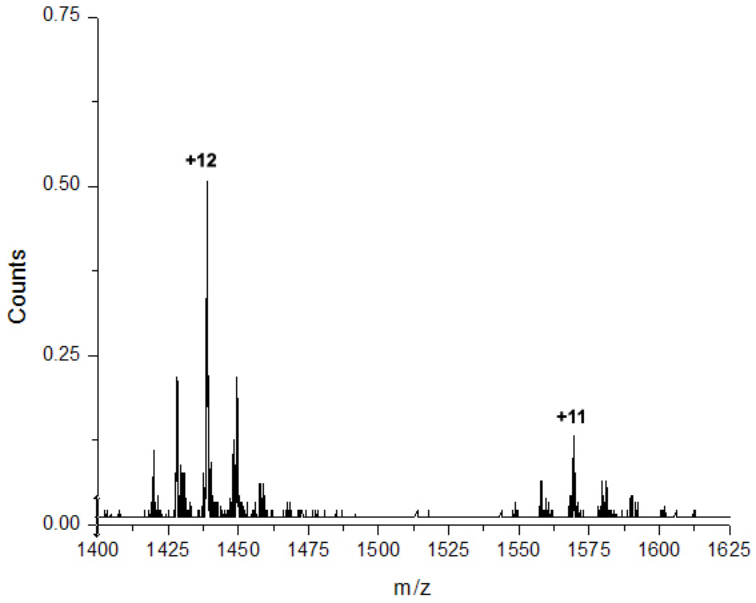

Figure 41. Low ESI Charge States for a Sample of Apo A-II

Over the entire range of the ESI spectra, there were 5 charge states observed in total for the dominant ion of apo A-II, and increasingly higher numbers of peaks of apo A-II as the number of charge states decreased (Table 12). The dominant ion is in bold font, ions that are smaller than the dominant ion have a negative Δ m/z, and larger ions have a positive Δ m/z value. Looking at differences in m/z ratios, an average difference was calculated of approximately 110-129 Da for each subsequent peak, which did not correlate well with the molecular weight of TFA as was previously seen with apo A-I. This observation revealed that the distribution of peaks in the ESI spectra of apo A-II were more likely to be post-translational modifications, and not adducts of TFA.

Table 12. Summary of Apo A-II ESI Calculations

Ion Number	Ion (m/z)	Δ m/z of Dominant Ion	(Δ m/z) / (MW of TFA)
1	**17,253.58**	**0.00**	**0.00**
2	17,125.37	-128.21	--
3	17,024.59	-228.99	--
4	17,382.41	128.83	1.13
5	17,491.07	237.49	2.08

Of the three apolipoproteins analyzed by LC-MS, the apo C-I standard had the least complex ESI spectra although it was observed to be asymmetric with regards to the dominant ion (Figure 42). The spectrum was not as convoluted as the other apolipoproteins so focusing on specific regions to reveal peak structure was not necessary in this case. Only a single peak existed that had a lower m/z than the dominant ion, and the remaining five peaks had a higher m/z ratio.

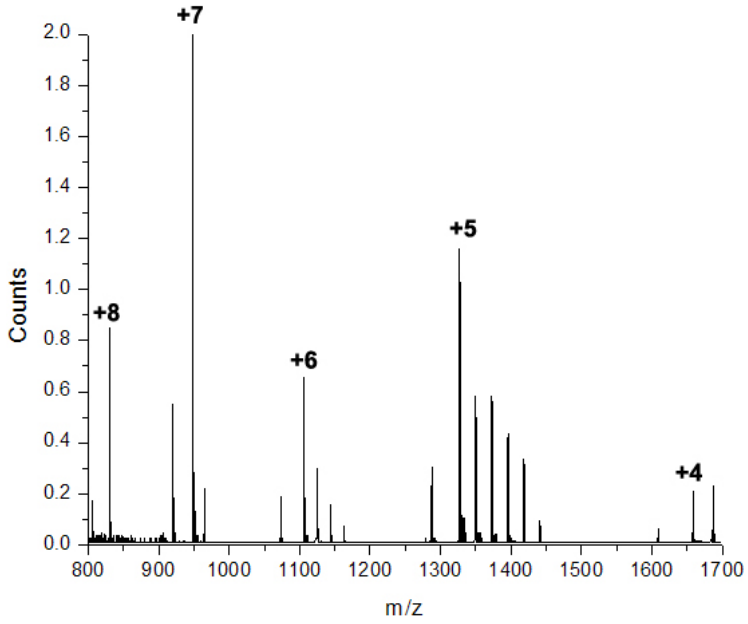

Figure 42. ESI Spectra for a Standard of Apo C-I at a Concentration of 5.00mg/dL

The charge states ranged from +4 to +8, and the charge state at +7 was observed to be the most prevalent ion. The highest number of peaks was seen in the region with a

charge state of +5. The average mass was determined for apo C-I in the same manner as for apo A-I and apo A-II and was found to be 6630.39 Da, with a RSD% of 0.01. This mass was lower than the literature value for apo C-I mass by 0.21 mass units. The ion with a lower m/z than the dominant ion differed by 197 Da and ions with a higher m/z increased in mass by increments of 110-120 Da (Table 13).

Table 13. Summary of Apo C-I ESI Calculations

Ion Number	Ion (m/z)	Δ m/z of Dominant Ion	(Δ m/z) / (MW of TFA)
1	**6,630.39**	**0.00**	**0.00**
2	6,432.92	-197.47	--
3	6,740.15	109.76	0.96
4	6,861.31	230.93	2.02
5	6,973.80	343.42	3.01
6	7,087.42	457.03	4.01
7	7,201.43	571.05	5.01

Analysis of the ESI spectra in detail enabled correct classification of the different apolipoprotein peaks in the patient samples, and offered a means to compare peak distribution and intensity between different samples. For the twelve patient samples, there were not significant density-dependent or patient-dependent differences in the ESI spectra of apo A-I in numbers of post-translational modifications that could be seen (Figure 43). However, there were observable differences in the peak intensities between samples.

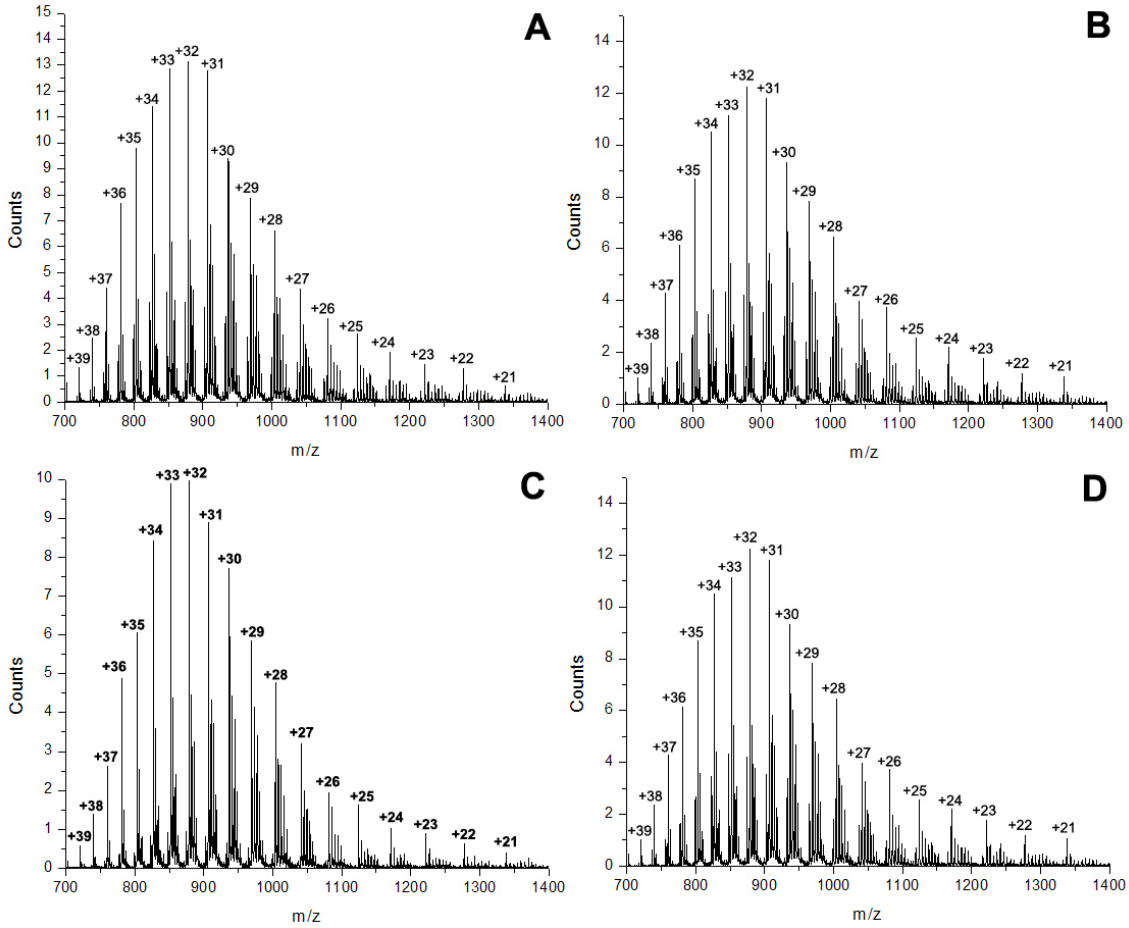

Figure 43. ESI Spectra of Apo A-I for (A) CAD HDL-2, (B) CAD HDL-3, (C) Control HDL-2, and (D) Control HDL-3

With a more detailed look at the three selected zones, differences between the control group and the CAD group could more easily be determined (Figures 44-46). In every case, the HDL-2 and HDL-3 fractions for both cohorts appeared to contain the same number of peaks at the same masses as one another, indicating that adduct formation of TFA with the apolipoproteins behaved similarly for both cohorts. A subtle difference could be seen when comparing the intensity of the ion to the left of the predominant peak for both the control and CAD groups. It was observed that this ion was in lower abundance in the CAD samples than in the controls, and this observation was consistent across the entire ESI spectrum. The most dramatic example of this was

seen in the low charge state region of the ESI spectrum, where this ion was not detected at all in the CAD group, but gave a good signal in the control group. This ion was calculated to be 121.49 Da smaller than the dominant ion of Apo A-I, and indicated that a truncated form of apo A-I was more prevalent in the control group. Previous research in our laboratory identified a truncated form of apo A-I, designated as apo A-I' and having a mass of 27974.84 Da, which was 14.61 Da smaller than the mass reported here.

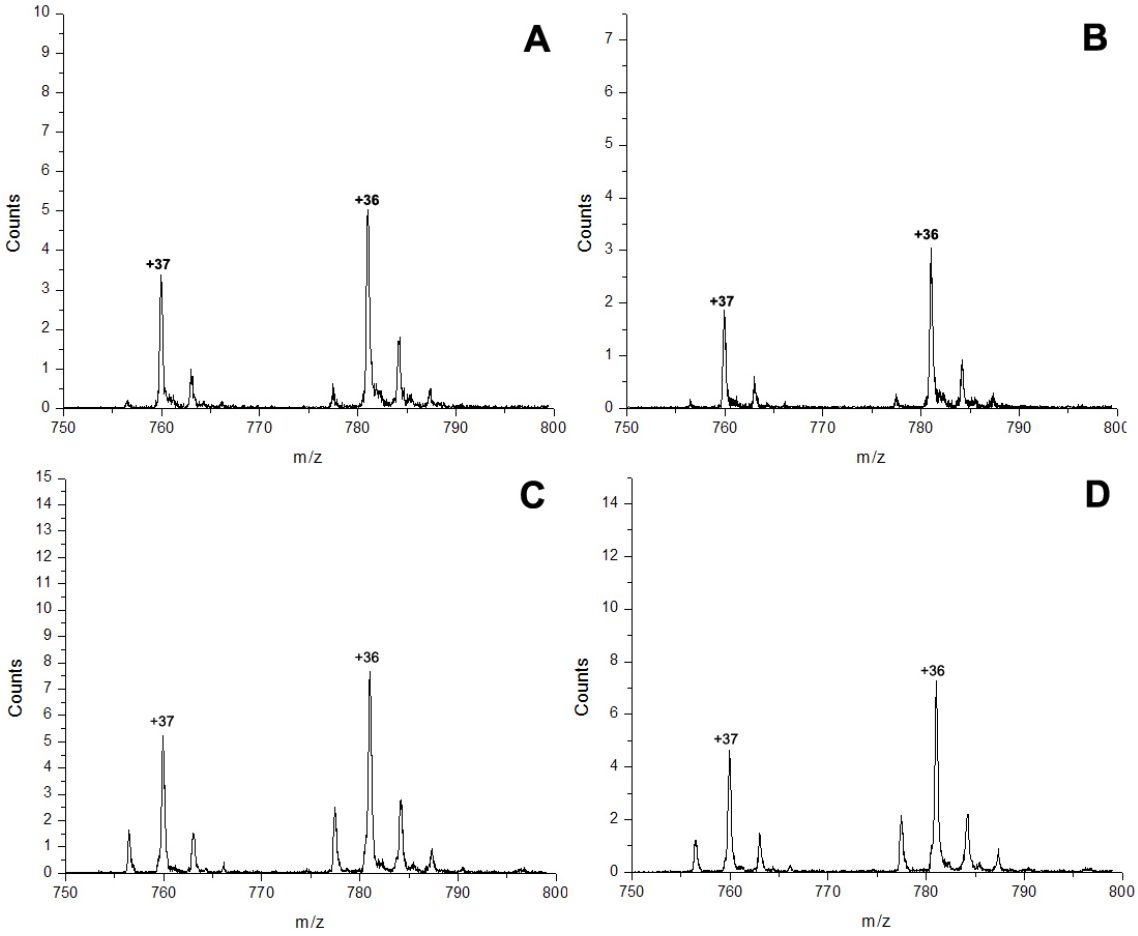

Figure 44. ESI Spectra of High Charge States of Apo A-I for (A) CAD HDL-2, (B) CAD HDL-3, (C) Control HDL-2, and (D) Control HDL-3

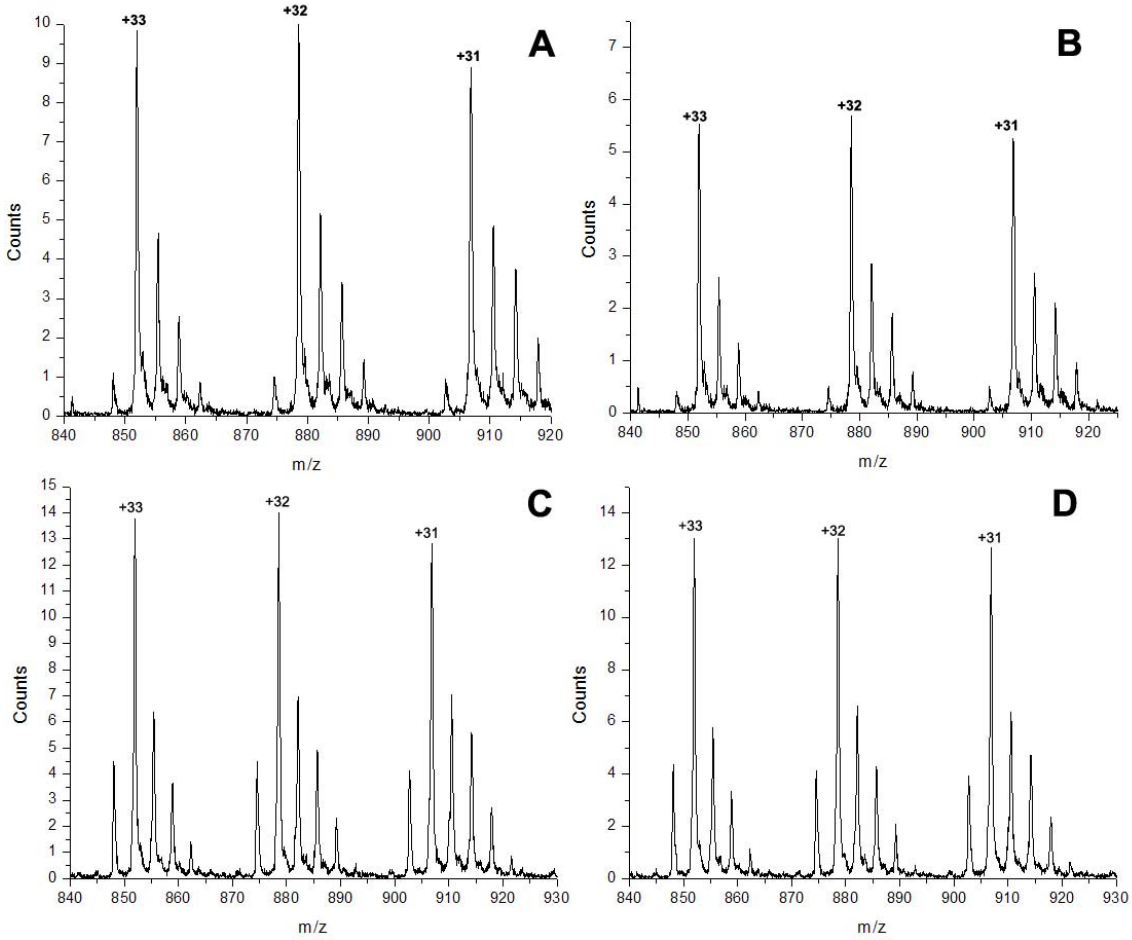

Figure 45. ESI Spectra of the Most Prominent Charge States of Apo A-I for (A) CAD HDL-2, (B) CAD HDL-3, (C) Control HDL-2, and (D) Control HDL-3

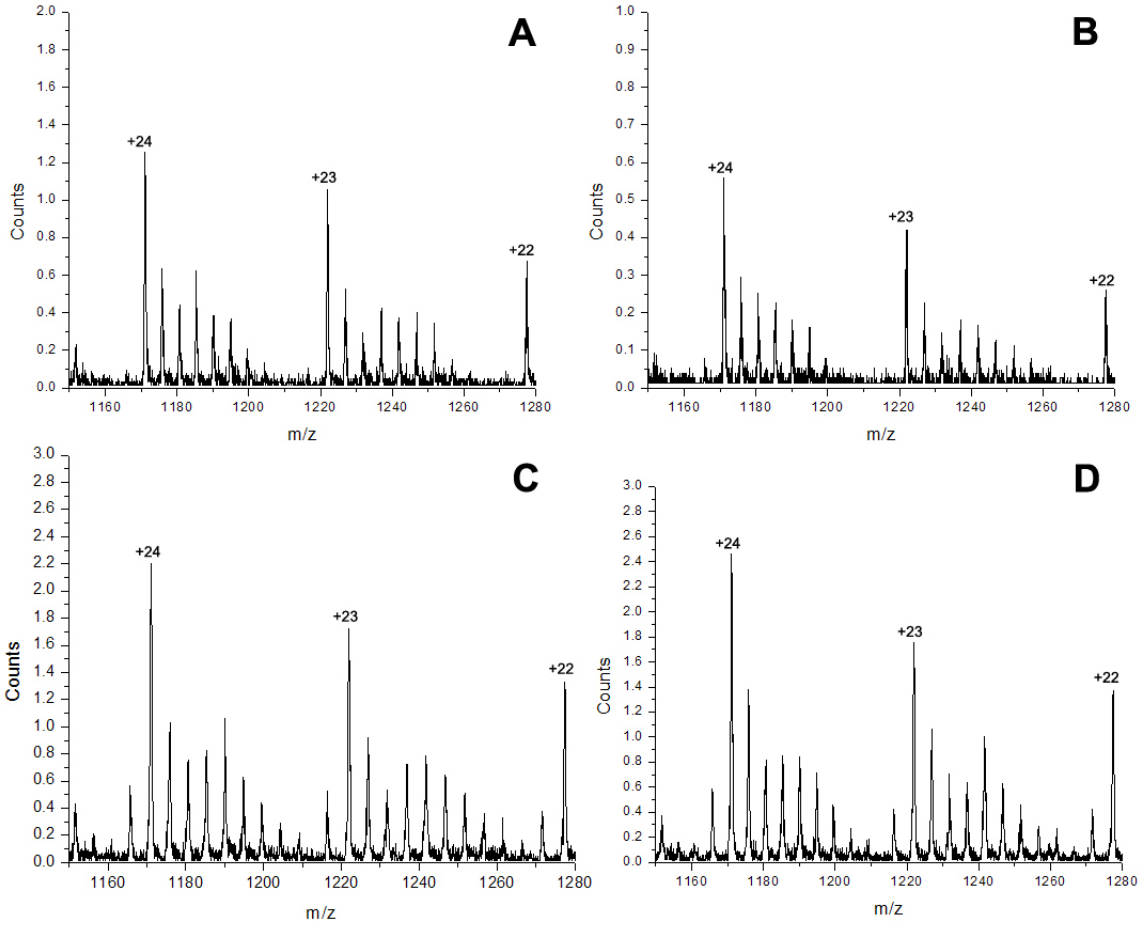

Figure 46. ESI Spectra of Low Charge States of Apo A-I for (A) CAD HDL-2, (B) CAD HDL-3, (C) Control HDL-2, and (D) Control HDL-3

A considerable difference was seen between density-distinct subclasses for control and CAD subjects in the analysis of apo A-2 by ESI. A significant increase in the intensity of the peaks was observed in the HDL-3 fractions of both the control and the CAD sample. This result correlated well with literature that explains that particles containing both apo A-I and apo A-II are predominately present in HDL-3.[200] A surprising feature of the apo A-II analysis by ESI was that the HDL-3 spectrum for the CAD patient was shifted towards higher charge states while the HDL-2 fraction from the CAD patient and both of the control fractions displayed similar charge state distributions. Beyond the shifting of the charge states, the distribution of peaks for each

was largely the same and can be viewed in the appended data section. This result demonstrated that patient-to-patient variability can have a large impact on the analysis.

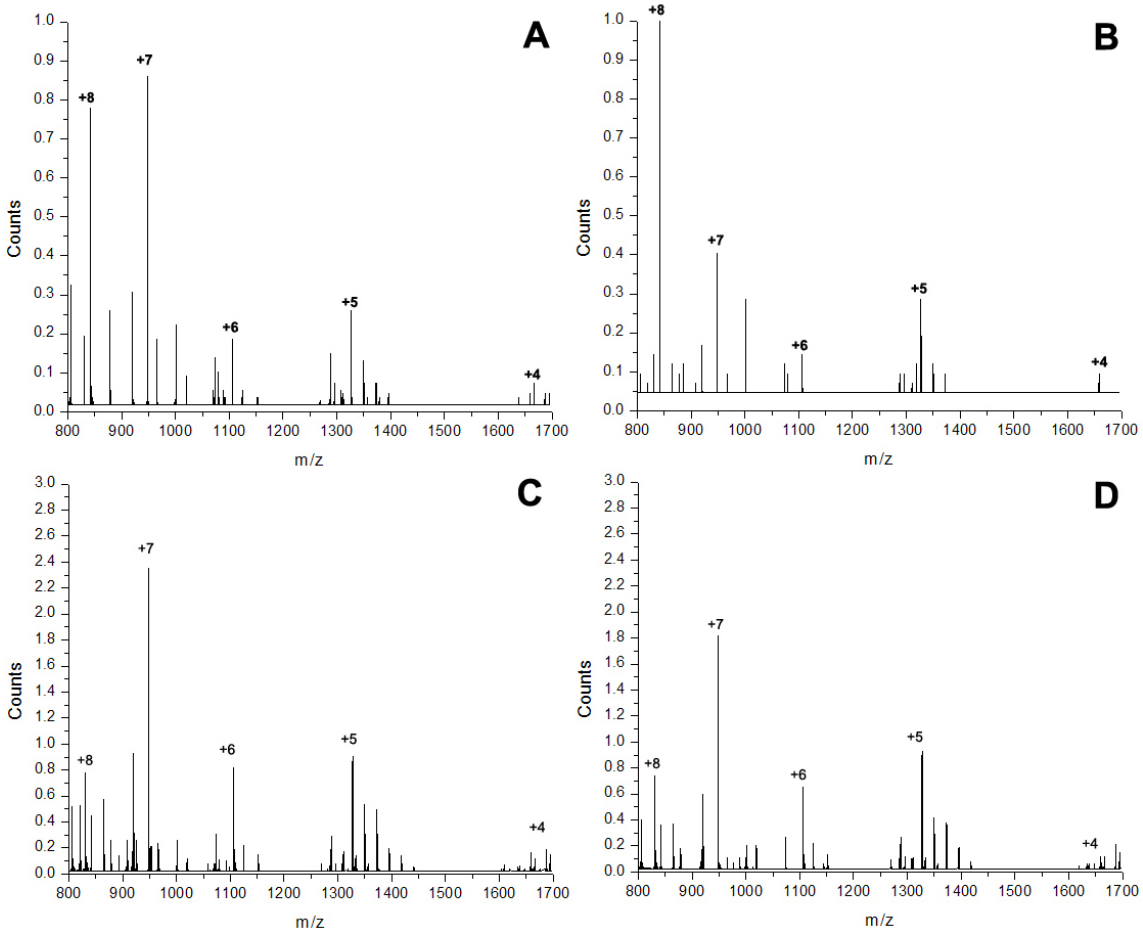

Figure 47. ESI Spectra of Apo C-I for (A) CAD HDL-2, (B) CAD HDL-3, (C) Control HDL-2, and (D) Control HDL-3

The ESI spectra of apo C-I also displayed a large variation in the distribution of charge states that appeared to be dependent on whether the sample was a control or a CAD subject (Figure 47). The most prominent ion in the apo C-I standard and in both HDL-2 and HDL-3 of the control sample appeared at a charge state of +7. In the CAD subject, the +8 charge state was nearly equally predominant with the +7 ion in the HDL-2 fraction and very predominant in the HDL-3 fraction. This information indicated that

apo C-I from CAD samples had a higher proton affinity than those found in control samples. The intensity of the truncated form of apo C-I' peak also appeared to scale with the intensity of the apo C-I peak and was consistently observed at approximately one-third of its height.

3.1.5.3 Identification and Quantification of HDL Apolipoproteins by Ion Extraction

A novel function of the Q-Star LC-MS software was the ability to isolate known ions of a particular protein from the total ion current for simplified quantification. This entailed choosing an m/z value that correlated with the average molecular mass for each apolipoprotein and dividing by the charge state of the most abundant ion. In the LC trace for the apolipoprotein standards, there appeared to be an abundance of impurities that masked the peaks for the apolipoproteins themselves, but the use of ion-extraction generated a much cleaner spectra. This entailed filtering out ions that did not have the correct m/z, so that only the ions of interest were displayed (Table 14).

Table 14. Ion Extractions for Apolipoproteins A-I, A-II, and C-I

Apolipoprotein	Avg. MW	Most Abundant Ion	Ion Extraction
Apo A-I	28,078.60	+32	877.46
Apo A-II	17,379.94	+14	1,241.42
Apo C-I	6,630.60	+7	947.23

As with the LC traces, Origin software was again utilized to integrate the spectra to link the concentration of the standards with the instrument response (Figures 48-53). Of note, is that in the apo A-I standard, a doublet appeared to exist in the ion extraction trace, indicating that there likely were post-translational modifications of apo A-I contained in the commercial standard. In the apo C-I standard, only a singlet peak was seen, indicating that either the standard contained only a single mass for apo C-I, or that the concentration was sufficiently low to prevent seeing a second mass peak.
The lowest concentration of apo A-I that was visible in the ion extraction trace was 62.5μg/mL, while the lowest concentration of apo C-I was 25.0μg/mL. The integrated areas of apo A-I appeared to track well with concentration, whereas changing the

concentration of apo C-I by a factor of two drastically reduced the instrument response by nearly a factor of five. The quantification based on ion extraction, while an improvement over quantification based on the LC trace, still has limitations.

By dividing the molecular weight of each apolipoprotein by the charge state of its most abundant mass, the instrumental response will be biased towards only the most abundant ion. For example, the m/z values for the +32 charge state of apo A-I ranged from 873.76 to 910.19 Da, and also ranged from 918.49 to 1028.78 Da for the +7 charge state of apo C-I. Selecting the most abundant ions for each respective apolipoprotein served to filter out much of the background noise seen in the LC trace, but also altered the intensity of peaks that were filtered out. In cases where multiple adducts of TFA were observed, the high MW ions were filtered out of the resulting spectrum through selection of the most abundant ions of the two apolipoproteins. By combining the adduct formation between TFA and the apolipoproteins, and choosing a narrow mass window around the most abundant ions of each, the concentration of the two apolipoproteins were expected to be underestimated.

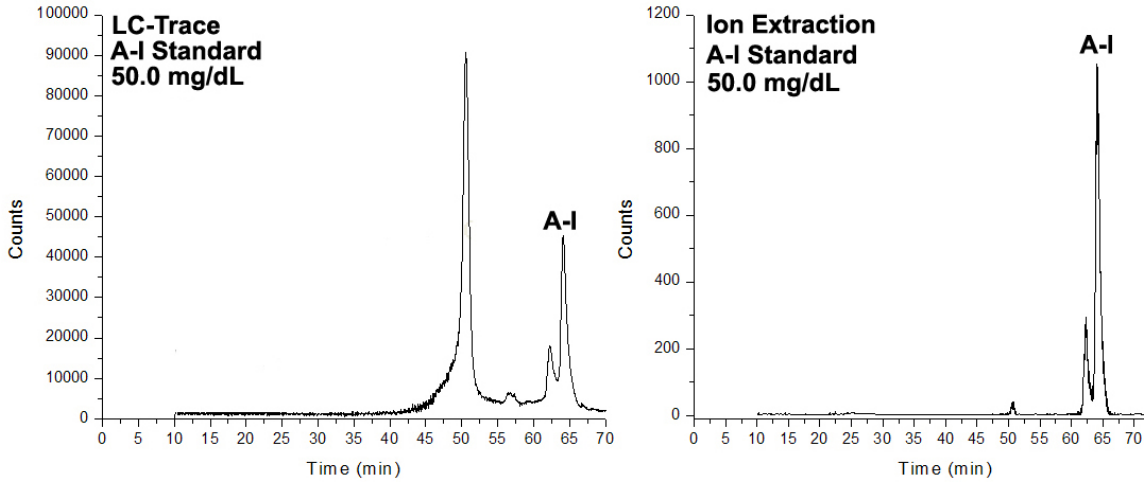

Figure 48. Ion Extraction of Apo A-I Standard at a Concentration of 50.0mg/dL

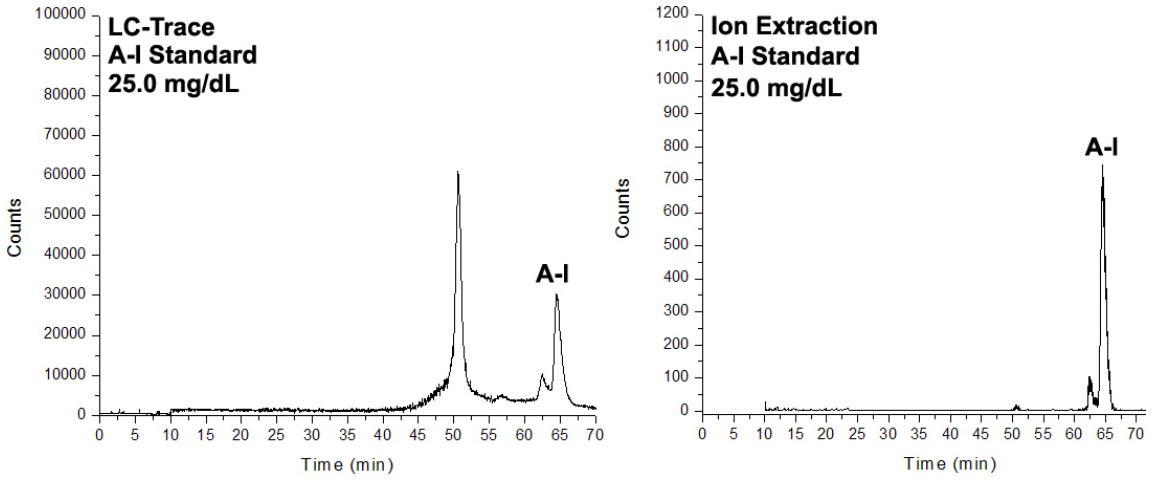

Figure 49. Ion Extraction of Apo A-I Standard at a Concentration of 25.0mg/dL

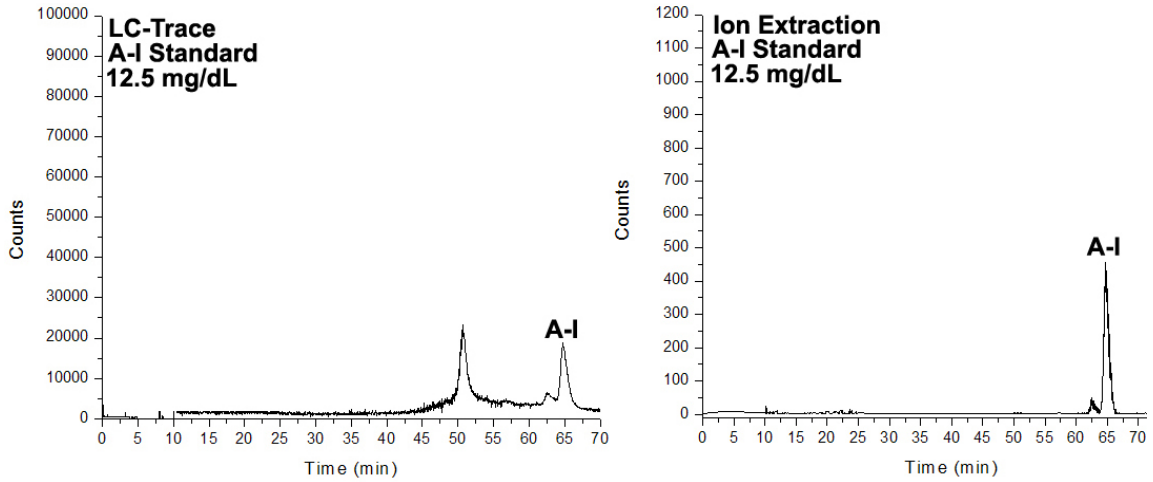

Figure 50. Ion Extraction of Apo A-I Standard at a Concentration of 12.5mg/dL

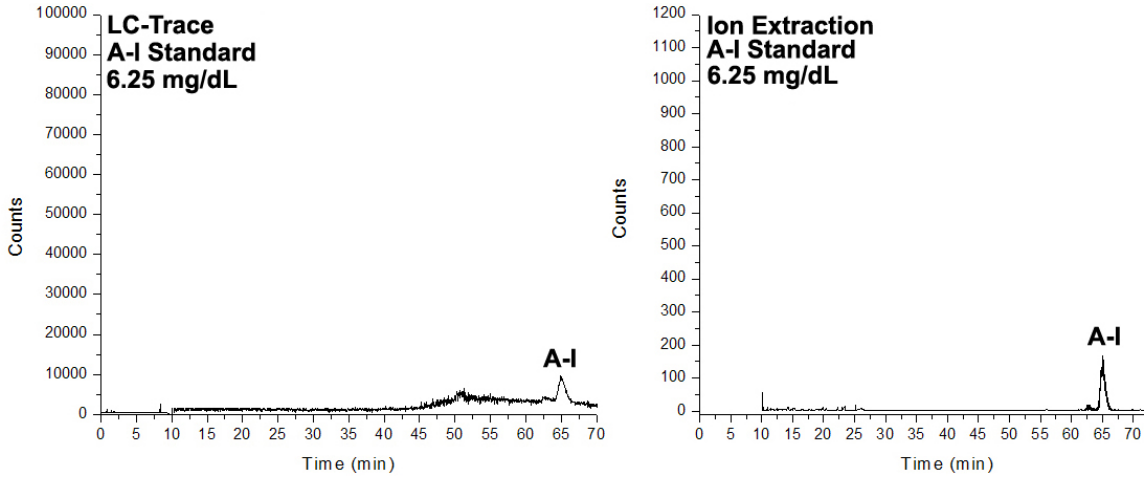

Figure 51. Ion Extraction of Apo A-I Standard at a Concentration of 6.25mg/dL

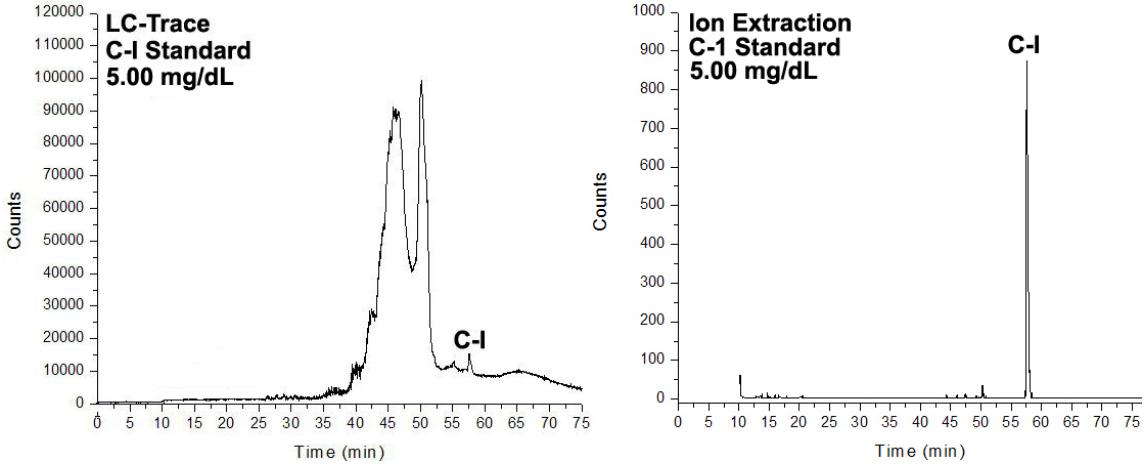

Figure 52. Ion Extraction of Apo C-I Standard at a Concentration of 5.00mg/dL

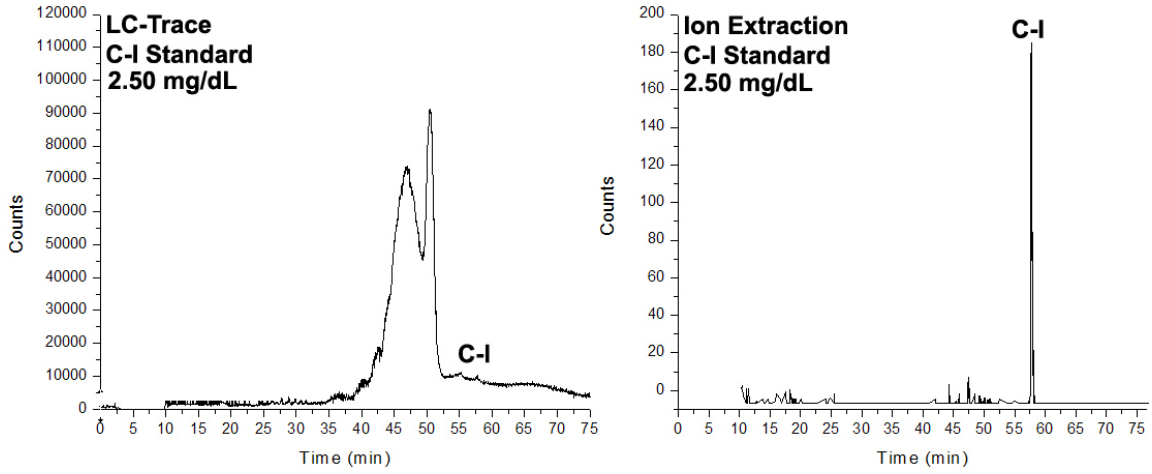

Figure 53. Ion Extraction of Apo C-I Standard at a Concentration of 2.50mg/dL

Calibration curves were generated for both the LC traces and ion extraction traces for the apo A-I and apo C-I standards in order to determine the level of quantification with both methods. It was seen that there was a very high background in the LC-traces for both apolipoproteins, as determined by the large y-intercept of the calibration curve (Figures 54,55). The relationship between the instrument response and concentration appeared to track fairly well despite the high background. As for the ion extraction calibration curves, the background was greatly reduced, but the instrument response was not as linear as in the LC mode (Figures 56,57). The effect of extracting only the ions of interest diminished the background current of any co-eluting ions, but selection of ions likely played a large role in quantifying the amount of apo A-I or apo C-I that was detected. This was seen very well in the calibration for apo C-I because the instrument response dropped nearly a factor of five for a two-fold decrease in concentration. Dividing the average mass of apo C-I (6630.60 Da) by its most abundant ion (+7), resulted in an ion extraction value of 947.23 Da. A narrow mass window around this predominant ion would filter out the truncated form of apo C-I possessing an average mass of 6430.60 Da, and an extracted value of 918.66 Da. Because the truncated apo C-I ions would not be present in the ion extraction trace, the resulting value for the integrated intensity would be lower than expected.

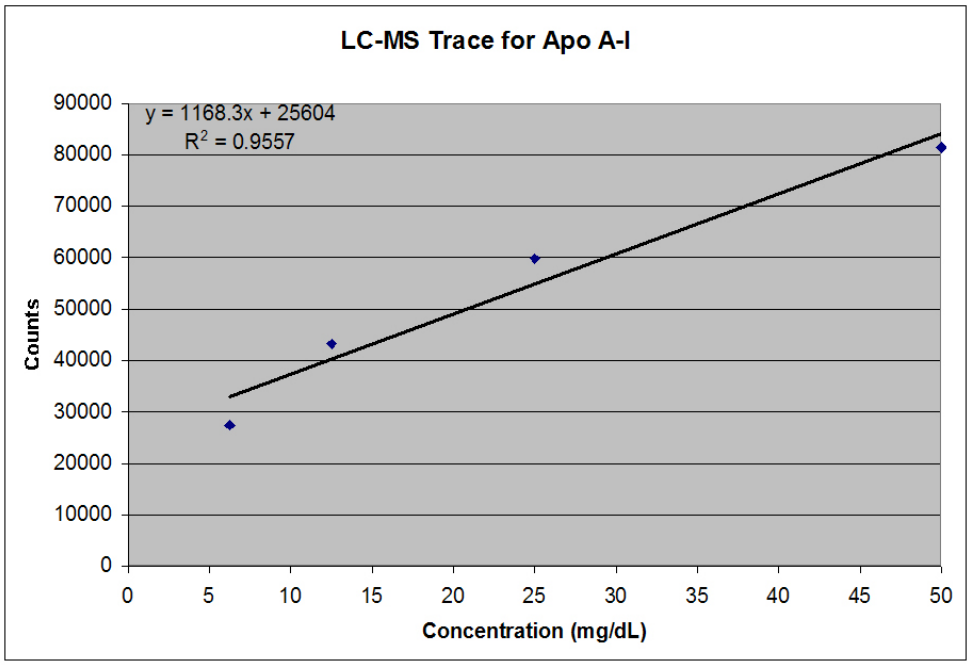

Figure 54. Calibration of Apo A-I by LC Trace

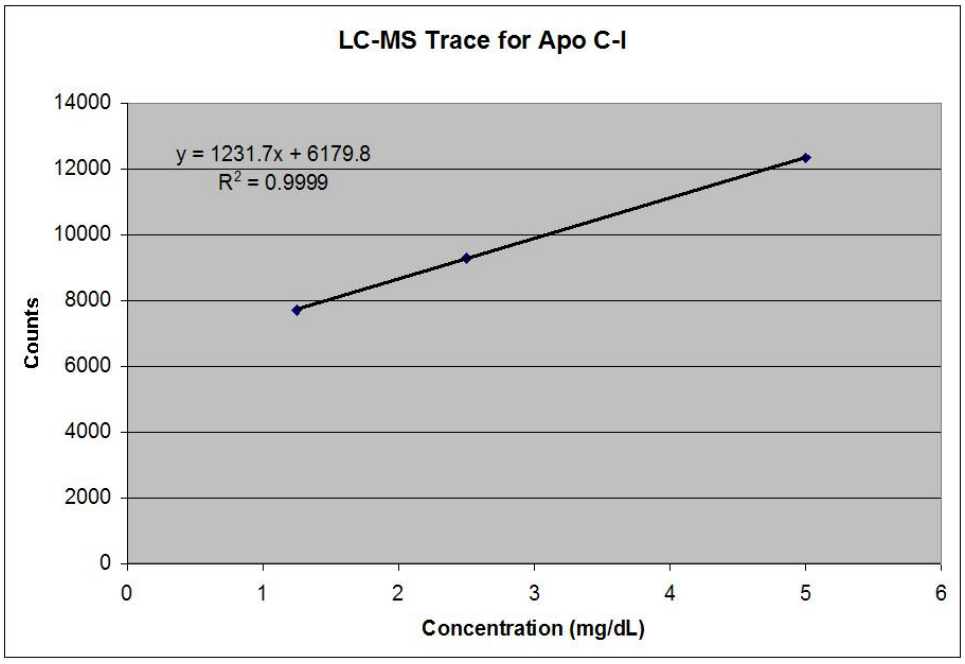

Figure 55. Calibration of Apo C-I by LC Trace

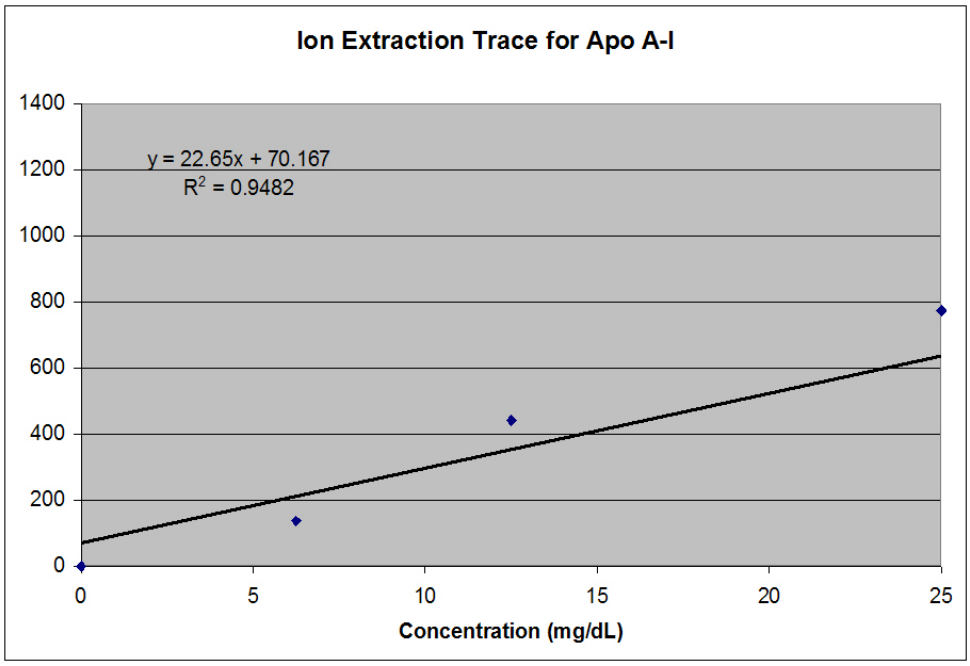

Figure 56. Calibration of Apo A-I by Ion Extraction

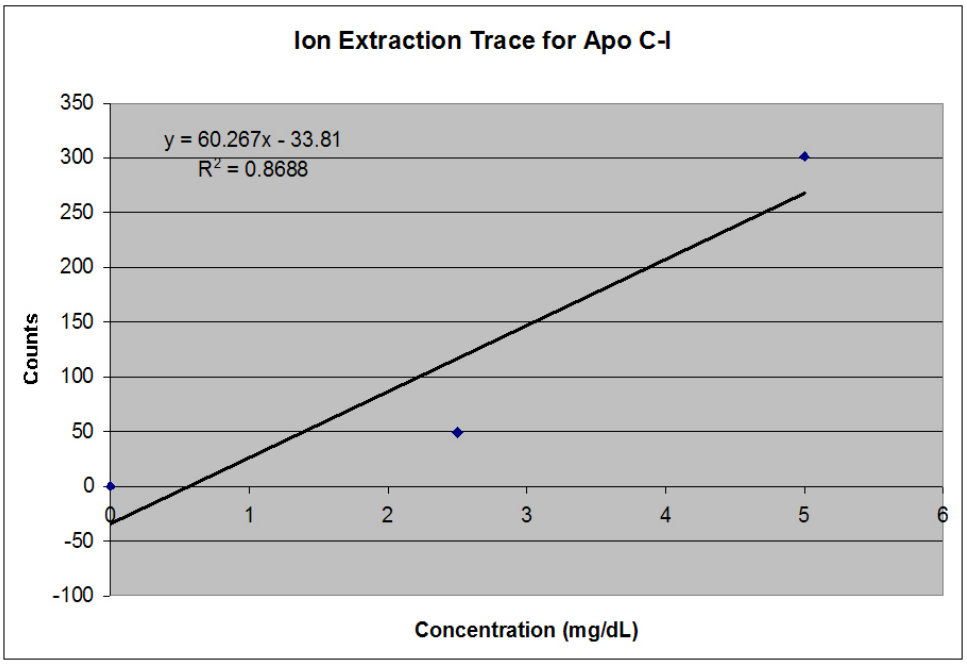

Figure 57. Calibration of Apo C-I by Ion Extraction

3.1.5.4 Comparison of Patient Samples

LC-MS was chosen as one of the methods for secondary analysis following preparative UC in order to determine what, if any, differences existed between two HDL subclasses in known CAD samples and control samples. Qualitatively, it was of interest to determine if different mass distributions of apolipoproteins were visible based on their density or which of the two cohorts the sample belonged to. Quantitatively, the focus was to determine whether differences could be seen in the relative abundance of apo A-I and the hypothesized atherogenic apo C-I.

Three patients from each cohort were selected, and preparative UC was used in order to selectively remove the buoyant HDL-2 and dense HDL-3 subclasses from the rest of the serum profile. SPE was performed on these fractions, which were then reconstituted in 100μL of 0.1% TFA/H_2O for the LC-MS experiment. In total, twelve samples were then analyzed by LC-MS (Figures 42-47). It was observed that the order the apolipoproteins eluted from the reverse phase LC column followed what was previously seen with the reverse phase SPE column, with the most hydrophobic apolipoproteins requiring the longest amount of time to elute. Any HSA that was not successfully washed off the column during the SPE procedure eluted early in the LC trace. Apo C-I eluted as a doublet with the first peak appearing very broad, while the second very sharp in comparison. Apo A-I eluted as a tall peak with a shoulder on the left side that could not be identified. The more hydrophobic apo A-II eluted after the other apolipoproteins at an intermediate intensity between apo C-I and apo A-I. Any small molecular weight lipids that were successfully eluted during SPE, eluted after the apo A-II peak. These peaks were designated as lipids because they were the most hydrophobic portion of the samples and also because they had a much lower observed molecular weight than the apolipoproteins.

There were a few striking differences between samples of HDL-2 and HDL-3 in the LC traces. When HSA was visible, it appeared to be more pronounced in the HDL-3 fraction, as was the case for every sample except for sample 10. The presence of lipids was also more prevalent in samples of HDL-2. The peak shapes for the apolipoproteins

were largely the same throughout the entire batch of samples, but it was clear that the intensities fluctuated greatly between samples. Quantification was performed by integrating the area under each apolipoprotein in Origin software and comparing the integrated intensity to the calibration curves previously established.

From the LC traces, ion extraction traces were generated by isolating the most prominent charge states for the apolipoproteins, then using Origin software in order to plot them on the same axis (Figures 58, 59). This presentation gave a better picture of the distribution of the apolipoproteins by minimizing the background noise of the LC trace. Though it was not necessary in this case, this feature could have been used to help identify the most probable migration time for molecules in the sample if the LC trace includes peaks that co-elute but formed different ions during electrospray. In all cases, the apolipoproteins in the ion extraction traces were seen as very sharp single peaks. Note also that the peaks for HSA and any lipids are completely missing from the original LC trace. This occurred because the ions formed by ESI of both the HSA and the lipids were filtered out by the choice of ions to be used in the ion extraction. Quantification was performed by integrating the area under each apolipoprotein in Origin software and comparing the integrated intensity to the calibration curves previously established.

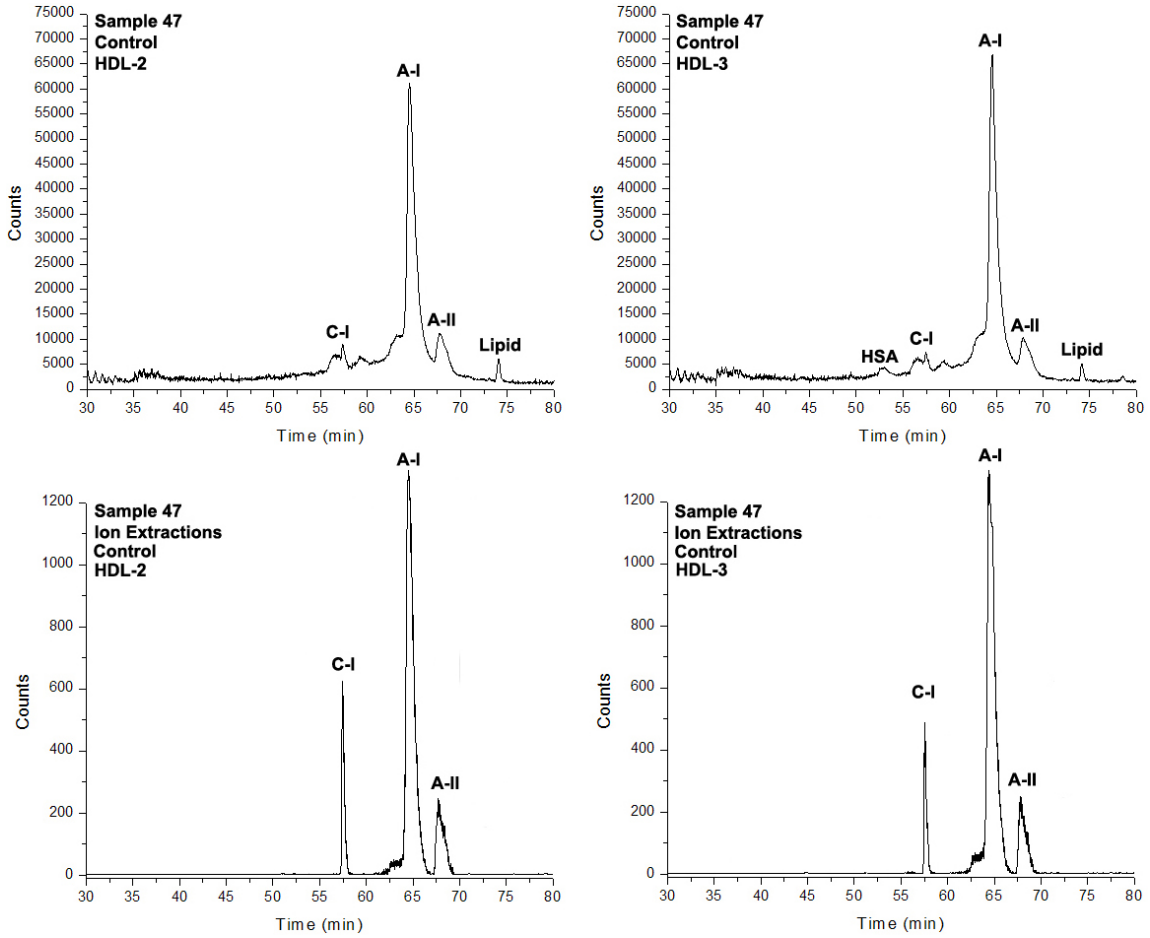

Figure 58. LC Total Ion Current and Ion Extractions for Sample #47

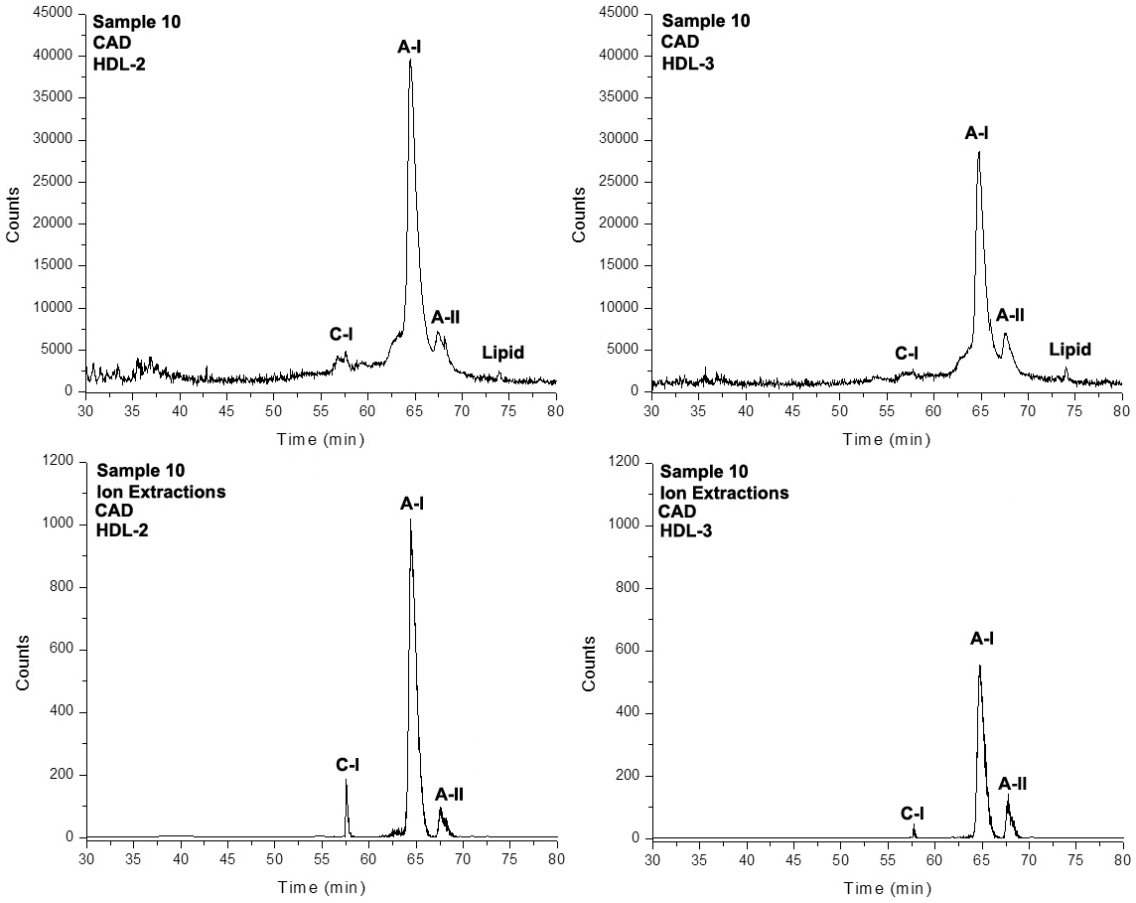

Figure 59. LC Total Ion Current and Ion Extractions for Sample #10

By comparing the twelve samples to the calibration curves for both the LC trace and the ion extraction trace, the relative amounts of apo A-I and apo C-I were calculated (Figures 60, 61). From the concentration of each apolipoprotein in mg/dL, the MW of each and the volume of serum samples could be used to determine the number of moles of each apolipoprotein. This experiment was designed to determine if the amount of apo C-I can be linked to whether a sample is a control or CAD, so the number of moles of apo C-I were divided by the number of moles of apo A-I to give a means of comparing the samples against one another.

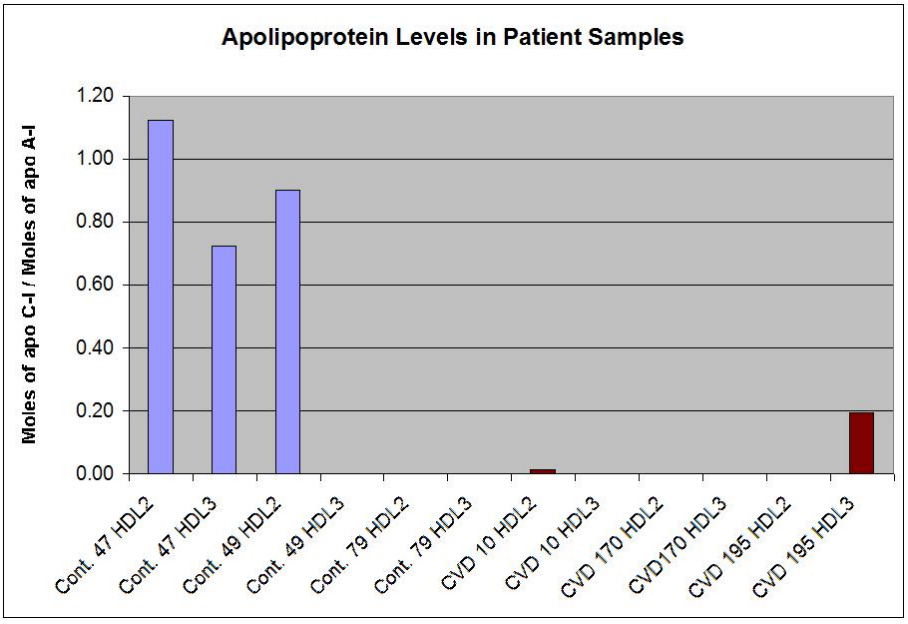

Figure 60. Quantification of Apolipoproteins by LC Trace

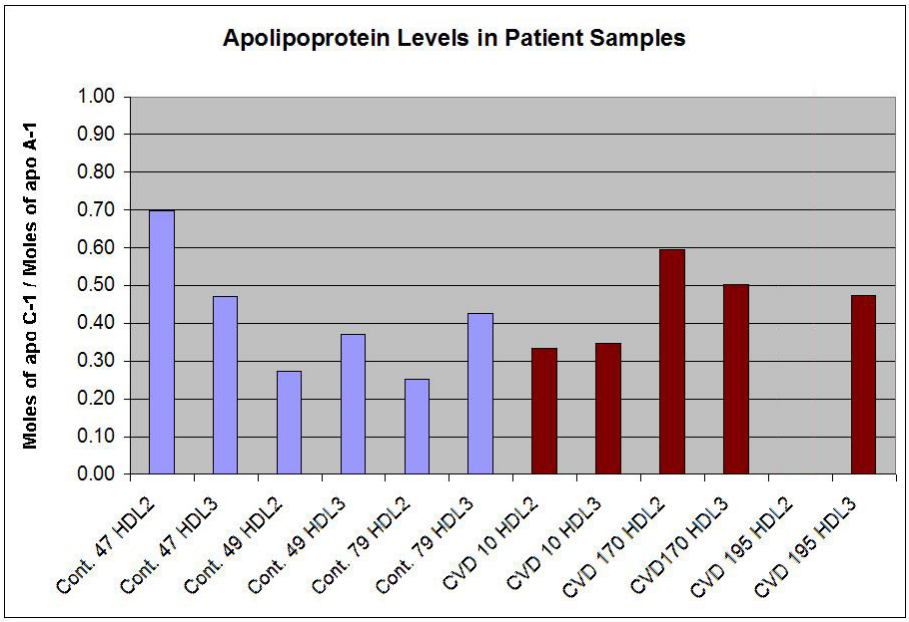

Figure 61. Quantification of Apolipoproteins by Ion Extraction

By definition, an HDL particle must contain at least one apo A-I, but does not necessarily have to contain apo C-I, so this ratio yielded information regarding the

stoichiometry between the two apolipoproteins. On a mole-to-mole ratio between apo C-1 and apo A-1 in a normo-lipidemic sample, this ratio was expected to be between 0.169 and 0.254. In other words, approximately one in five HDL particles should have both apo A-I and apo C-I. Looking at the reported values for the calibration based on the LC trace, several samples had an apo C-I to apo A-I ratio that was barely above zero, one sample that was at the expected ratio, and three samples that had a much higher than expected ratio. This was not surprising given that the very high background in the LC trace would negatively effect the calibration. Looking at the reported values for the calibration based on ion extraction, however, about seven of the twelve samples had ratios in range of the expected ratio, while the remaining five had ratios that were much higher than expected. The better signal/noise in the ion extraction traces accounted for the better quantification than looking at the LC trace alone, but ionization efficiency should be expected to play a role in the quality of these values. As a result, quantification by LC-MS generated a rough assessment of the apolipoprotein content of the HDL samples.

3.1.6 CE Analysis of HDL Fractions

Capillary Electrophoresis (CE) was another method chosen for secondary analysis following preparative UC in order to determine if there were differences in the electrophoretic properties between HDL subclasses in known CAD samples and control samples. Qualitatively, it was of interest to determine whether post-translational modifications could be detected by changes in the inherent mobility of the apolipoproteins of HDL in these samples. Another goal focused on analyzing the differences in distributions of the various apolipoproteins as a function of density. Quantitatively, the focus was to determine whether differences could be seen in the relative abundance of apo A-I and the hypothesized atherogenic apo C-I throughout the selected samples.

Three patients from each cohort were selected, and preparative UC was used in order to selectively remove the buoyant HDL-2 and dense HDL-3 subclasses from the

rest of the serum profile. SPE was performed on these fractions, which were then reconstituted in 100μL of a CE buffer consisting of 12.5mM sodium borate, 3.5mM SDS, and 20% (v/v) ACN. This buffer system was chosen in order give a strong EOF, due to the high pH of approximately 9.00, and to ensure a high amount of negative charge on the apolipoprotein particles due to their interaction with the anionic surfactant. These conditions served to minimize apolipoprotein/apolipoprotein interactions and apolipoprotein wall interactions. The electrophoresis experiment was performed in normal polarity, such that the electroosmotic flow (EOF) moves from the anode to the cathode. Integration of peak areas was performed manually. In total, twelve samples were analyzed by CE.

3.1.6.1 Identification and Quantification of HDL Apolipoproteins by CE

Serial dilutions were performed on stock 1.000mg/mL standard solutions of apo A-1 and apo C-1 in order to generate a concentration range that would include the dynamic range of each apolipoprotein expected in a serum sample. The average molar concentration of apo C-I is a factor of twenty times less than that of apo A-I in normo-lipidemic serum, which was reflected in the establishment of these calibration curves (Figures 62-65). In these figures, the electropherograms for each dilution of apo A-I and apo C-I were staggered in order to better visualize the peak shapes at each concentration. The migration times of the EOF marker and both of the apolipoprotein standards did not fluctuate during the construction of the calibration curve.

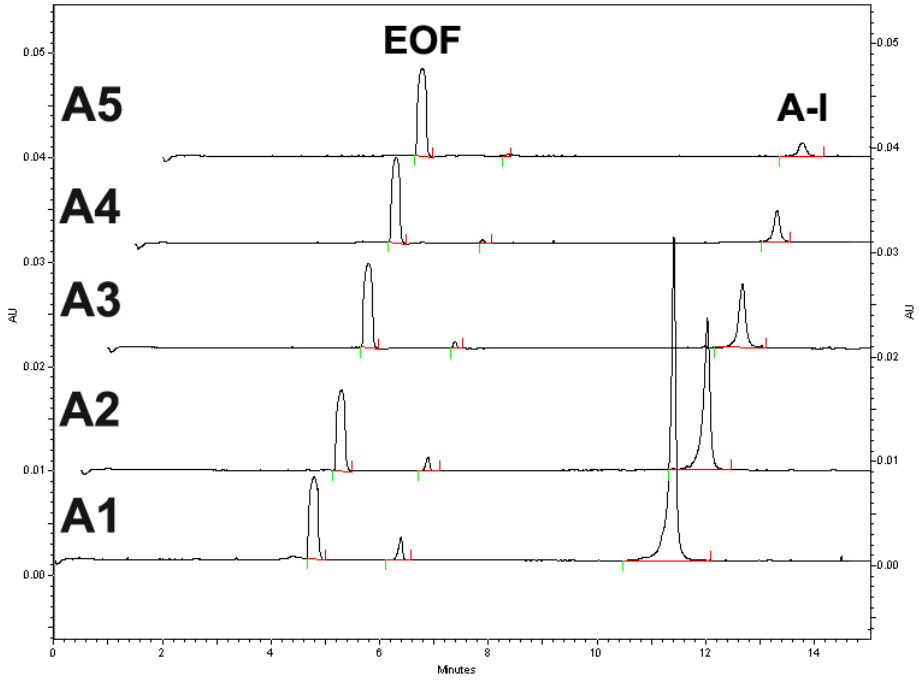

Figure 62. Electropherograms for Apo A-I Calibration. Conditions: 12.5mM Sodium Borate, 3.5mM SDS (70%), 20% (v/v) ACN, 5s Injection, 17.5kV

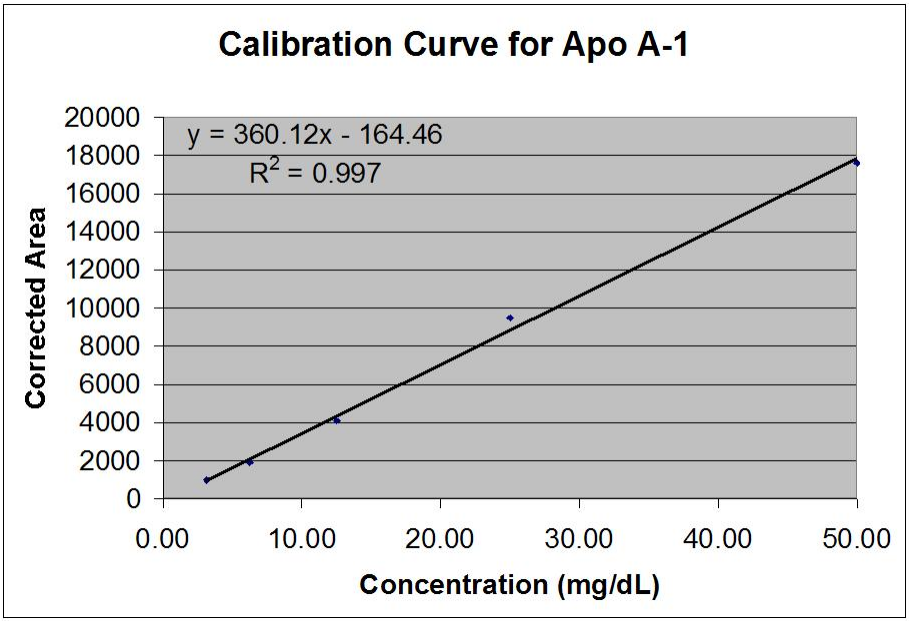

Figure 63. Apo A-I Calibration Curve by CE

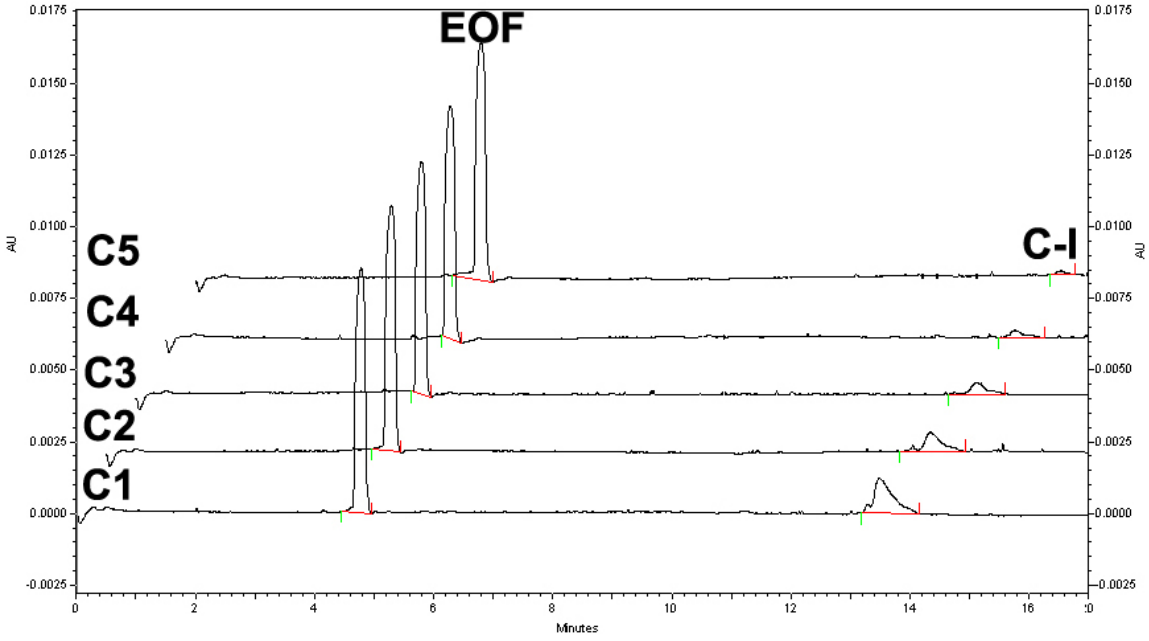

Figure 64. Electropherograms for Apo C-I Calibration. Conditions as Above

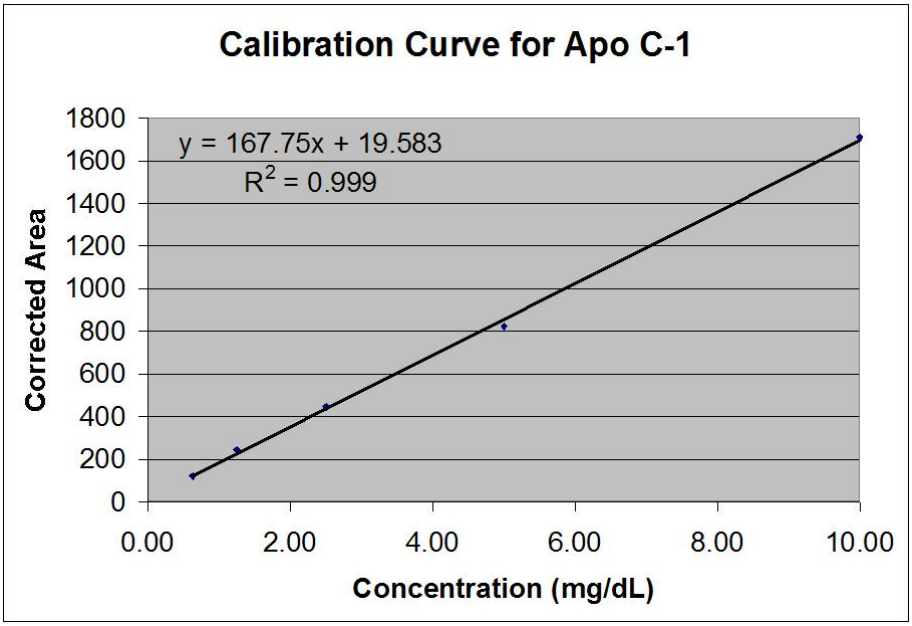

Figure 65. Apo C-I Calibration Curve by CE

In these curves the neutral marker, labeled EOF, eluted past the detector at approximately 5 minutes, apo A-I eluted at approximately 11.5 minutes, and apo C-I

eluted at approximately 13.5 minutes. By combining the migration time of the neutral marker, the migration time of analyte ions, and the dimensions of the capillary, the mobility of these species could be determined. The mobility for the apolipoproteins in the standards was found to be -25.9 x$10^{-5}$$cm^2$/Vs and -28.9 x$10^{-5}$$cm^2$/Vs for apo A-I and apo C-I respectively. Integration of the peak areas was performed manually. The calibration curves showed a strong linear relationship between concentration and UV absorbance over the selected concentration range for both apolipoproteins. The corrected area (Corr Area) of peaks that migrated past the detector was calculated as a function of the integrated area and velocity of the peaks, length to the detector (L_D) in cm, and the migration time of the peak (t_M) in seconds, as they eluted through the capillary. (Eq. 26)

$$Corr\ Area = (Area) \times (\frac{L_D}{t_M}) \qquad (26)$$

The corrected area accounts for peak widening that occurred to ions that took longer to migrate past the detector, and prevented the instrument from reporting higher areas for the slower moving peaks.

3.1.6.2 Comparison of Patient Samples

It was observed that the order the apolipoproteins eluted from capillary column differed from what was seen in both SPE and LC-MS. Because this was not a chromatography experiment, the apolipoproteins were separated by differences in electrophoretic mobility, dictated by their size/charge ratio. Larger particles with low charges were expected to have lower mobilities than small particles that were highly charged. These CE experiments were performed in normal polarity, so the only ions that reached the detector were anions that possessed a lower mobility than the EOF marker. In a sense, anions with mobilities lower than the EOF were driven by electrophoresis to the anode, but were pulled by electroosmosis past the detector to the cathode. The

balance between size and charge can be used to explain the elution order of the apolipoproteins. The observed elution order of peaks in the electropherograms was: EOF marker, HSA, apo A-II, a mixture of apo C-II/C-III, followed by apo A-I, then finally apo C-I. The elution profile of these apolipoprotein samples correlated well with data previously obtained in our laboratory.[201] This could also be explained in part by mass spectrometry results that gave details on the size/charge of these various apolipoproteins. HSA is larger than any of the apolipoproteins of HDL (~66 kDa) and also had a high number of charge states. Its large size kept its mobility low compared to the other apolipoproteins. Apo A-I was the next largest apolipoprotein (~28 kDa), but displayed a high number of charge states in ESI. This combination of size and charge explained why apo A-I had a higher mobility than every other apolipoprotein except for apo C-I. Though apo C-I formed very low charge states by ESI, its MW is much lower than the other lipoproteins (~6.6 kDa), which explained its relatively high mobility. Apo A-II displayed more charge states in ESI than apo C-I, but less that apo A-I and it also possessed an intermediate MW between apo A-I and apo C-I (~17.5 kDa). This combination of size and charge gave Apo A-II an intermediate mobility between apo A-I and apo C-I.

There were a few striking differences between samples of HDL-2 and HDL-3 for the two patient cohorts in the resulting electropherograms (Figures 66-67). The peak shapes for the apolipoproteins were largely the same throughout the entire batch of samples, but it was clear that the intensities fluctuated greatly between both patients and density regions. Any HSA that was not successfully washed off the column during the SPE procedure was typically seen as a broad peak early in the electropherogram and appeared to be more dominant in the HDL-3 fraction. Apo A-II was typically seen as a medium intensity single peak with a fairly broad base. It appeared to have a more erratic peak shape in CAD samples, and typically had a small shoulder peak on the left side. The apolipoproteins apo C-II and apo C-III were seen as very small sharp peaks between apo A-II and apo A-I and were generally easier to visualize in control samples. Apo A-I eluted as a dominantly tall peak with a shoulder on the right side that could not be

identified beyond assumption that it may be a modified version of the apolipoprotein as supported by evidence of post-translational modifications seen in both MALDI and ESI results. Apo C-I eluted very late in the electropherogram as a doublet with the first peak appearing sharper than the later peak. Because apo C-I has a known truncated form of approximately 6.4 kDa, it was hypothesized that the later of the two peaks for apo C-I was the truncated form because its lower size should give it a higher mobility. Mass spectral data also indicated that the truncated apo C-I' had a lower intensity than the native apo C-I, which further verified this hypothesis. Because of the low intensity of apo C-I relative to the other apolipoproteins, a zoomed in view of that region of the electropherogram was added to each figure to better illustrate this feature. Quantification was performed by comparing the calculated corrected areas for each apolipoprotein to the generated calibration curves from the standards of apo A-I and apo C-I. Note that both the primary and shoulder peak of apo A-I were integrated together, and the two peaks for apo C-I were integrated together for this comparison to the standards.

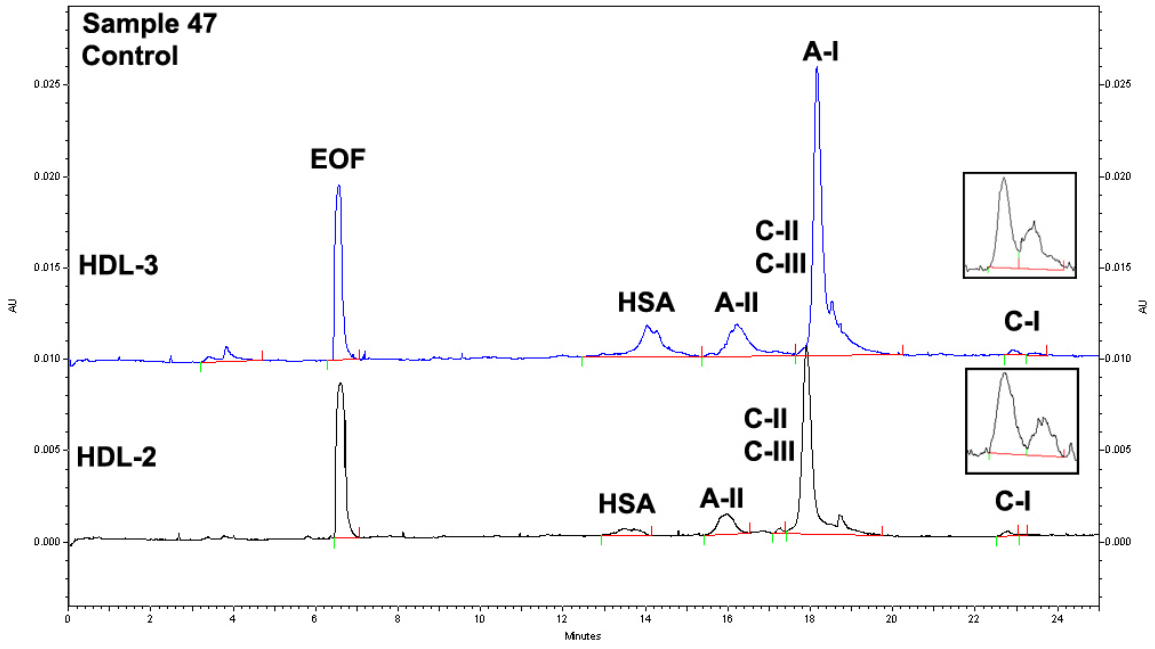

Figure 66. Electropherograms of HDL Fractions for Sample #47. Conditions as Above

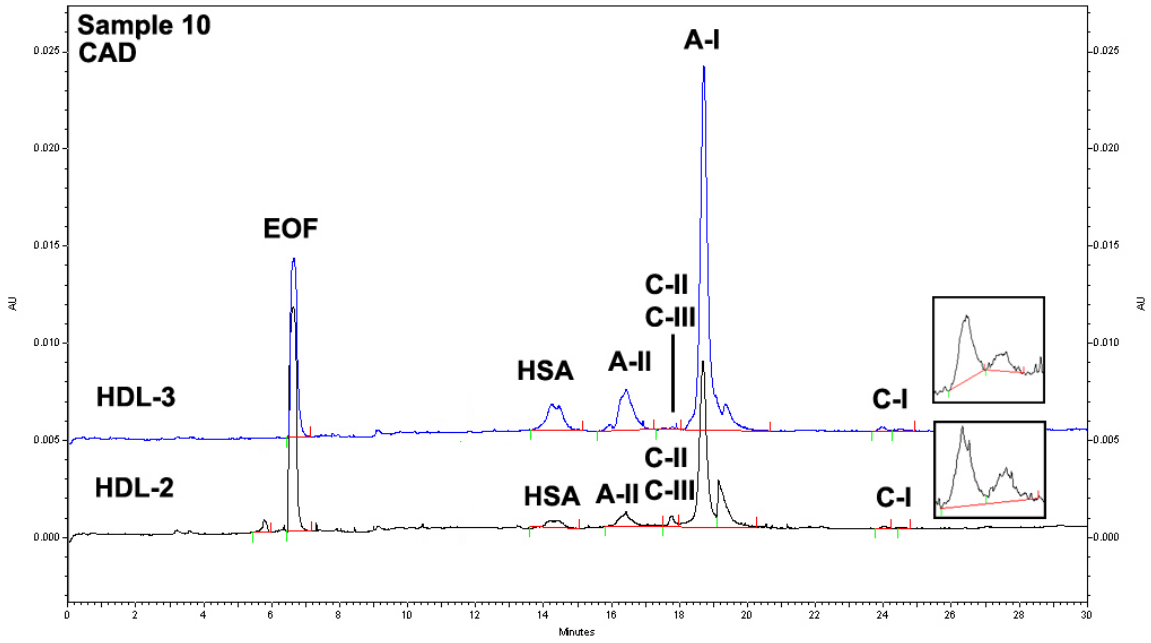

Figure 67. Electropherograms of HDL Fractions for Sample #10. Conditions as Above

It was observed that the migration time of the EOF marker appeared to drift towards progressively later times over the lifetime of the capillary column. This peak shifting phenomenon was most easily visualized in the analysis of HDL-2 in sample 195 and HDL-2 of sample 79 as seen in the appended electropherograms. EOF peak drift did not impact classification of the apolipoproteins because the mobility values for each did not change, and the corrected area calculation accounted for changes in peak velocity.

It was originally hypothesized that apo C-I may play a role in the early onset of cardiovascular disease, and early studies questioned whether buoyant HDL-2 was enriched with this apolipoprotein. Based on the quantification of apo A-I and apo C-I by CE, it was apparent that HDL-2 has a higher concentration of apo C-I relative to apo A-I in every sample but one (Figure 68).

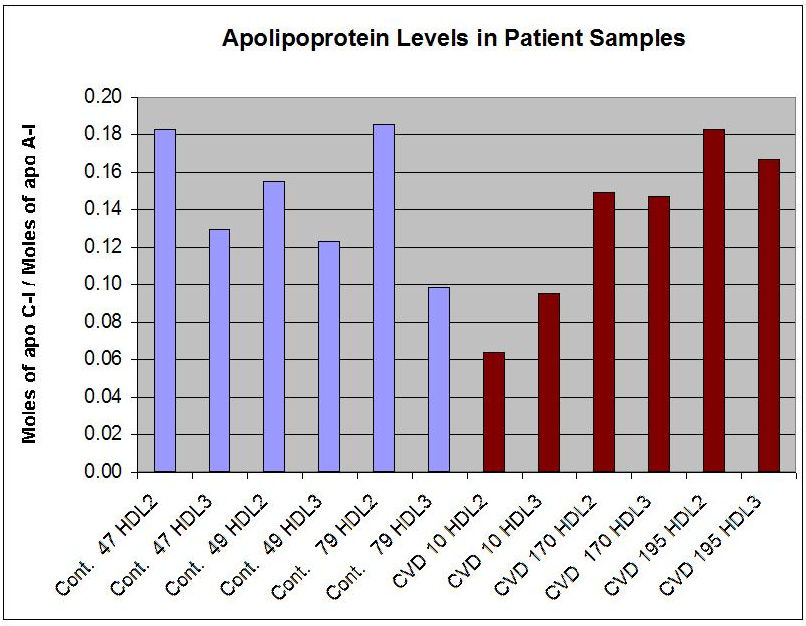

Figure 68. Quantification of Apo A-I and Apo C-I by CE

The mole-to-mole ratio between apo C-1 and apo A-1 in a normo-lipidemic sample was expected to be between 0.169 and 0.254 which correlates reasonably well with the calculated CE data. There appeared to be a larger disparity between the concentrations of these two apolipoproteins between HDL-2 and HDL-3 in the control samples, and a very minor difference between the two density regions in CAD samples. Data obtained from the CE gave the best quantification of the apolipoproteins out of the methods utilized in this study. Qualitatively the data indicated that there is a slightly higher ratio of apo C-I to apo A-I in the buoyant fraction of HDL, and supported the mass spectral evidence of the presence of subclasses of apo A-I and apo C-I.

3.1.7 IEF Analysis of HDL Fractions

3.1.7.1 Identification of HDL Apolipoproteins

The immobilized pH Gradient (IPG) gels used in this study gave good resolution of the various apolipoproteins of HDL and appeared to reveal several post-translational modifications for apo A-I, apo A-II, and apo C-I. It was observed that for each of these

apolipoproteins, there was typically a dominant peak that appeared at a reproducible pI value of ranging no more than ±0.10 pI units from sample to sample. The observed pI values correlated fairly well with values that were previously seen in our laboratory.[141] Apo A-I was very easily recognized at a pI value centered about 5.24, as was apo C-I at a pI value centered about 6.65. Apo A-II was not well resolved from the other apo C proteins, but was typically seen at a pI value centered about 4.70. In any samples in which the HSA was not fully removed by SPE, a broad peak was seen between pI values of 5.60 to 6.00. Though accurate quantification was not possible, a rough estimation of apolipoprotein concentration was determined through comparison of relative peak intensities within and between samples. Observation of the peak qualities throughout the cohort of 12 samples revealed that banding in the gels were typically very sharp, with very little smearing of bands across the gels. It was suspected that the loading capacity of the gel was likely approached, or even met in some cases, for apo A-I and HSA, as evidenced by very dark staining and distortion of band shape in these pI regions.

3.1.7.2 Comparison of Patient Samples

When comparing density-dependent regions of HDL and the two cohorts of patients, qualitative differences such as the presence/absence of peaks, pI values of dominant peaks, and distribution of peaks for a given apolipoprotein were the primary focus. Rough quantification, based on darkness of staining, was useful in determining which peaks were the most dominant in each density region for both cohorts of patients. Upon initial analysis, each sample revealed a high number of bands across the entire pI region, but possessed a particularly complex distribution in the apo A-II and apo A-I region (Figures 69, 70). As expected, it was also seen that HSA was not present in every sample, as was the case in both mass spec experiments and in CE electropherograms.

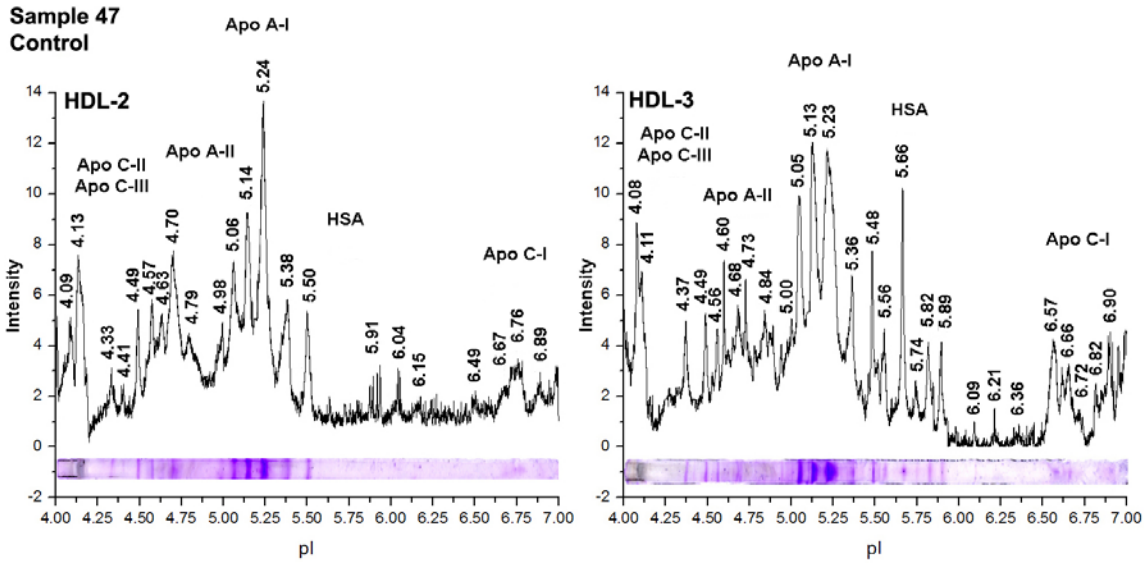

Figure 69. pI Profile for Sample #47 with a 13cm, pH 4-7 IPG Strip

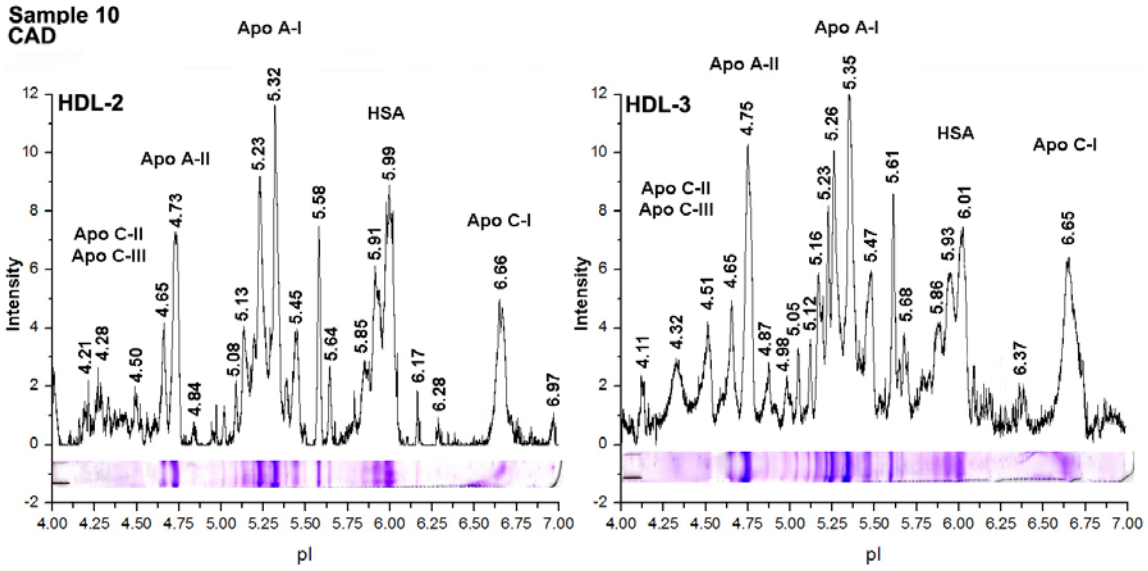

Figure 70. pI Profile for Sample #10 with a 13cm, pH 4-7 IPG Strip

As few as 5, and as many as 7 bands were seen for apo A-I, which correlates well with what was seen in the MALDI and LC-MS. Two dominant peaks existed at pI values of approximately 5.23 and 5.32 in the majority of the samples. There was a medium intensity band at a more basic pI value of between 5.36 and 5.46 that was

common across the 12 samples as well. Only in the more acidic region at pI values between 5.05 and 5.20 did differences between samples particularly begin to stand out.

Apo A-II was primarily visualized at a pI value of approximately 4.75 throughout the various samples. A single more basic band was seen at a pI range of 4.80 to 4.90 and several more acidic bands between 4.50 and 4.70. This apolipoprotein was more predominant in fractions of HDL-3, which agrees with literature observations that the majority of apo A-II was reported to be found in dense HDL.[202]

The analysis of apo C-I was much more informative than the other apolipoproteins. In some cases, only a single pI value was observed, but as many as 4 were seen. Contrary to what was observed in the other methods, the bands corresponding to apo C-I appeared to be more intense in the dense HDL-3 fractions than in the buoyant HDL-2. However, the concentration of apo C-I must be compared to the concentration of apo A-I in order to determine if it is indeed enriched with apo C-I. Since quantification with this technique was not possible, the distribution of pI values will yield much more meaningful information. The three CAD samples, displayed markedly different apo C-I pI banding from one another and from the controls. The banding pattern in sample 10 revealed a single dominant apo C-I peak at a pI value of 6.66 in both HDL-2 and HDL-3. Sample 170 displayed very minimal peaks for apo C-I, with a singlet in HDL-2 and a doublet in HDL-3. There were several apparent modified versions of apo C-I in sample 195, which showed three medium intensity bands at pI values between 6.60 and 6.86 in HDL-2 and more basic pI values in HDL-3. The control samples, with the exception of sample 49, displayed low intensity bands for apo C-I, particularly in the HDL-2 fraction. Sample 49 however, showed a very intense triplicate of apo C-I bands in the HDL-3 fraction with pI values at 6.61, 6.67, and 6.79.

The most striking difference between the CAD and control samples appeared to be differences in apo C-I intensity and distribution between the two HDL fractions. Banding patterns for apo A-I and apo A-II tended to vary less between patient samples and density regions than apo C-I and did not offer a great deal of insight as to differences between the two sample cohorts. Control samples were observed to display only very

minor bands for apo C-I in the HDL-2 fraction, but much more intense bands in the HDL-3 fraction. CAD samples on the other hand, tended to display similarly intense bands for apo C-I in both HDL fractions, which was particularly true with samples 10 and 195. This result gave further evidence that there is both a quantitative and qualitative difference in the apolipoprotein distribution found in density-distinct subclasses from the two patient cohorts.

3.2 Clinical Studies

3.2.1 Aortic Smooth Muscle Cell Apoptosis

The Chatterjee laboratory at The Johns Hopkins University, was responsible for analyzing the apoptotic capacity of samples of HDL that were generated by means of preparative UC. Samples of HDL-2 and HDL-3 were isolated and then desalted and sterilized as described in the materials and methods section prior to shipment. It was previously seen that HDL particles enriched in apo C-I from the cord blood of infants markedly induced apoptosis via the N-SMase pathway.[186] The mitochondria within cells releases cytochrome C in response to pro-apoptotic stimuli. This cytochrome C then interacts with the inositol triphosphate receptor (IP3R) found in the endoplasmic reticulum of the cell, triggering a release of calcium. Increased calcium levels in turn trigger an increased release of cytochrome C by the mitochondria, creating a positive feedback loop. Ultimately, the high cytochrome C levels activate various caspases which are responsible for destroying the cell from within.

Recent analyses of the HDL fractions from patient samples were also observed to induce apoptosis involving the same pathway. By combining 4'-6-Diamidino-2-phenylindole (DAPI) as a stain of the aortic smooth muscle cell (ASMC) cultures with fluorescent antibodies against cytochrome C and caspase-3, the response of the cell cultures to outside stimuli could be monitored. ASMCs were photographed under a phase contrast fluorescent microscope in order to visualize any apoptosis-inducing interactions (Figure 71).

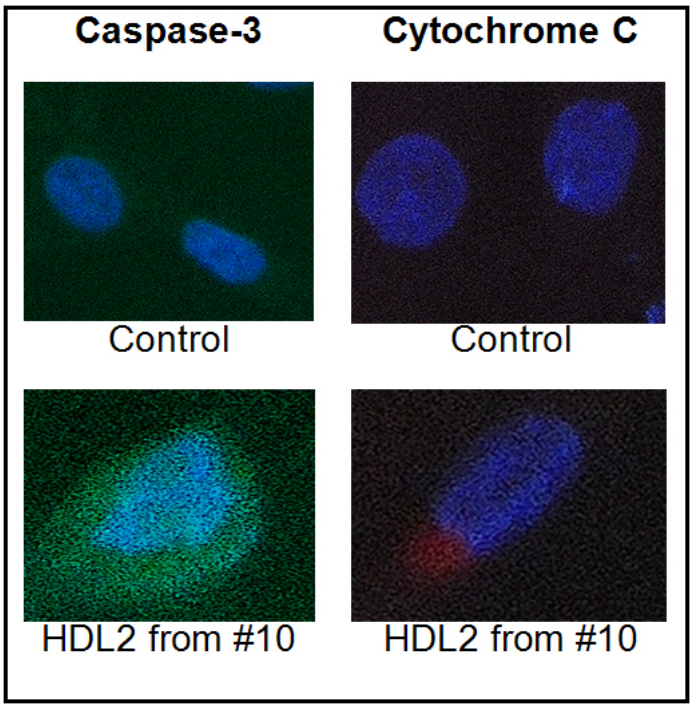

Figure 71. Activation of Caspase-3 and Cytochrome-C in ASMC by the HDL-2 Fraction of Sample #10

When the HDL-2 fraction from sample #10 was introduced to the ASMC culture, a strong reaction of the fluorescent antibodies towards caspase-3 and cytochrome-C was observed. In the control sample, no noticeable reaction was observed.

It was discovered that the buoyant HDL-2 fraction from CAD samples readily induced apoptosis in ASMCs while HDL-3 fractions from the same patient did not. Several hundred cells were counted to determine the number of apoptotic cells (Figure 72). Pre-incubation of the ASMC cultures with an inhibitor of N-SMase, GW4869, was seen to greatly inhibit apoptosis. ASMC apoptosis was not seen in either fraction from control patients.

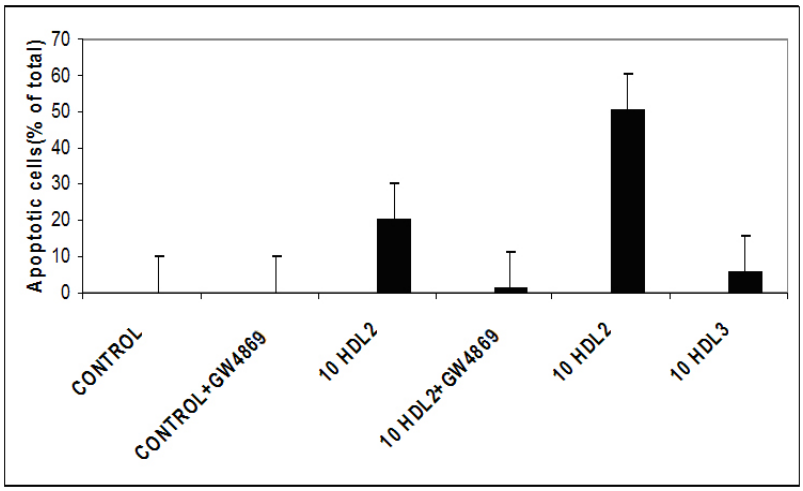

Figure 72. Percentage of ASMCs that Underwent Apoptosis after Introduction of Samples

3.2.2 Human Arterial Endothelial Cell Apoptosis

In a related study by the Chatterjee laboratory, the apoptotic effect of LDL and HDL fractions was also measured for human arterial endothelial cells (HAEC). It was observed that neither the HDL-2 nor the HDL-3 fraction from CAD samples induced HAEC apoptosis. However, the LDL fraction did induce apoptosis of these cell cultures. This result suggested the possibility that small molecules of HDL could penetrate the endothelial wall and cause substantial apoptosis of smooth muscle cells. HAEC were also incubated with the HDL-2 fractions from CAD and control samples, and then stained with 4'5'-diamino fluoroscein diacetate (DAF-2), which is a marker for nitric oxide. It was seen that the HDL-2 from the CAD samples produced a strongly positive reaction as compared to the HDL-2 from a control sample (Figure 73). Pre-treatment of the HAECs with pyrrolidine dithiocarbamate (PDTC), a membrane permeable anti-oxidant, was observed to reverse this reaction.

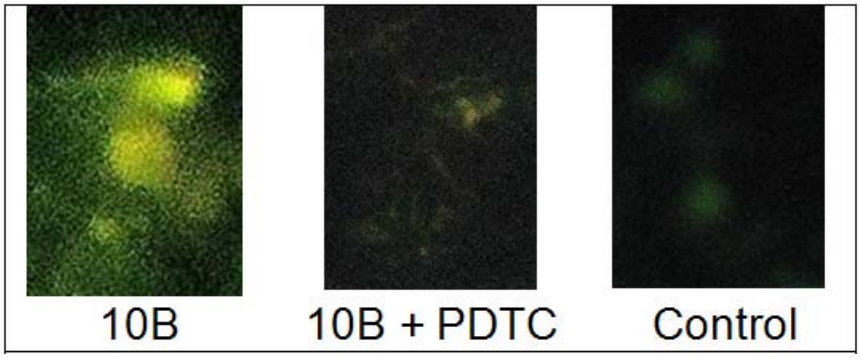

Figure 73. Effects of Serum Lipoproteins on Nitric Oxide Levels

Nitrite is a stable product formed from endothelial nitric oxide synthase (eNOS) activity towards nitric oxide. Measurement of nitrite levels in HAEC using the Greiss reagent also suggested that HDL-2 from CAD samples markedly increased nitrite levels, which is indicative of increased eNOS activity.[203] Since increased levels of nitric oxide can induce apoptosis by reaction with superoxides and peroxynitrite generation, it is very curious as to why these buoyant samples of HDL-2 induce apoptosis in ASMC but not in HAEC.

3.3 Statistical Analysis

The aim of this study was to determine the feasibility of classifying subjects from two groups of samples, controls and CAD, by utilizing a statistical analysis software package. Data from the integrated fluorescence intensities of subclasses contained in lipoprotein density profiles was inputted into this software and statistical analyses methods were then used to determine which group a particular sample belonged to. Classification utilized both linear discriminate analysis (LDA) and sliced average variance estimation (SAVE), in which both attempted to determine a linear combination of variables. LDA attempted to find a linear combination of the variables, which in this case is the integrated intensities of the various subclasses. SAVE attempted to find a linear combination of the same variables by also using the mean, variance, and covariance. In this study, a cohort consisting of 15 controls and 15 CAD samples were

analyzed by lipoprotein density profiling that utilized both a 0.2000M solution of NaBiY and a 0.2000M solution of Cs_2CdY.

Results from the LDA and SAVE analyses are reported for both solute systems. The equations generated by each statistical method were log-transformed functions that include the ratios of the most significant variables inputted. In other words, variables that were found to be statistically insignificant contained low exponential values, and therefore did not appear in the final equations. For the 30 patient samples analyzed, the resulting LDA equation for NaBiY can be approximated by (Eq. 27), and for Cs_2CdY by (Eq. 28).

$$LDA = 3.29 \log\left[\frac{(HDL-3a)\times(HDL-2b)^{0.39}}{(HDL-3b)^{0.78}\times(LDL-3)^{0.38}\times(HDL-2a)^{0.37}}\right] \tag{27}$$

$$LDA = 3.19 \log\left[\frac{(LDL-3)\times(HDL-3b)^{0.57}\times(bTRL)^{0.47}}{(dTRL)^{0.60}\times(LDL-4)^{0.40}\times(HDL-2a)^{0.40}}\right] \tag{28}$$

For the LDA analysis, the most significant variables were found to be HDL-3a and HDL-3b for the NaBiY analysis and LDL-3, HDL-3b, and both TRL subclasses for the Cs_2CdY analysis. By simply changing the solute system, the statistical classification was observed to dramatically change as a result of the difference in separation achieved by each of the solutes. The NaBiY solute system was capable of separating 12 density-distinct subclasses in the lipoprotein profile, while Cs_2CdY was not able to resolve the TRL subclasses from the buoyant LDL subclasses, resulting in only 10 density-distinct subclasses. The dense HDL subclasses of HDL-3a and HDL-3b appeared as significant variables in both solute systems, indicating that this region of the lipoprotein profile is statistically important in categorizing a sample into one of the two cohorts. Curiously, the LDA analysis determined that HDL-3a was the most important variable in the NaBiY separation, while LDL-3 was the most important variable in the Cs_2CdY

separation. The difference in weighting of the variables likely occurred due to the lower number of resolved subclasses in the Cs_2Cdy solute system.

The SAVE analysis, reported two equations, SAVE1 and SAVE2, in order to express the linear combination of variables from each of the two sample groups. The resulting equations for the NaBiY solute system were given by (Eqns. 29 and 30):

$$SAVE1 = 13.77 \log\left[\frac{(HDL-3a)\times(HDL-2b)^{0.15}}{(HDL-3b)^{0.74}\times(HDL-2a)^{0.54}}\right] \tag{29}$$

$$SAVE2 = -10.33 \log\left[\frac{(HDL-3b)\times(LDL-2)^{0.42}\times(LDL-4)^{0.25}}{(HDL-3c)^{0.60}\times(HDL-3a)^{0.57}\times(LDL-3)^{0.29}}\right] \tag{30}$$

The resulting equations for the Cs2CdY solute system were given by (Eqns. 31 and 32):

$$SAVE1 = -7.46 \log\left[\frac{(HDL-3b)\times(bTRL)^{0.34}\times(LDL-4)^{0.21}}{(HDL-3a)^{0.84}\times(HDL-3c)^{0.64}\times(dTRL)^{0.33}\times(LDL-5)^{0.26}}\right] \tag{31}$$

$$SAVE2 = -2.38 \log\left[\frac{(HDL-3a)\times(LDL-4)^{0.70}\times(HDL-3c)^{0.47}\times(HDL-2a)^{0.32}}{(bTRL)^{0.78}\times(HDL-3b)^{0.67}\times(LDL-3)^{0.47}\times(HDL-2b)^{0.27}}\right] \tag{32}$$

For the SAVE1 analysis with the NaBiY solute system, the most significant variables were found to be associated with the subclasses HDL-3a and HDL-3b due to their high exponent relative to the other subclasses. Similarly, the most significant variables seen in SAVE2 were associated with the subclasses of HDL-3b and HDL3-c. This meant that of all of the 12 subclasses analyzed, the fluorescence intensity of the dense HDL subclasses influenced the group assignment made by the statistical software more heavily than the other variables. For the SAVE1 analysis with the Cs_2CdY solute system, the most significant variables were found to be associated with HDL-3a and

HDL-3b as was seen in the NaBiY analysis, but HDL-3c was also seen to be statistically significant. The SAVE2 analysis for Cs_2CdY however, reported that HDL-3a, LDL-4, and b-TRL were all statistically significant. This result indicated that serum levels of two common risk factors for atherogenesis, dense LDL and triglycerides, were important in the classification.

A graphical representation of this data plotted LDA, also known as SIR1, along with SAVE1, and SAVE2 (Figures 74, 75). In these figures the row and column determined the axis on which the statistical solution was plotted. SIR1 was plotted against SAVE1 in the upper left panel and against SAVE2 in the upper right panel. SAVE1 and SAVE2 were plotted against each other in the bottom right panel. By arranging the data in this manner, each of the three statistical solutions were plotted against one another, giving three combinations in a single concise graphic. The three combinations included: SIR1 vs SAVE1, SIR1 vs. SAVE 2, and SAVE1 vs. SAVE2 Group 1, the control group, was represented by the black trace, and group 2, the CAD group, was represented by the red trace.

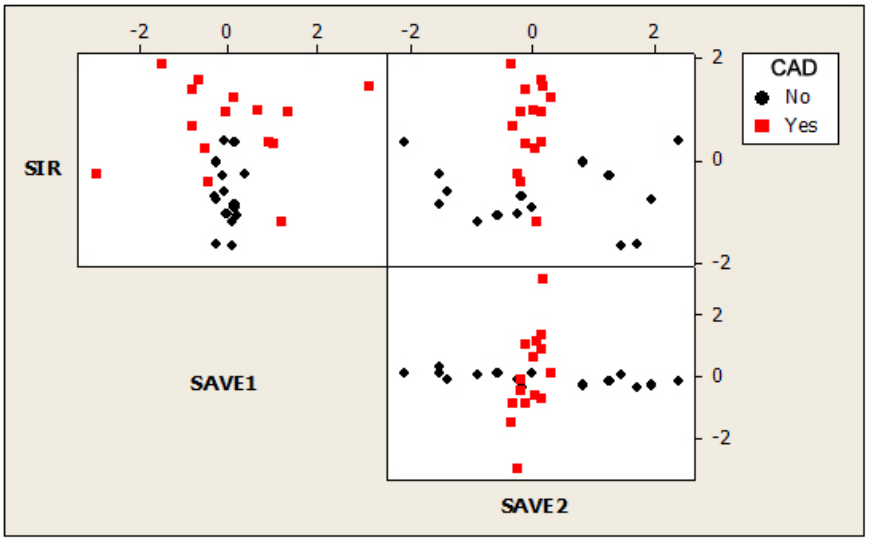

Figure 74. Statistical Plots for 6μL of Serum at Saturating NBD (C_6-ceramide) Conditions, Spun in 0.2000M NaBiY for 6 Hours at 120,000 RPM and 5ºC

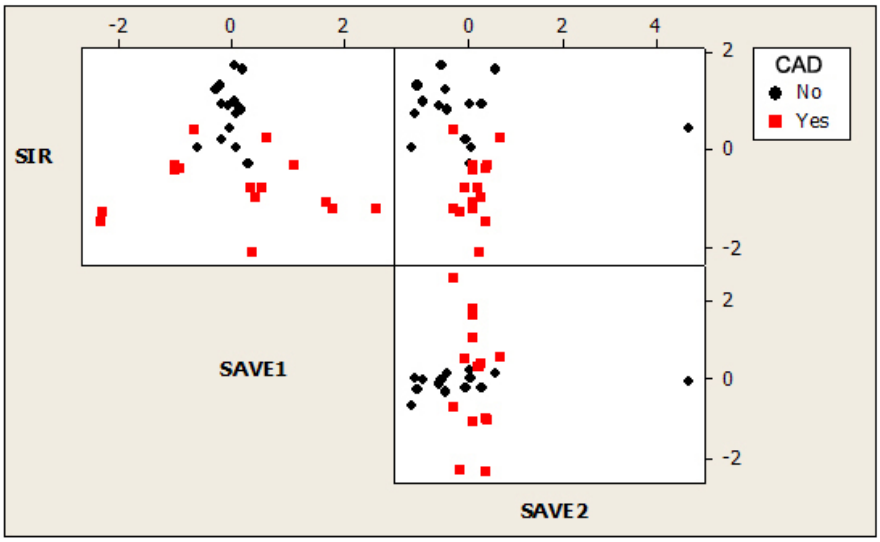

Figure 75. Statistical Plots for 6µL of Serum at Saturating NBD (C_6-ceramide) Conditions, Spun in 0.2000M Cs_2CdY for 6 Hours at 120,000 RPM and 5ºC

It was observed that the SAVE1 vs. SAVE2 plots, as seen in the lower right panels of each figure, yielded the most discernible classification between the two groups for both solute systems. It was also readily apparent that the difference between the two groups was remarkably different when comparing the slopes of the two fitted lines. The values of SAVE1 for the control group were relatively constant over the data range of the 15 subjects in this group even though the values for SAVE2 were quite different. The inverse appeared to be true for the CAD group, in which SAVE1 drastically changed between subjects, while SAVE2 remained relatively constant. A surprising result was seen when the extremities of the two data sets also fell nearly perfectly on their respective fitted lines. Even where the two data sets intersected, there was not appreciable deviation of individual data points from their respective classification lines.

It was also observed that the scatter of the data was considerably better in the NaBiY solute system than in the Cs_2CdY system. This largely stemmed from the loss of two variables in the Cs_2CdY system since the two most buoyant subclasses of LDL could not be isolated from the two TRL subclasses. The best classification appeared in the SAVE1 vs. SAVE2 plot of the NaBiY data where two distinct groupings of data

were apparent. The same plot in the Cs_2CdY figure was similar in appearance to the SAVE1 vs. SAVE2 seen with NaBiY, but there was considerably more scatter in the data. This indicated that a classification was possible with the Cs_2CdY system, but it did not yield as good of a separation between the two groups. Comparison of these two results indicated that the EDTA solute system chosen for the analysis was an important parameter that greatly impacted the end result. Another important observation is that a large distribution of acceptable values for the various subclasses exists that still enabled a sample to be correctly classified.

CHAPTER IV

CONCLUSIONS

The overall objective of this research was to develop a combination of methods for an in-depth analysis of the apolipoproteins of HDL subclasses and to apply these methods to clinical samples. This objective was achieved by combining novel density gradient separations with secondary analyses that yielded information regarding the size, charge, structure, abundance, and distribution of the desired analytes. By applying these methods to a cohort of patients who exhibited a range of cardiovascular health, a better assessment of an individual's cardiovascular risk could be reached, thereby showing feasibility for potential early detection of the onset of CAD.

The heavy metal EDTA complexes, when used as a solute system in UC, generated highly reproducible gradients between individual spins and between different batches of solution. This reproducibility offered a rugged method which allowed a high degree of control over the separation of lipoprotein particles, both for fluorometric analysis, and for preparative UC. The use of these solute systems also offered higher sample throughput than separations that require time-consuming sequential centrifugation steps.

Through combination of preparative UC and MALDI-MS, an interesting correlation was observed between different density classes of HDL and degrees of post-translational modifications for its primary apolipoproteins. There appeared to be variable protease activity in the different density regions of HDL which suggests that various proteases are also associated with a specific density region of the lipoprotein profile.

The technique of LC-MS enabled both a qualitative analysis of the distribution of apolipoproteins and a semi-quantitative means of determining the concentration of apo A-I and apo C-I. Analysis of the ESI spectra in detail enabled correct classification of the different apolipoprotein peaks in the patient samples, and offered a means of comparison in terms of numbers of peaks seen in the spectra for each. For the twelve

patient samples, there were no significant density-dependent or patient-dependent differences in the ESI spectra of the three apolipoproteins in numbers of post-translational modifications that could be seen. Quantification of the apolipoproteins throughout the batch of samples provided a rough assessment of apolipoprotein levels and indicated that on average, the buoyant HDL-2 fraction possessed a higher relative concentration of apo C-I.

Based on the quantification of apo A-I and apo C-I by CE, it was apparent that fractions of HDL-2 possessed a higher ratio of apo C-I to apo A-I in every sample but one. The relative ratio of these two apolipoproteins also closely agreed with expected literature values. Qualitatively, this experiment also revealed that there were two mobility separated components of both apo A-I and apo C-I which correlated with the numbers of post-translational modifications seen in MALDI-MS and LC-MS.

Gel electrophoresis experiments further revealed the complex nature of the apolipoprotein population from various fractions of HDL, and appeared to correlate well with results seen in the ESI spectra. A striking difference was seen in the relative abundance of apo C-I between the buoyant and dense fractions of HDL from control and CAD samples. Apo C-I was observed to generate the most intense bands on an IPG gel for the buoyant HDL-2 sample for CAD patients and moderately intense bands in the dense HDL-3 sample. Little to no difference was seen when comparing both density regions of control patients. This result further validated the hypothesis that apo C-I enriched HDL is found in the buoyant fraction.

Cell culture studies from an outside laboratory focused on the capacity of various intact HDL fractions to induce apoptosis of both ASMC and HAEC cultures. It was observed that only the buoyant fraction of HDL from CAD samples induced significant apoptosis of ASMC. There was little to no apoptosis in the dense region of HDL from CAD samples, or from any fraction of HDL in control samples. It was also seen that the same sample fractions that previously caused significant apoptosis of ASMC induced little to no apoptosis of HAEC cultures. This result yields crucial data about the

biological activity of the samples that were previously analyzed by chemical means and reveals a possible scheme to explain the instigation of atherogenesis.

Statistical analysis demonstrated a new approach at analyzing the compositional differences seen in the distribution of lipoproteins with the goal of classifying a patient's risk of developing atherosclerosis. Despite the array of traditional risk factors, there exists a segment of the population that still develops CAD for currently unknown reasons. By combining the separatory power of DGU with EDTA solute systems, modern statistical methods have shown a very effective, and nearly perfect, classification of two patient cohorts from one another.

Though the focus of research on lipoproteins has typically centered on the intact structure of these particles, as well as quantification of cholesterol levels, the field is beginning to shift towards changes in lipoprotein structure itself. Modifications to either the lipid component or in the apolipoproteins themselves have become increasingly important, particularly in studies involving the effects of oxidation. The combination of these methods demonstrated strength in their ability to not only quantify the amounts of key apolipoproteins, but also to analyze differences in their structure from very different perspectives. The research reported here established a foundation of analytical tools to assist in distinguishing differences between healthy samples and those that are at risk of developing CAD. Future applications of this research will explore the use of these techniques in determining additional risk factors that can be applied to a broader cohort of samples for a more complete assessment of cardiovascular risk.

REFERENCES

(1) Jehle, A.J.; *Circulation* **2002**, *106*, 3143-3421.

(2) Havel, R. J.; Eder, H. A.; Bragdon, J. H. *J. Clin. Invest.* **1955**, *34*, 1345-1353.

(3) Hosken, B. D.; Cockrill, S. L.; Macfarlane, R. D. *Anal. Chem.* **2005**, *77*, 200-207.

(4) Johnson, J. D.; Bell, N. J.; Donahoe, E. L.; Macfarlane, R. D. *Anal. Chem.* **2005**, *77*, 7054-7061.

(5) Beverly, M. B.; Voorhees, K. J. *Anal. Chem.* **2000**, *72*, 2428-2432.

(6) Roussis, S. G.; Fedora, J. W. *Anal. Chem.* **1997**, *69*, 1550-1556.

(7) Pacholski, M. L.; Cannon, D. M.; Ewing, A. G.; Winograd, N. *J. Am. Chem. Soc.* **1999**, *121*, 4716-4717.

(8) Shieh, I.; Lee, C.; Shiea, J. *J. Prot. Res.* **2005**, *4*, 606-612.

(9) Levander, F.; James, P. *J. Prot. Res.* **2004**, *4*, 71-74.

(10) Schmitz, G.; Mollers, C.; Richter, V. *Electrophoresis* **1997**, *18*, 1807-1813.

(11) Ceriotti, L.; Shibata, T.; Folmer, B.; Weiller, B. H.; Roberts, M. A.; de Rooij, N. F.; Verpoorte, E. *Electrophoresis* **2002**, *23*, 3615-3622.

(12) Cruzado, I. D.; Cockrill, S. L.; McNeal, C. J.; Macfarlane, R. D. *J. Lipid Res.* **1998**, *39*, 205-217.

(13) Bjellqvist, B.; Ek, K.; Righetti, P. G.; Gianazza, E.; Gorg, A.; Westermeir, R.; Postel, W. *J. Biochem. Biophys. Methods* **1982**, *6,* 317-339.

(14) Righetti, P. G.; In *Laboratory Techniques in Biochemistry and Molecular Biology*; Burdon, R.H., van Knippenberg, P. H., Eds.; Elsevier Science Publishers: Amsterdam, 1990; Vol. 20, pp 117-179.

(15) Tulenko, T. N.; Summer, A. E. *J. Nucl. Cardiol.* **2002**, *9*, 638-649.

(16) Dominiczak, M. H.; In *Apolipoproteins and Lipoproteins in Human Plasma;* The American Association for Clinical Chemistry, Inc.: Washington D.C., 1997.

(17) Caslake, M. J.; Packard, C. J.; In *Handbook of Lipoprotein Testing*; Rifai, N., Warnick, G. R., Dominiczak, M. H., Eds.; The American Association for Clinical Chemistry, Inc.: Washington D.C., 1997, pp 509-529.

(18) Mjos, O. D.; Faergeman, O.; Hamilton, R. L.; Havel, R. J. *J. Clin. Invest.* **1975**, *56*, 603-615.

(19) Austin, M.; Breslow, J.; Hennekens, C.; Buring, J.; Willett, W.; Krauss, R. M. *JAMA* **1988**, *260*, 1917-1921.

(20) Austin, M.; King, M.-C.; Vranizan, K.; Krauss, R. M. *Circulation* **1990**, *82*, 495-506.

(21) Austin, M.; King, M.-C.; Vranizan, K.; Newman, B.; Krauss, R. M. *Am. J. Hum. Genet.* **1988**, *43*, 838-846.

(22) Austin, M.; Brunzell, J. D.; Fitch, W. L.; Krauss, R. M. *Arteriosclerosis* **1990**, *10*, 520-530.

(23) McNamara, J.; Campos, H.; Ordovas, J. M.; Peterson, J.; Wilson, P.; Schaefer, E. *Arteriosclerosis* **1987**, *7*, 483-490.

(24) Patsch, J. R.; Gotto, A. M.; Olivercrona, T. *Proc. Nat. Acad. Sci.* **1978**, *75*, 4519-4523.

(25) Miller, N. E.; Hammett, F.; Saltissi, S. *Br. Med. J.* **1981**, *282*, 1741-1744.

(26) Ballantyne, F. C.; Clark, R. S.; Simpson, H. S. *Metabolism* **1982**, *31*, 433-439.

(27) Stampfer, M. J.; Sacks, F. M.; Salvini, S. *N. Engl. J. Med.* **1991**, *325*, 377-381.

(28) Mackenzie, S. L.; Sundaram, G. S.; Sodhi, H. S. *Clin. Chim. Acta.* **1973**, *43*, 223-229.

(29) Sundaram, G. S.; Mackenzie, S. L.; Sodhi, H. S. *Biochim. Biophys. Acta* **1974**, *337*, 196-203.

(30) Grundy, S. M.; Becker, D.; Clark, L. T.; Cooper, R. S.; Denke, M. A.; Howard, W. J.; Hunninghake, D. B.; Illingworth, R.; Luepker, R. V.; McBride, P.; McKenney, J. M.; Pasternak, R. C.; Stone, N. J.; Van Horn, L. *JAMA* **2001**, *285*, 2486-2497.

(31) Mahley, R. W.; Innerarity, T. L.; Rall, S. C.; Weisgraber, K. H. *J. Lipid Res.* **1984**, *25,* 1277-1294.

(32) Nestruck, A. C.; Suzue, G.; Marcel, Y. L. *Biochim. Biophys. Acta* **1980**, *617,* 110-121.

(33) Menzel, H. J.; Kladetzky, R. G.; Assmann, G. J. *J. Lipid Res.* **1982**, *23,* 915-922.

(34) Lux, S. E.; John, K. M.; Ronan, R.; Brewer Jr., H. B. *J. Biol. Chem.* **1972**, *247,* 7519-7127.

(35) Lagocki, P. A.; Scanu, A. M. *J. Biol. Chem.* **1980**, *255,* 3701-3706.

(36) Pastier, D.; Dugue, E.; Boisfer, V.; Atger, N. Q.; Tran, A.; von Trol, M. J.; Chapman, J.; Chambaz, J.; Laplaud, P. M.; Kalopissis, A.-D. *Biochemistry* **2001**, *40*, 12243-12253.

(37) Soutar, A. K.; Garner, C. W.; Baker, H. N.; Sparrow, J. T.; Jackson, R. L.; Gotto, A. M.; Smith, L. C. *Biochemistry* **1975**, *14*, 3057-3064.

(38) Blanco-Vaca, F.; Escola-Gil, J. C.; Martin-Campos, J. M.; Julve, J. *J. Lipid Res* **2001**, *42,* 1727-1739.

(39) Wu, A. L.; Windmueller, H. G. *J. Biol. Chem.* **1979**, *254,* 7316-7322.

(40) Medstrand, P.; Landry, J.-R.; Mager, D. L. *J. Biol. Chem.* **2001**, *276,* 1896-1903.

(41) Gabelli, C.; Bilato, C.; Fojo, S. S.; Marini, S.; Brewer Jr., H. B.; Crapaldi, G.; Baggio, G. *Eur. J. Clin. Invest.* **1993**, *23,* 522-528.

(42) Weisgraber, K. H.; Mahley, R. W.; Kowal, R. C.; Herz, J.; Goldstein, J. L.; Brown, M. S. *J. Biol. Chem.* **1990**, *265,* 22453-22459.

(43) Gautier, T. D.; Masson, J.-P.; de Barros, P.; Athias, A.; Gambert, P.; Aunis, D.; Metz-Boutiques, M.-H.; Lagrost, L. *J. Biol. Chem.* **2001**, *276,* 37504-37509.

(44) Havel, R. J.; Fielding, C. J.; Olivecrona, G. *Biochemistry* **1973**, *12*, 1828-1833.

(45) Brown, W. V.; Baginsky, M. L. *Biochem. Biophys. Res. Commun.* **1972**, *46*, 375-382.

(46) Curry, M. D.; McConathy, W. J.; Fesmire, J. D.; Alaupovic, P. *Clin. Chem.* **1981**, *27,* 543-548.

(47) Westerterp, M.; Berbee, J. F. P.; Pires, N. M. M.; van Mierlo, G. J. D.; Kleemann, R.; Romijin, J. A.; Havekes, L. M.; Rensen, P. C. N. *Circulation* **2007**, *116,* 2173-2181.

(48) Westerterp, M.; Van Eck, M.; de Haan, W.; Offerman, E. H.; Van Berkel, T. J. C.; Havekes, L. M.; Rensen, P. C. N. *Atherosclerosis* **2007**, *195*, e9-e16.

(49) Bier, D. M.; Havel, R. J. *J. Lipid Res.* **1970**, *11,* 565-570.

(50) LaRosa, J. C.; Levy, R. I.; Herbert, P.; Lux, S. E.; Fredrickson, D. S. *Biochem. Biophys. Res. Commun.* **1970**, *41*, 57-62.

(51) Breckenridge, W. C.; Little, J. A.; Steiner, G.; Chow, A.; Poapst, M. *N. Engl. J. Med.* **1978**, *298,* 1265-1273.

(52) Shelburne, F.; Hanks, J.; Meyers, W.; Quarffordt, S. *J. Clin. Invest.* **1980**, *65,* 652-658.

(53) Windler, E.; Chao, Y.-S.; Havel, R. J. *J. Biol. Chem.* **1980**, *255,* 5475-5480.

(54) Connelly, P. W.; Maguire, G. F.; Hofmann, T.; Little, J. A. *Proc. Nat. Acad. Sci.* **1987**, *84,* 270-273.

(55) Kinnunen, P. K.; Ehnholm, C. *FEBS Lett.* **1976**, *65,* 354-357.

(56) Hodis, H. N.; Mack, W. J.; Azen, S. P.; Alaupovic, P.; Pogoda, J. M.; LaBree, L.; Hemphill, L. C.; Dramsch, D. M.; Blankenhorn, D. H. *Circulation* **1994**, *90,* 42-49.

(57) Alaupovic, P.; Mack, W. J.; Knight-Gibson, C.; Hodis, H. N. *Arterioscler. Thromb. Vasc. Biol.* **1997**, *17*, 715-730.

(58) Sacks, F. M.; Alaupovic, P.; Moye, L. A.; Cole, T. G.; Sussex, B.; Stampfer, M. J.; Pfeffer, M. A.; Braunwald, E. *Circulation* **2000**, *102,* 1886-1892.

(59) Rall, S. C.; Weisgraber, K. H.; Mahley, R. W. *J. Biol. Chem.* **1982**, *257,* 4171-4178.

(60) Weisgraber, K. H.; Rall, S. C.; Mahley, R. W. *J. Biol. Chem.* **1981**, *256,* 9077-9083.

(61) Mahley, R. W.; Innerarity, T. L. *Biochim. Biophys. Acta* **1983**, *737*, 197-222.

(62) Kesaniemi, Y. A.; Ehnholm, C.; Miettinen, T. A. *Clin. Invest.* **1987**, *80,* 578-581.

(63) Mahley, R. W.; Weisgraber, K. H.; Innerarity, T. L. *Biochim. Biophys. Acta* **1979**, *575*, 81-91.

(64) Huang, Y.; Liu, X. Q.; Rall, S. C. *J. Biol. Chem.* **1998**, *273,* 26388-26393.

(65) Nakashima, Y.; Plump, S. S.; Raines, E. W. *Arterioscler. Thromb. Vasc. Biol.* **1994**, *14*, 133-140.

(66) Carlquist, J.; Anderson, J. L. *Curr. Opin. Cardiol.* **2007**, *22*, 352-358.

(67) Kwiterovich, J., P.O.; Cockrill, S. L.; Virgil, D. G.; Garrett, E. S.; Otvos, J. D.; Knight-Gibson, C.; Alaupovic, P.; Forte, T.; Zhang, L.; Farwig, Z. N.; Macfarlane, R. D. *JAMA* **2005**, *293*, 1891-1899.

(68) Koopmans, S. J.; Jong, M. C.; Que, I.; Dahlmans, V. E. H.; Pijl, H.; Radder, J. K.; Frolich, M.; Havekes, L. M. *Diabetologia* **2001**, *44*, 437-443.

(69) Ensign, W.; Hill, N.; Heward, C. B. *Clin. Chem.* **2006**, *52*, 1722-1727.

(70) Rainwater, D. L.; Andres, D. W.; Ford, A. L.; Lowe, W. F.; Blanche, P. J.; Krauss, R. M. *J. Lipid Res.* **1992**, *33*, 1876-1881.

(71) Georgieva, A. M.; van Greevenbroek, M. M. J.; Krauss, R. M.; Brouwers, M. C. G. J.; Vermeulen, V. M. M.-J.; Robertus-Teunissen, M. G.; van der Kallen, C. J. H.; de Bruin, T. W. A. *Arterioscler. Thromb. Vasc. Biol.* **2004**, *24*, 744-749.

(72) Hirany, S. V.; Othman, Y.; Kutscher, P.; Rainwater, D. L.; Jialal, I.; Devaraj, S. *Am. J. Clin. Pathol.* **2003**, *119*, 1-7.

(73) Kulkarni, K. R.; Garber, D. W.; Jones, M. K.; Segrest, J. P. *J. Lipid. Res.* **1995**, *36*, 2291-2302.

(74) Kulkarni, K. R.; Marcovina, S. M.; Krauss, R. M.; Garber, D. W.; Glasscock, A. M.; Segrest, J. P. *J. Lipid Res.* **1997**, *38*, 2353-2364.

(75) Blake, G. J.; Otvos, J. D.; Rifai, N.; Ridker, P. M. *Circulation* **2002**, *106*, 1930-1937.

(76) Tsai, M. Y.; Georgopoulos, A.; Otvos, J. D.; Ordovas, J. M.; Hanson, N. Q.; Peacock, J. M.; Arnett, D. K. *Clin. Chem.* **2004**, *50*, 1201-1204.

(77) Lounila, J.; Ala-Korpela, M.; Jokisaari, J. *Phys. Rev.* **1994**, *72*, 4049-4052.

(78) Friedewald, W. T.; Levy, R. I.; Fredrickson, S. D. *Clin. Chem.* **1972**, *18*, 499-502.

(79) Freifelder, D. M. In *Principles of Physical Chemistry With Applications to the Biological Sciences 2nd Edition*; Jones and Bartlett Publishers, Inc.: Portola Valley, CA, 1984, pp 495-565.

(80) Atkins, P. In *Physical Chemistry, 6th Edition*; W. H. Freeman & Co.: New York, 1998, pp 686-689.

(81) Swinkels, D. W.; Hak-Lemmers, H. L.; Demacker, P. N. *J. Lipid Res.* **1987**, *28*, 1233-1239.

(82) Bozoky, Z.; Fulop, L.; Kohidai, L. *Fur. Biophys. J.* **2001**, *29*, 621-627.

(83) Luchansky, J. B.; dePasquale, D. A.; Hehl, G. L. *Biotechniques* **1991**, *11*, 336-338.

(84) Muratsugu, M. *J. Health Sci.* **2005**, *51*, 584-589.

(85) Rickwood, D.; Ford, T.; Graham, J. *Anal. Biochem* **1982**, *123*, 23-31.

(86) Nielsen, S. U.; Bassendine, M. F.; Alastair, D. B.; Martin, C.; Pumeechockchai, W.; Toms, G. L. *J. Virology* **2006**, *80,* 2418-2428.

(87) Okazaki, M.; Usui, S.; Fukui, A.; Kubota, I.; Tomoike, H. *Clin. Chem.* **2006**, *52*, 2049-2053.

(88) Fisher, R. A. *Annals of Eugenics* **1936**, *7*, 179-188.

(89) Truett, J.; Cornfield, J.; Kannel, W. *J. Chron. Dis.* **1967**, *20*, 511-524.

(90) Sheather, S. J.; McKean, J. W.; Crimin, K. *Comput Stat Data An* **2007, in press**.

(91) Cook, R. D.; Yin, X. *Aust. NZ J. Stat.* **2001**, *43,* 147-199.

(92) Park, Z.; Russell, D. H. *Anal. Chem.* **2001**, *73*, 2558-2564.

(93) Ruotolo, B. T.; Gillig, K. J.; Stone, E. G.; Russell, D. H.; Fuhrer, K.; Gonin, M.; Schultz, J. A. *IJMS* **2002**, *219,* 253-267.

(94) Ruotolo, B. T.; Verbeck, G. F.; Thomson, L. M.; Woods, A. S.; Gillig, K. J.; Russell, D. H. *J. Prot. Res.* **2002**, *1,* 303-306.

(95) Ruotolo, B. T.; Gillig, K. J.; Woods, A. S.; Egan, T. F.; Ugarov, M. V.; Schultz, J. A.; Russell, D. H. *Anal. Chem.* **2004**, *76*, 6727-6733.

(96) Karas, M.; Hillenkamp, F. *Anal. Chem.* **1988**, *60*, 2299-2301.

(97) Karas, M.; Bachmann, D.; Bahr, U.; Hillenkamp, F. *Int. J. Mass Spectrom. Ion. Processes* **1987**, *78*, 53-68.

(98) Zenobi, R.; Knochenmuss, R. *Mass Spectrom. Rev.* **1988**, *17*, 337-366.

(99) Karas, M.; Gluckman, M.; Schafer, J. *J. Mass Spectrom.* **2000**, *35*, 1-12.

(100) Hillenkamp, F.; Karas, M.; Beavis, R. C.; Chait, B. T. *Anal. Chem.* **1991**, *63*, 1193A-1202A.

(101) Noble, D. *Anal. Chem.* **1995**, *67*, 497A.

(102) Kinsel, G. R.; Gimon-Kinsel, M.; Gillig, K. J.; Russell, D. H. *J. Mass Spectrom.* **1999**, *34,* 684-690.

(103) Wiley, W. C.; Maclaren, I. H. *Rev. Sci. Instr.* **1955**, *26*, 1150-1157.

(104) Brown, R. S.; Lennon, J. J. *Anal. Chem.* **1995**, *67*, 1998-2003.

(105) Mamyrin, B. A.; Karataev, V. I.; Shmikk, D. V.; Zagulin, V. A. *Zhurnal Eksperimental'noi i Teoreticheskoi Fiziki* **1973**, *64*, 82-89.

(106) Vestal, M. L.; Juhasz, P.; Martin, S. A. *Rap. Commun. Mass Spectrom.* **1995**, *9*, 1044-1050.

(107) Gimon-Kinsel, M.; Preston-Schaffter; Kinsel, G. R.; Russell, D. H. *J. Am. Chem. Soc.* **1997**, *199,* 2534-2540.

(108) Skoog, D. A.; Holler, J. F.; Nieman, T. A. In *Principles of Instrumental Analysis, 5th Edition*; Harcourt Brace & Company: Orlando, Florida, 1998, pp 498-532.

(109) Beavis, R. C.; Chaudhary, T.; Chait, B. T. *Org. Mass Spectrom.* **1992**, *27*, 156-158.

(110) Vorm, O.; Roepstorff, P.; Mann, M. *Anal. Chem.* **1994**, *66*, 3281-3287.

(111) Bonk, T.; Humeny, A. *Neuroscientist* **2001**, *7*, 6-12.

(112) Arpino, P.; Inc., J. W. S., Ed., 1992; Vol. 11, pp 3-40.

(113) Arpino, P.; Inc., J. W. S., Ed., 1989; Vol. 8, pp 35-55.

(114) Murray, K. K.; Inc., J. W. S., Ed., 1998; Vol. 16, pp 283-299.

(115) Skoog, D. A.; Holler, J. F.; Nieman, T. A. In *Principles of Instrumental Analysis, 5th Edition*; Harcourt Brace & Company: Orlando, Florida, 1998, pp 725-765.

(116) Vestal, M. L. *Anal. Chem.* **1983**, *55* (11), 1741.

(117) Bakhtiar, R.; Hofstadler, A.; Smith, R. D. *J. Chem. Educ.* **1996**, *73,* A118-A123.

(118) Taylor, G. I. *Proc. R. Soc. A.* **1964**, *280,* 383.

(119) Kebarle, P. *J. Mass Spectrom.* **2000**, *35,* 804-817.

(120) Tadey, T.; Purdy, W. *J. Chrom. B.* **1995**, *671,* 237-253.

(121) Skoog, D. A.; Holler, J. F.; Nieman, T. A. In *Principles of Instrumental Analysis, 5th Edition*; Harcourt Brace & Company: Orlando, Florida, 1998, pp 778-795.

(122) Williams, R. L.; Vigh, G. *J. Chrom. A* **1996**, *730,* 273-278.

(123) Williams, R. L.; Childs, B.; Dose, E. V.; Guiochon, G.; Vigh, G. *Anal. Chem.* **1997**, *69*, 1347-1354.

(124) Williams, R. L.; Childs, B.; Dose, E. V.; Guiochon, G.; Vigh, G. *J. Chrom. A* **1997**, *781,* 107-112.

(125) Lauer, H. H.; McManigill, D. *Anal. Chem.* **1989**, *58*, 166-170.

(126) Muijselaar, W. G.; de Bruin, C. H.; Everaerts, F. M. *J. Chrom.* **1992**, *605,* 115-123.

(127) McCormick, R. M. *Anal. Chem.* **1988**, *60*, 2322-2328.

(128) Tadey, T.; Purdy, W. *J. Chrom. A.* **1993**, *652,* 131-138.

(129) Tadey, T.; Purdy, W. *J. Chrom.* **1992**, *583,* 111-115.

(130) Bjellqvist, B.; Hughes, G. J.; Pasquali, C.; Paquet, N.; Ravier, F.; Sanchez, J. C.; Frutiger, S.; Hochstrasser, D. F. *Electrophoresis* **1993**, *14,* 1023-1031.

(131) Tanford, C. *Adv. Protein Chem.* **1968**, *23,* 121-282.

(132) Ui, N. *Biochim. Biophys. Acta* **1971**, *229,* 567-581.

(133) Helenius, A.; Simons, K. *Biochim. Biophys. Acta* **1975**, *415,* 29-79.

(134) Robinson, N. C.; Tanford, C. *Biochemistry* **1975**, *14*, 369-378.

(135) Strahler, J.; Hanash, S. M.; Somerlot, L.; Bjellqvist, B.; Gorg, A. *Electrophoresis* **1988**, *9,* 74-80.

(136) Rifai, N. *Arch. Path. Lab. Med.* **1986**, *110,* 694-701.

(137) Guzman, N. A. *Anal. Chem.* **2005**, *77,* 60A-67A.

(138) Beavis, R. C.; Chait, B. T. *Proc. Nat. Acad. Sci.* **1990**, *87,* 6873-6877.

(139) Bondarenko, P. V., Texas A&M University, College Station, TX, 1998.

(140) Bondarenko, P. V.; Farwig, Z. N.; McNeal, C. J.; Macfarlane, R. D. *Int. J. of Mass. Spec.* **2002**, *319*, 671-680.

(141) Farwig, Z. N., Texas A&M University, College Station, TX, 2002.

(142) Farwig, Z. N.; McNeal, C. J.; Little, D.; Baisden, C. E.; Macfarlane, R. D. *Biochem. Biophys. Res. Commun.* **2005**, *332*, 352-356.

(143) Bondarenko, P. V.; Cockrill, S. L.; Watkins, L. K.; Cruzado, I. D.; Macfarlane, R. D. *J. Lipid Res.* **1999**, *40*, 543-555.

(144) von Eckardstein, A.; Walter, M.; Holz, H.; Benninghoven, A.; Assmann, G. J.; Roetrige, A.; Kock, R. *J. Lipid Res.* **1991**, *32,* 1465-1476.

(145) Anantharamaiah; Hughes, G. M.; Iqbal, M.; Gawish, A.; Nearne, P. J.; Medley, M. F.; Segrest, J. P. *J. Lipid Res.* **1998**, *39,* 309-318.

(146) Pankhurst, G.; Wang, X. L.; Wilcken, D. E.; Baernthaler, G.; Panzenbock, U.; Raftery, M.; Stocker, R. *J. Lipid Res.* **2003**, *44,* 349-355.

(147) Pazenbock, U.; Kritharides, L.; Faftery, M.; Rye, K. A.; Stocker, R. *J. Biol. Chem.* **2000**, *275,* 19536-19544.

(148) Sommer, U.; Herscovitz, H.; Welty, F.; Costello, C. *J. Lipid Res.* **2006**, 47, 804-814.

(149) Hayakawa, J.; Okabayashi, Y. *J. Liquid Chrom. & Rel. Tech.* **2005**, *28,* 1473-1485.

(150) Hayakawa, J.; Ono, T.; Hanasaki, K.; Okabayashi, Y. *Analytical Letters* **2006**, *39,* 957-972.

(151) Yamaguchi, T.; Miyamoto, K.; Yagi, S.; Horgane, A.; Sato, M.; Takeuchi, M. *Fisheries Science* **2001**, *67,* 200-202.

(152) Pruzanski, W.; Lambeau, L.; Lazdunsky, M.; Cho, W.; Kopilov, J.; Kuksis, A. *Biochim. Biophys. Acta* **2005**, *1736*, 38-50.

(153) Urpi-Sarda, M.; Jauregui, O.; Lamuela-Raventos, R. M.; Jaeger, W.; Miksits, M.; Covas, M.; Andres-Lacueva, C. *Anal. Chem.* **2005**, *77*, 3149-3155.

(154) de la Torre-Carbot, K.; Chavez-Servin, J. L.; Jauregui, O.; Castellote, A. I.; Lamuela-Raventos, R. M.; Fito, M.; Covas, M.; Munoz-Aguayo, D.; Lopez-Sabater, M. C. *Analytica. Chimica Acta* **2007**, *583,* 402-410.

(155) Obama, T.; Kato, R.; Masuda, Y.; Takahashi, K.; Aiuchi, T.; Itabe, H. *Proteomics* **2007**, *7,* 2132-2141.

(156) Heller, M.; Stalder, D.; Schlappritzi, E.; Hayn, G.; Matter, U.; Haeberli, A. *Proteomics* **2005**, *5*, 2619-2630.

(157) Kay, R. G.; Gregory, B.; Grace, P. B.; Pleasance, S. *Rap. Commun. Mass Spectrom.* **2007**, *21,* 2858-2593.

(158) Mukhodaphyay, R. *Anal. Chem.* **2006**, *78*, 2109-2111.

(159) Schmitz, G.; Borgmann, U.; Assmann, G. J. *J. Chrom.* **1985**, *320*, 253-262.

(160) Hu, A. Z.; Cruzado, I. D.; Hill, J. W.; McNeal, C. J.; Macfarlane, R. D. *J. Chrom. A* **1995**, *717*, 33-39.

(161) Stocks, J.; Nanjee, M. N.; Miller, N. E. *J. Lipid Res.* **1998**, *39*, 218-227.

(162) Peterson, J. R.; Okorodudu, A. O.; Mohammad, A.; Payne, D. A. *Clin. Chim. Acta.* **2003**, *330,* 1-30.

(163) Stocks, J.; Miller, N. E. *J. Lipid Res.* **1998**, *39,* 1305-1309.

(164) Bon, G. B.; Cazzolato, G. *J. Lipid Res.* **1999**, *40,* 170-177.

(165) Schmitz, G.; Mollers, C. *Electrophoresis* **1994**, *15,* 31-39.

(166) Nowicka, G.; Bruning, T.; Grothaus, B.; Kahl, G.; Schmitz, G. *J. Lipid Res.* **1990**, *31,* 1173-1186.

(167) Cruzado, I. D.; Song, S.; Crouse, S. F.; O'Brien, B. C.; Macfarlane, R. D. *Anal. Biochem.* **1996**, *243*, 100-109.

(168) Neuhoff, V.; Stamm, R.; Eibl, H. *Electrophoresis* **1985**, *6,* 427-448.

(169) Patestos, N. P.; Fauth, M.; Radola, B. J. *Electrophoresis* **1988**, *9,* 488-496.

(170) Sprecher, D. L.; Taam, L.; Brewer Jr., H. B. *Clin. Chem.* **1984**, *30,* 2084-2092.

(171) Haase, R.; Menke-Mollers, I.; Oette, K. *Electrophoresis* **1988**, *9,* 569-575.

(172) Baumstark, M. W.; Berg, A.; Halle, M.; Keul, J. *Electrophoresis* **1988**, *9,* 576-579.

(173) Golaz, O.; Sanches, J.-C.; James, R. W.; Hochstrasser, D. F. *Electrophoresis* **1995**, *16,* 1184-1186.

(174) Holmquist, L. *Electrophoresis* **1998**, *19,* 511-513.

(175) Contiero, E.; Ferrari, R.; Vaselli, G. M.; Folin, M. *Electrophoresis* **1997**, *18,* 122-126.

(176) Campbell-Melnichenko, A. V., Texas A&M University, 2001.

(177) Kohlmeir, M.; Sinha, E.; Kottgen, E.; Righetti, P. G. *Protid. Biol. Fluids* **1989**, *36,* 437-444.

(178) Karlsson, H.; Leanderson, P.; Tagesson, C.; Lindahl, M. *Proteomics* **2005**, *5,* 551-565.

(179) Farwig, Z. N.; Campbell, A. V.; Macfarlane, R. D. *Anal. Chem.* **2003**, *75*, 3823-3830.

(180) Cruzado, I. D.; Hu, A. Z.; Macfarlane, R. D. *J. Cap. Elec.* **1996**, *1*, 25-29.

(181) Watkins, L. K.; Bondarenko, P. V.; Barbacci, D. C.; Song, S.; Cockrill, S. L.; Russell, D. H.; Macfarlane, R. D. *J. Chrom. A* **1999**, 183-189.

(182) Warnick, G. R.; Benderson, J.; Albers, J. J. *Clin. Chem.* **1982**, *28,* 1379-1388.

(183) Smith, P. K. *Anal. Biochem* **1985**, *150*, 76-85.

(184) http://cbsu.tc.cornell.edu/vanwijk/images/massspec/massspec_schem_maldi.gif.

(185) Biosystems, A.: Foster City, CA, 2004.

(186) Kolmakova, A.; Kwiterovich, J., P.O.; Virgil, D. G.; Alaupovic, P.; Knight-Gibson, C.; Martin, S. F.; Chatterjee, S. *Arterioscler. Thromb. Vasc. Biol.* **2004**, *24*, 264-269.

(187) Oldenburg, K.; Vogler, A. *Z. Naturforsch.* **1993**, *48b*, 1519-1523.

(188) Oldenburg, K.; Vogler, A. *J. Organomet. Chem.* **1996**, *515*, 245-248.

(189) Busenlehner, L. S.; Cosper, N. J.; Scott, R. A.; Rosen, B. P.; Wong, M. D.; Giedroc, D. P. *Biochemistry* **2001**, *40*, 4426-4436.

(190) Busenlehner, L. S.; Apuy, J. L.; Giedroc, D. P. *J. Biol. Inorg. Chem.* **2002**, *7*, 551-559.

(191) Harris, D. C. In *Quantitative Chemical Analysis*; W.H. Freeman & Co.: New York, 2003, pp 258-282.

(192) Ramachandram, B.; Samanta, A. *J. Phys. Chem. A* **1998**, *102*, 10579-10587.

(193) Lytton, S. D.; Mester, B.; Libman, J.; Shanzer, A.; Cabantchik, Z. I. *Anal. Biochem* **1992**, *205*, 326-333.

(194) De Costa, M. D. P.; Jayasinghe, W. A. P. A. *J. Photochem. Photobiol.* **2004**, *162,* 591-598.

(195) Hariharan, C.; Vijaysree, V.; Mishra, A. K. *J. Lumin.* **1997**, *75,* 205-211.

(196) Martell, A. E.; Smith, R. M. In *Critical Stability Constants*; Plenum: New York, 1974; Vol. 1, pp 204-211.

(197) Strachan, A. F.; Brandt, W. F.; Woo, P.; Van der Westhuyzen, D. R.; Coetzee, G. A.; DeBeer, M. C.; Shephard, E. G.; DeBeer, F. C. *J. Biol. Chem.* **1989**, *264,* 18368-18373.

(198) Whitehead, A. S.; DeBeer, M. C.; Steel, D. M.; Rits, M.; Lelias, J. M.; Lane, W. S.; DeBeer, F. C. *J. Biol. Chem.* **1992**, *267,* 3862-3867.

(199) de Hoffman, E.; Stroobant, V.; *Mass Spectrometry (Principles and Applications) 2nd Edition*; John Wiley & Sons, 2001, pp 37.

(200) Rifai, N.; Warnick, G. R.; Dominiczak, M. H.; *Handbook of Lipoprotein Testing*; Rifai, N., Warnick, G. R., Dominiczak, M. H., Eds.: Washington, D.C., 1997, pp 1-24.

(201) Barbacci, L. K., Texas A&M, College Station, 2000.

(202) Rifai, N.; Warnick, G. R.; Dominiczak, M. H.; *Handbook of Lipoprotein Testing*; Press, A., Ed., 1997, pp 12-13.

(203) Khan, B. V.; Harrison, D. G.; Olbrych, M. T.; Alexander, R. W.; Medford, R. M. *PNAS USA* **1996**, *93,* 9114-9119.

APPENDIX A

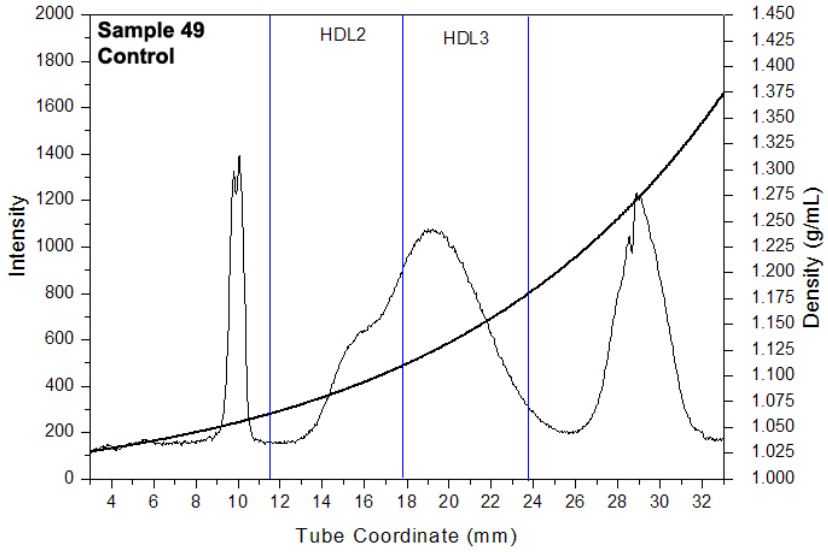

Figure A1. Lipoprotein Density Profile of Sample #49 in a 0.2000M Solution of NaBiY, Spun for 6 Hours at 120,000 RPM and 5ºC after DS Precipitation

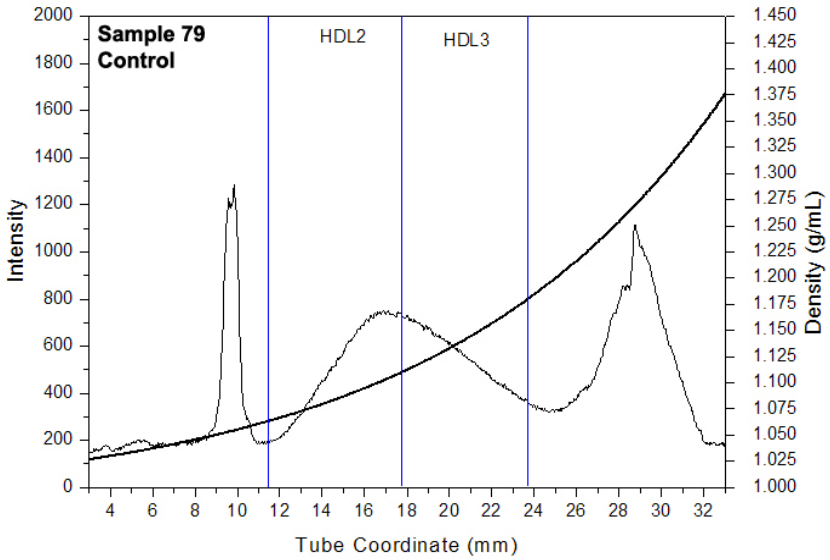

Figure A2. Lipoprotein Density Profile of Sample #79 in a 0.2000M Solution of NaBiY, Spun for 6 Hours at 120,000 RPM and 5ºC after DS Precipitation

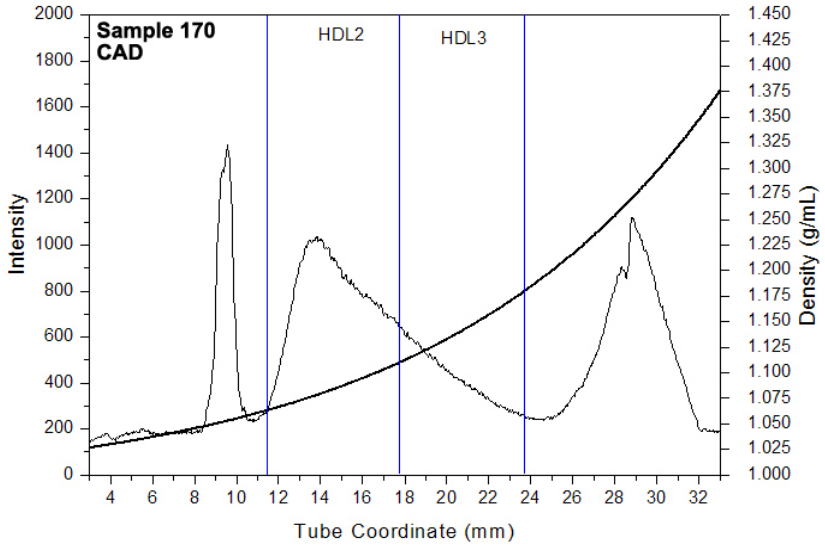

Figure A3. Lipoprotein Density Profile of Sample #170 in a 0.2000M Solution of NaBiY, Spun for 6 Hours at 120,000 RPM and 5ºC after DS Precipitation

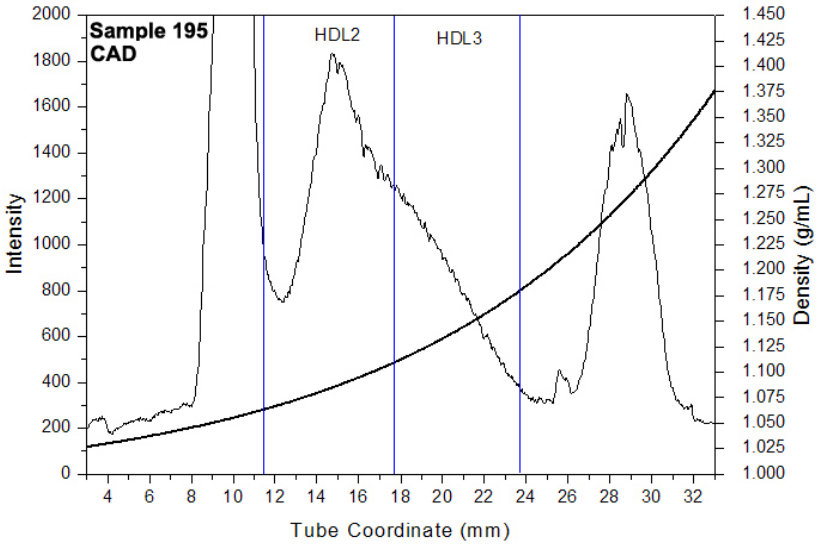

Figure A4. Lipoprotein Density Profile of Sample #195 in a 0.2000M Solution of NaBiY, Spun for 6 Hours at 120,000 RPM and 5ºC after DS Precipitation

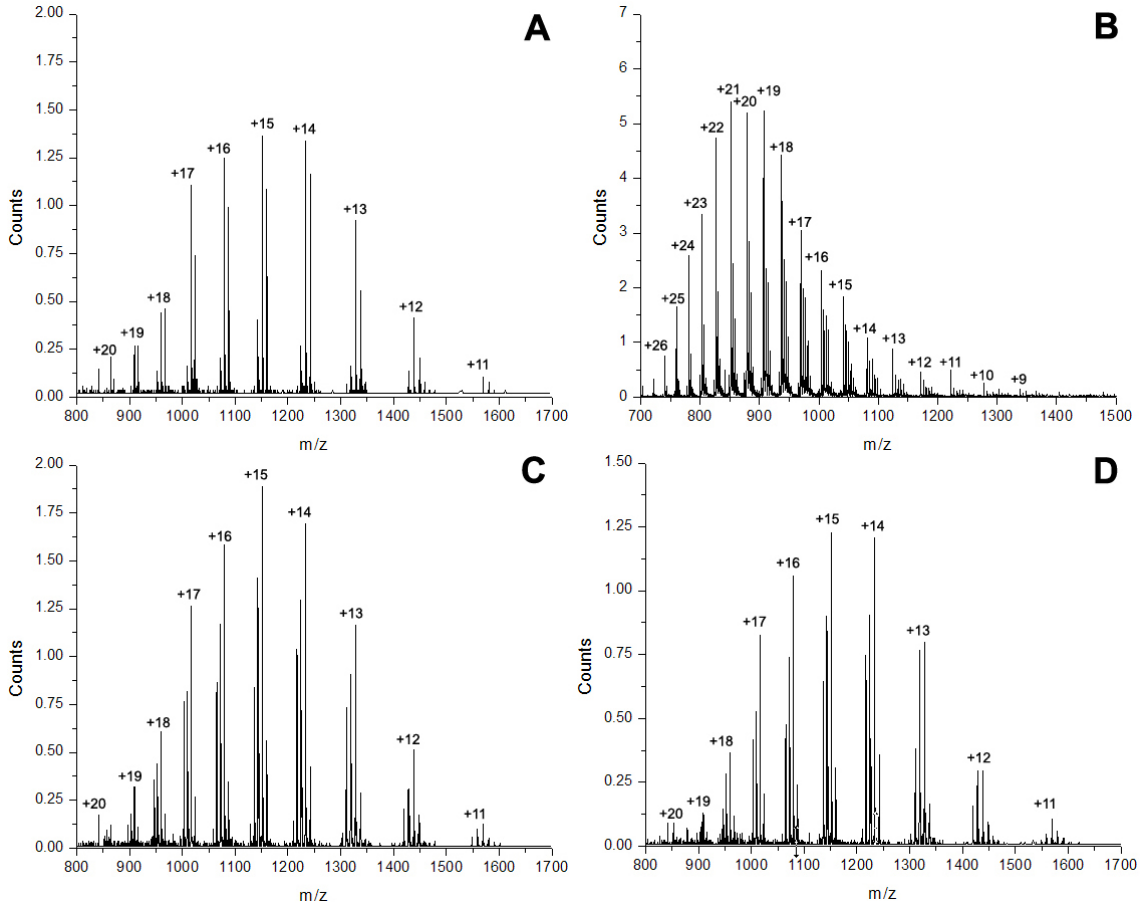

Figure A5. ESI Spectra of Apo A-II for (A) CAD HDL-2, (B) CAD HDL-3, (C) Control HDL-2, and (D) Control HDL-3

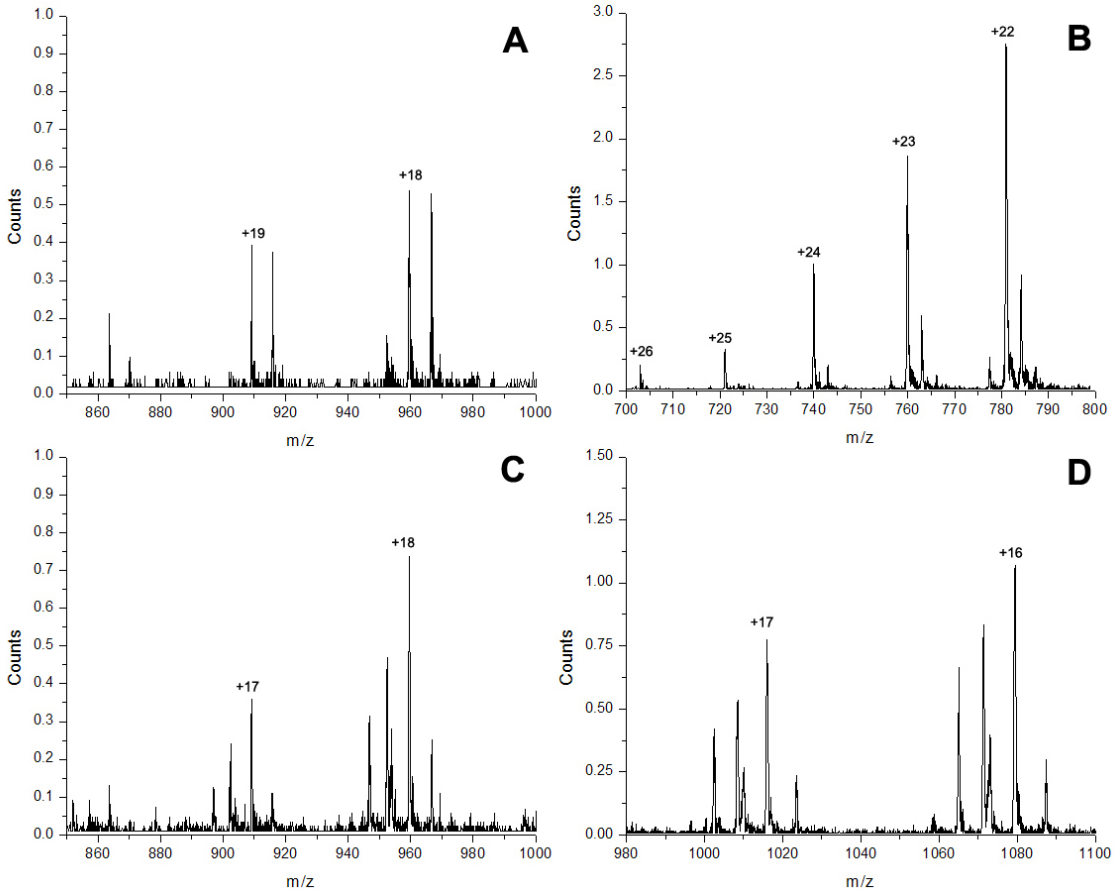

Figure A6. ESI Spectra High Charge States of Apo A-II for (A) CAD HDL-2, (B) CAD HDL-3, (C) Control HDL-2, and (D) Control HDL-3

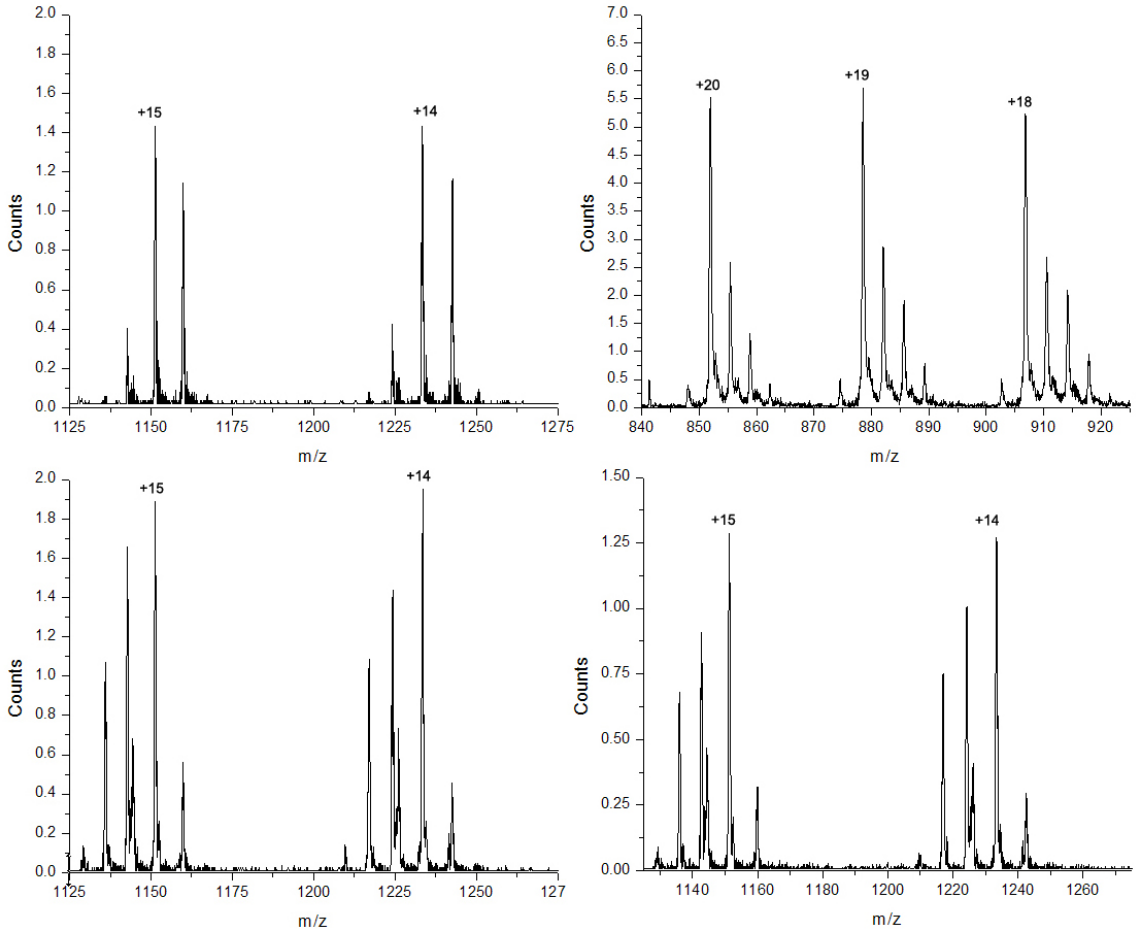

Figure A7. ESI Spectra Most Prominent Charge States of Apo A-II for (A) CAD HDL-2, (B) CAD HDL-3, (C) Control HDL-2, and (D) Control HDL-3

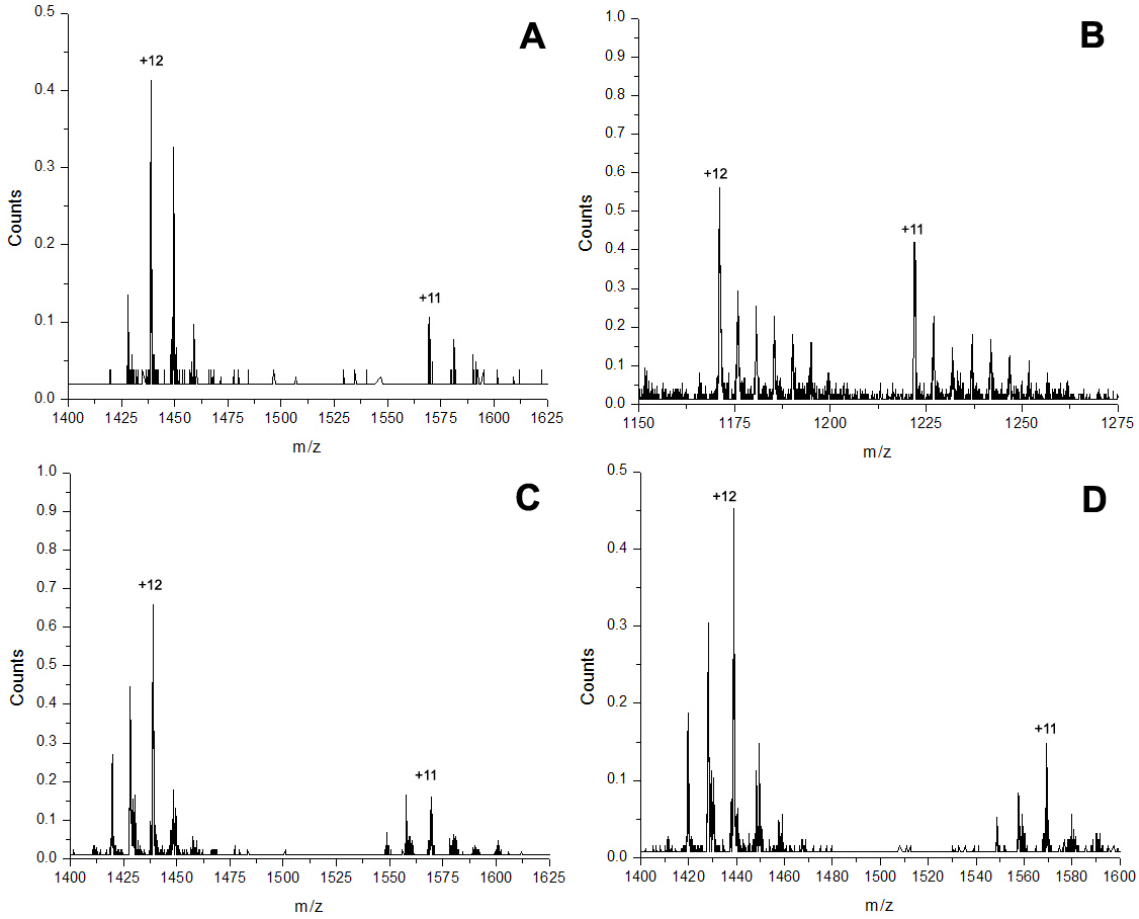

Figure A8. ESI Spectra Low Charge States of Apo A-II for (A) CAD HDL-2, (B) CAD HDL-3, (C) Control HDL-2, and (D) Control HDL-3

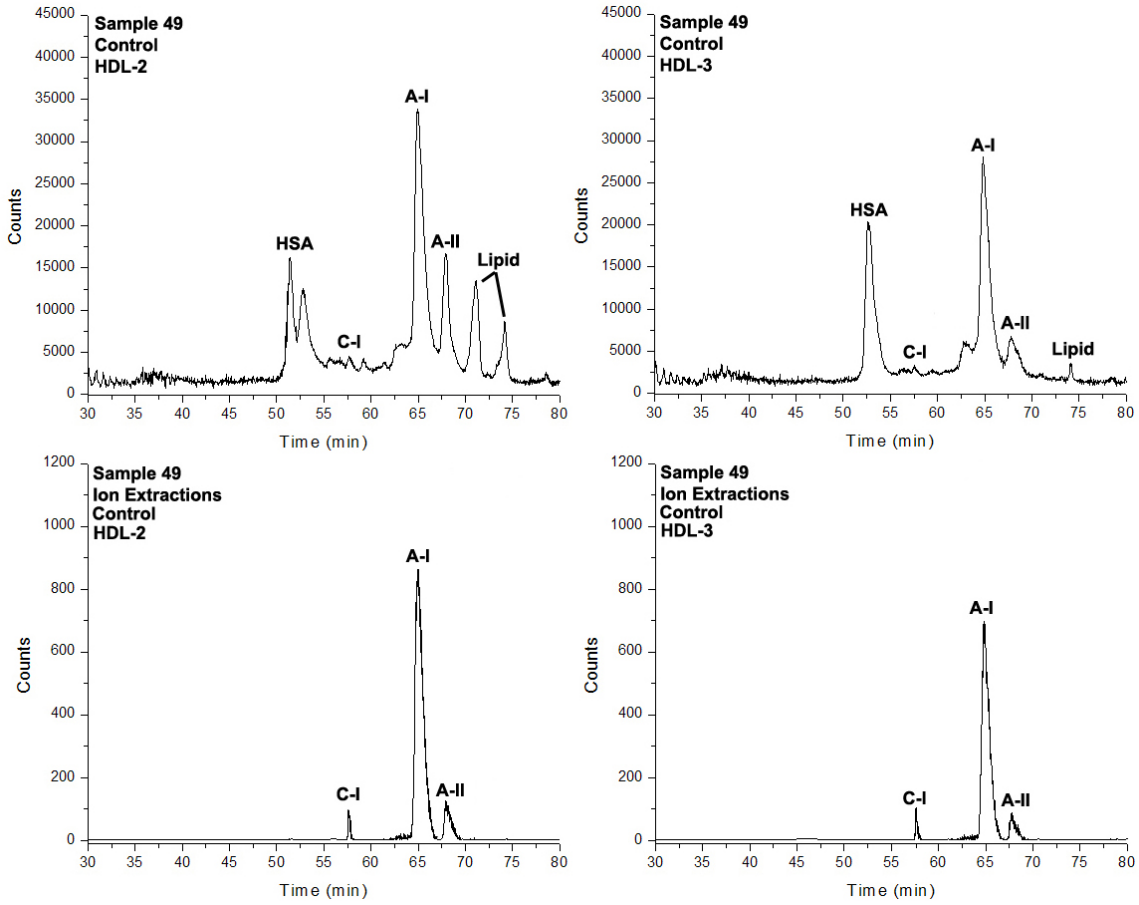

Figure A9. LC Total Ion Current for Sample 49

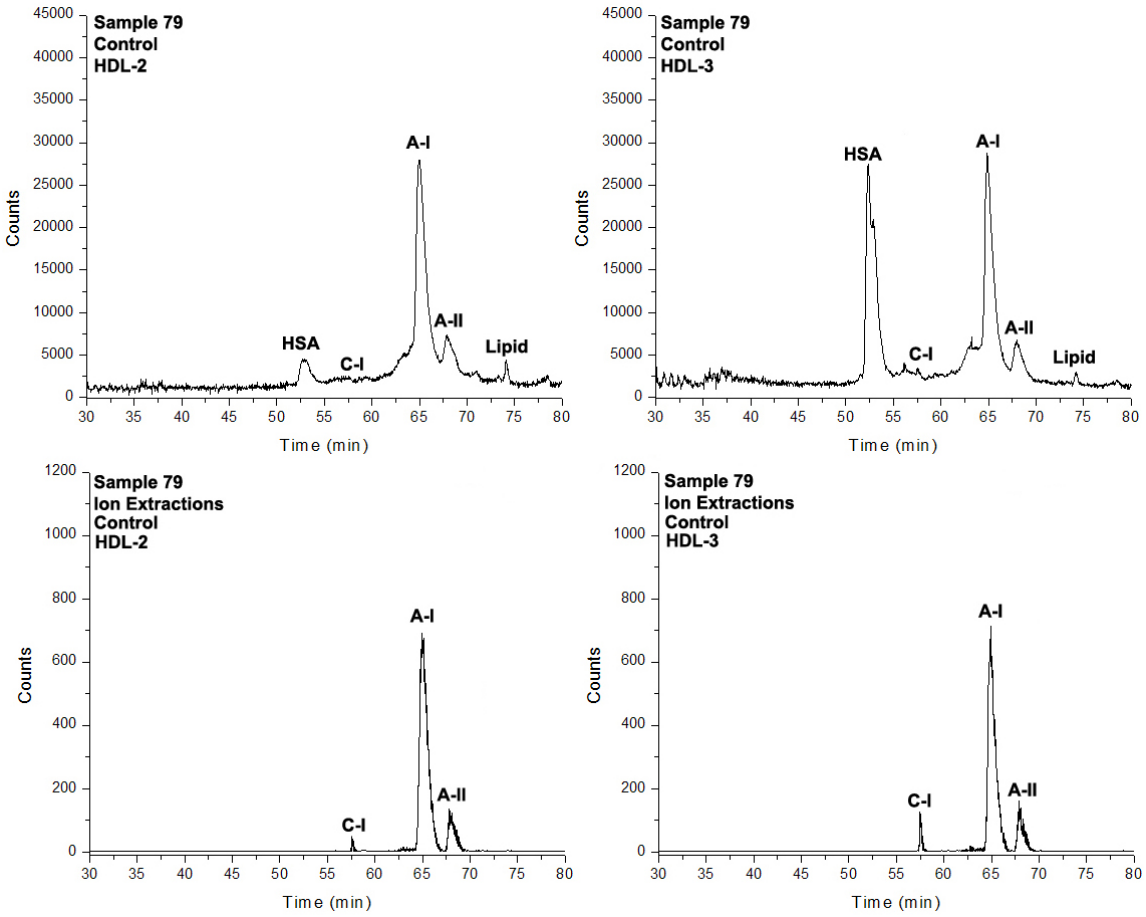

Figure A10. LC Total Ion Current for Sample 79

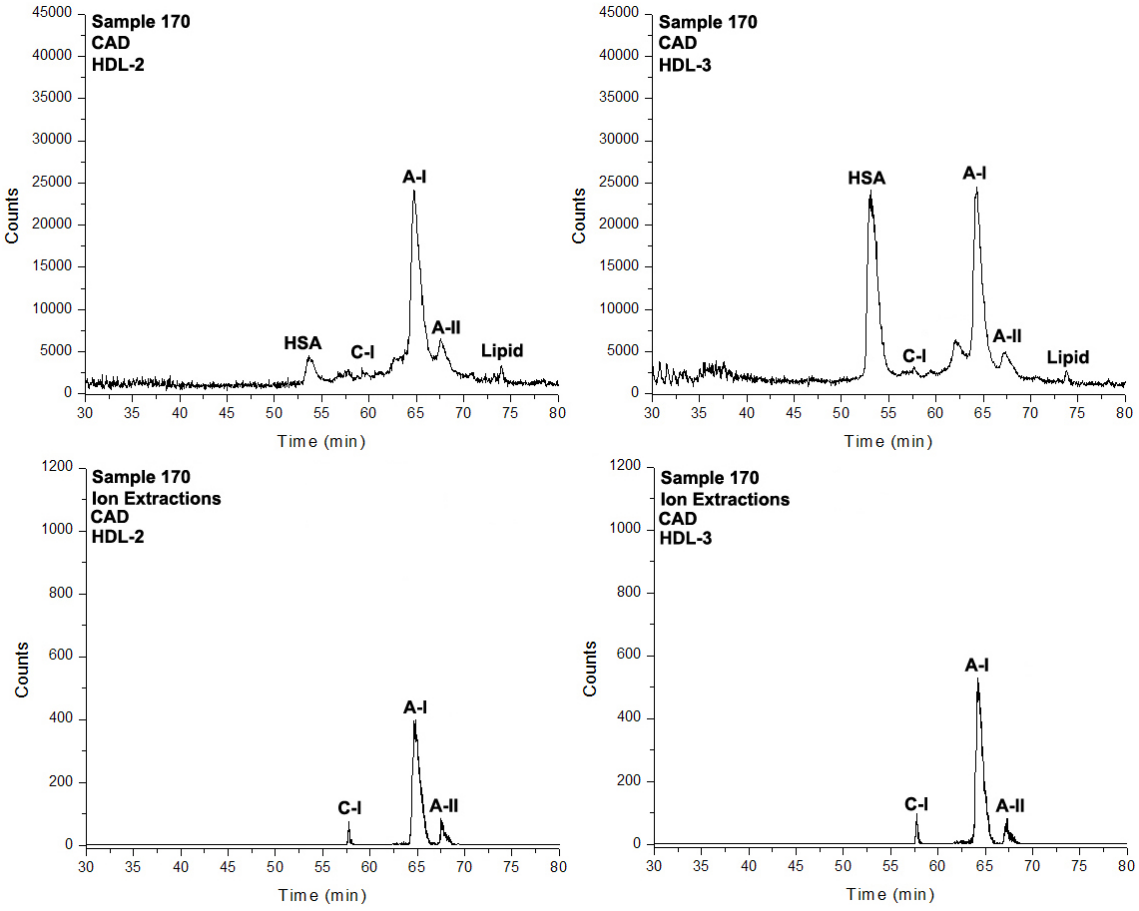

Figure A11. LC Total Ion Current for Sample 170

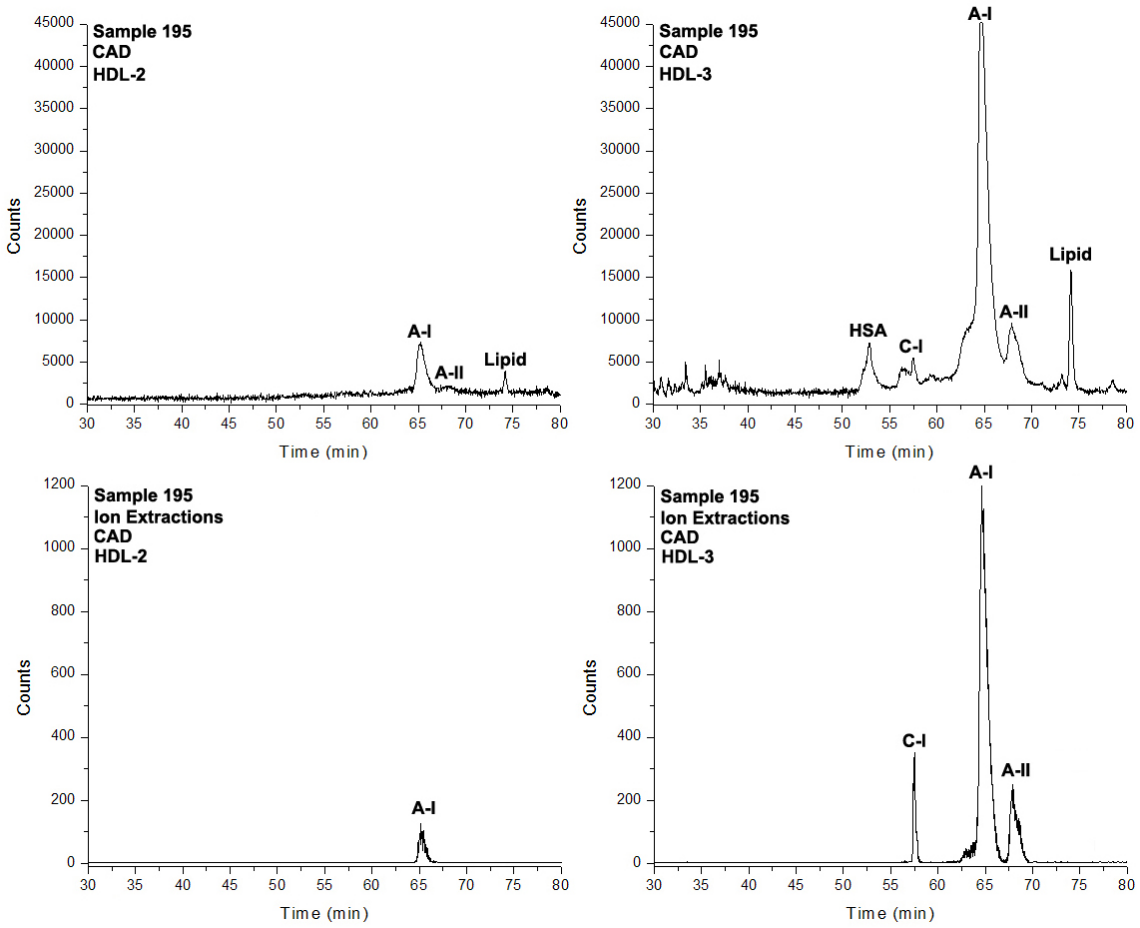

Figure A12. LC Total Ion Current for Sample 195

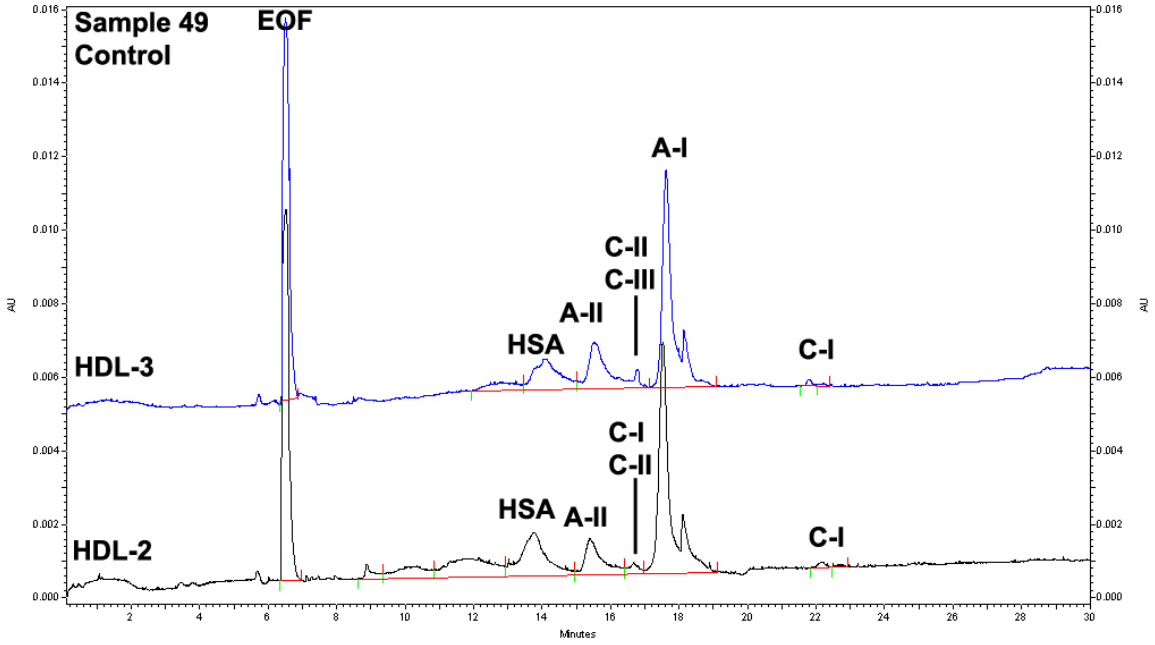

Figure A13. Electropherograms of HDL Fractions for Sample #49

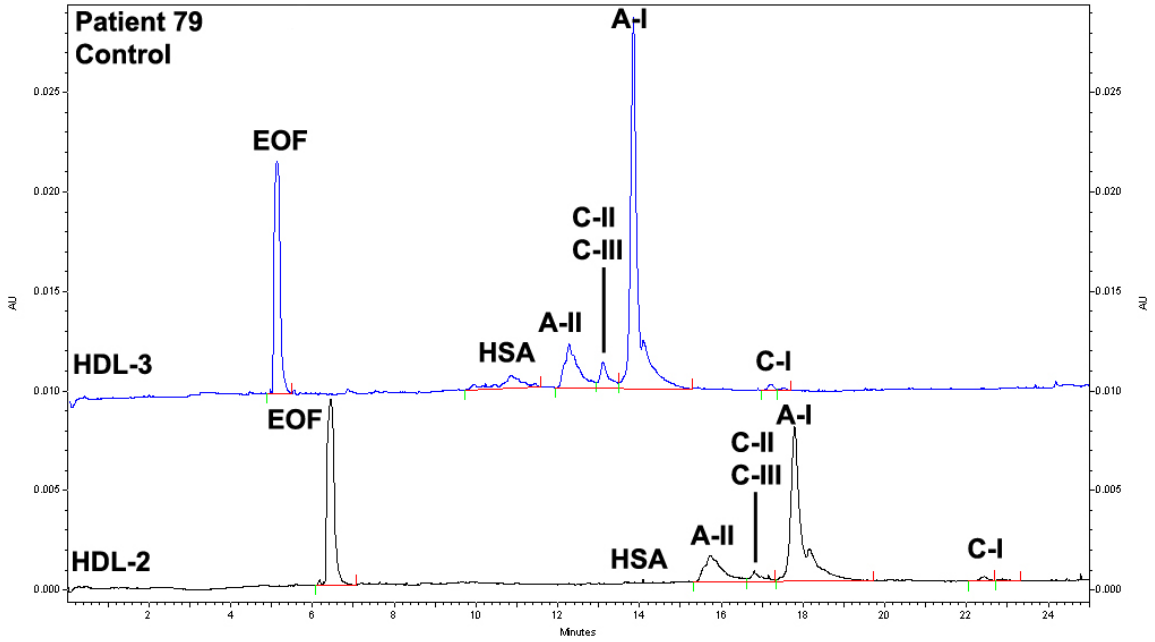

Figure A14. Electropherograms of HDL Fractions for Sample #79

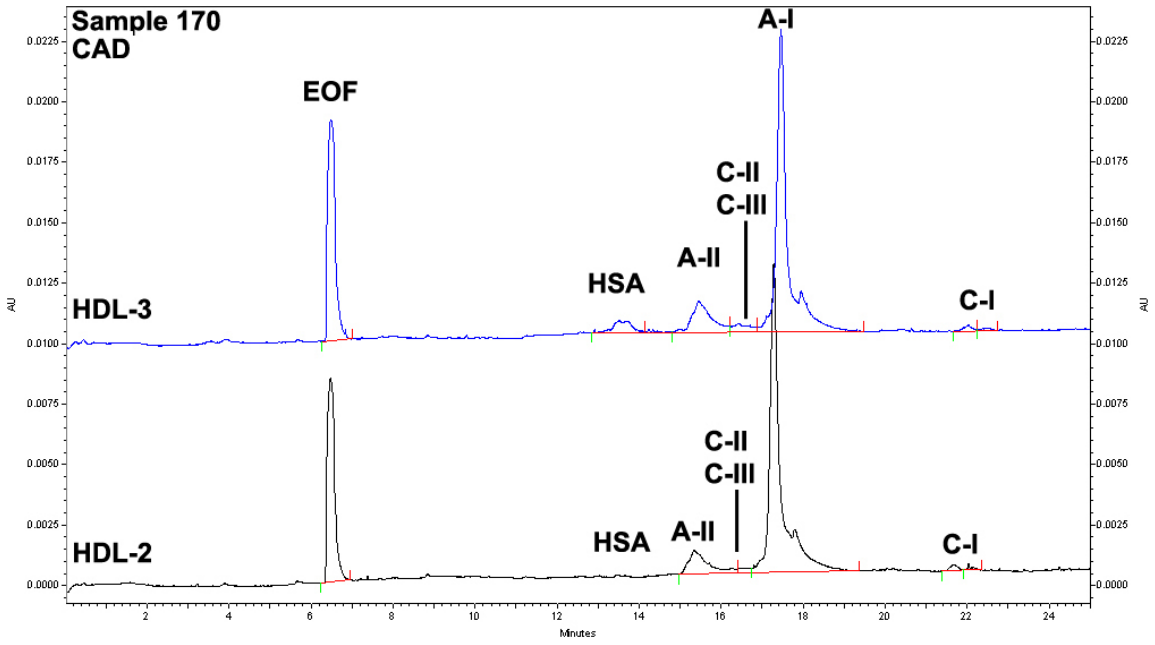

Figure A15. Electropherograms of HDL Fractions for Sample #170

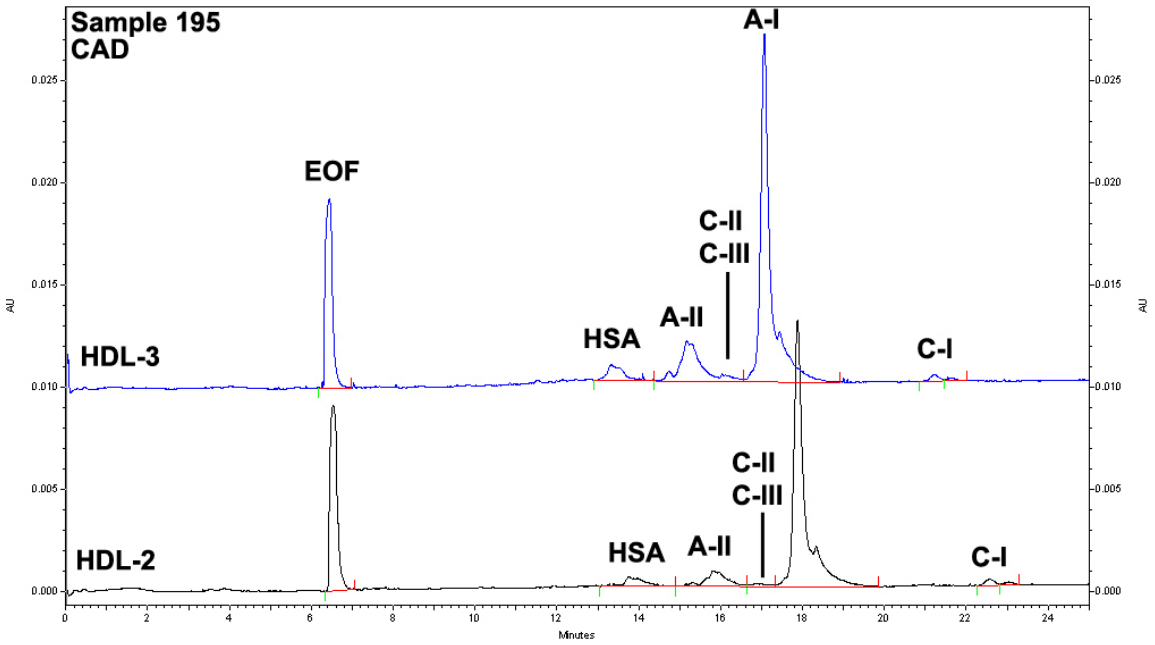

Figure A16. Electropherograms of HDL Fractions for Sample #195

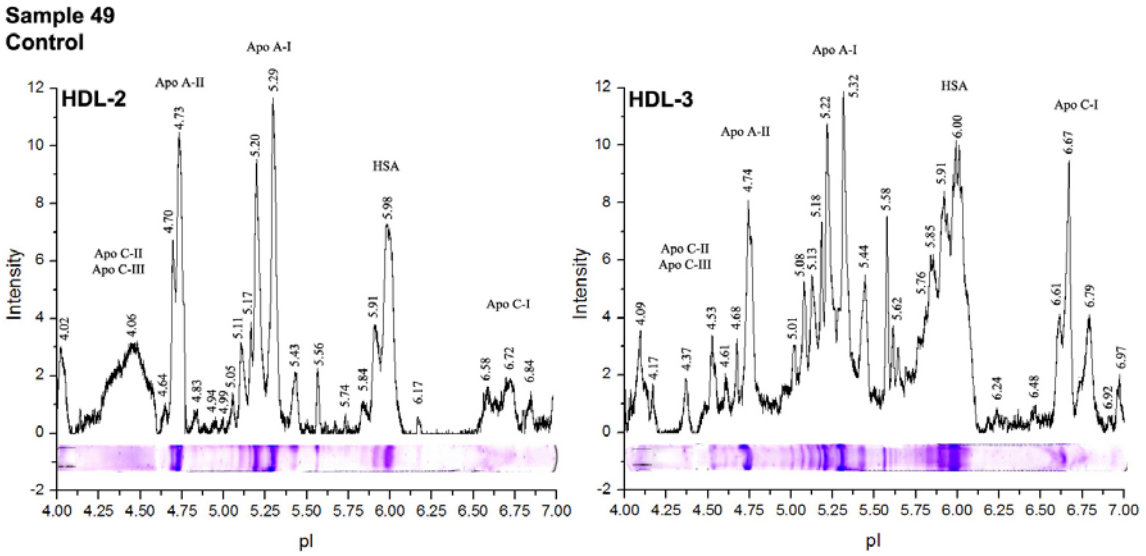

Figure A17. pI Values for Sample #49

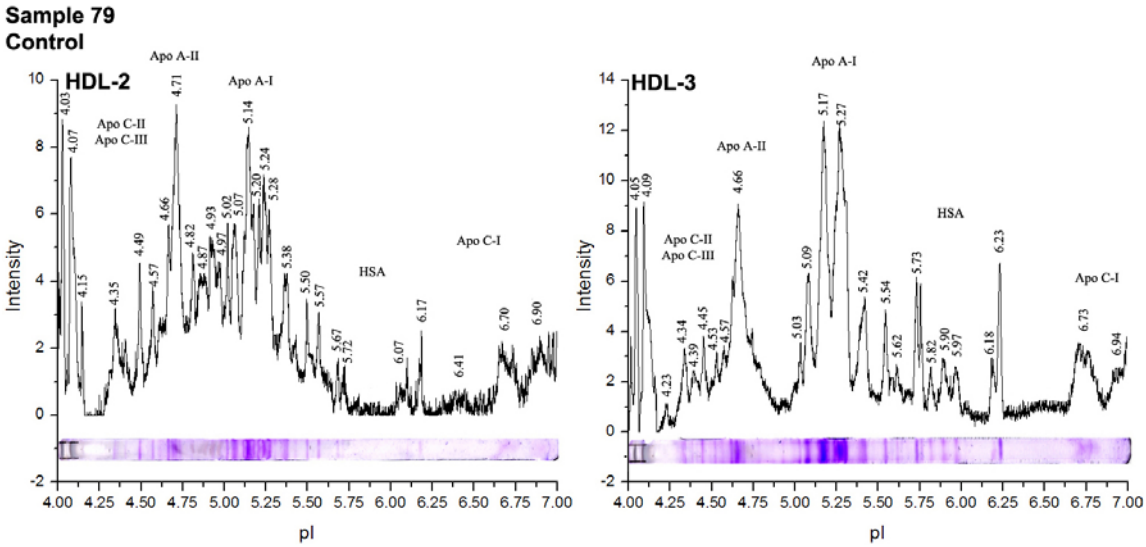

Figure A18. pI Values for Sample #79

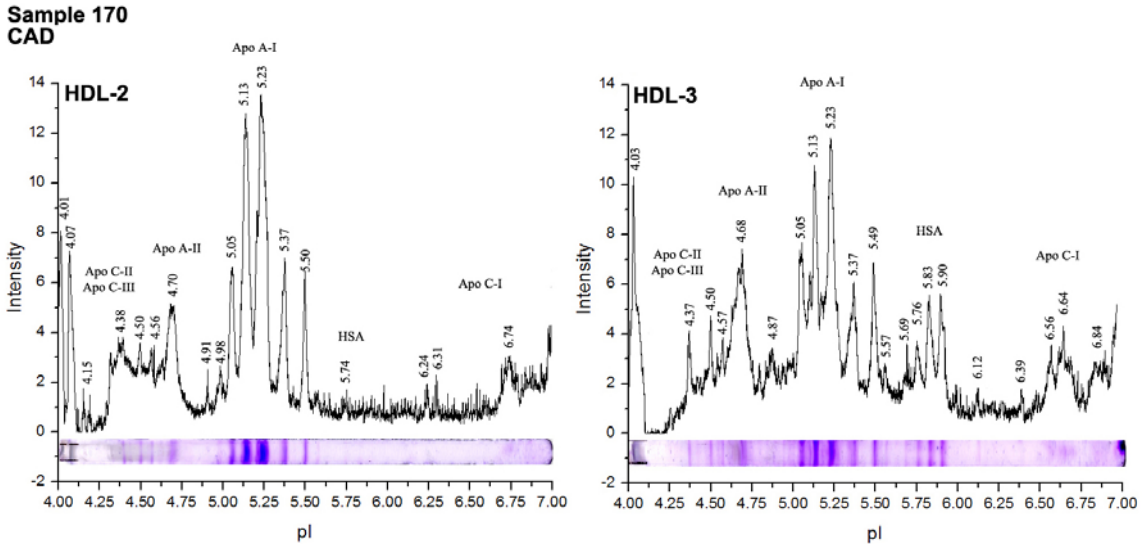

Figure A19. pI Values for Sample #170

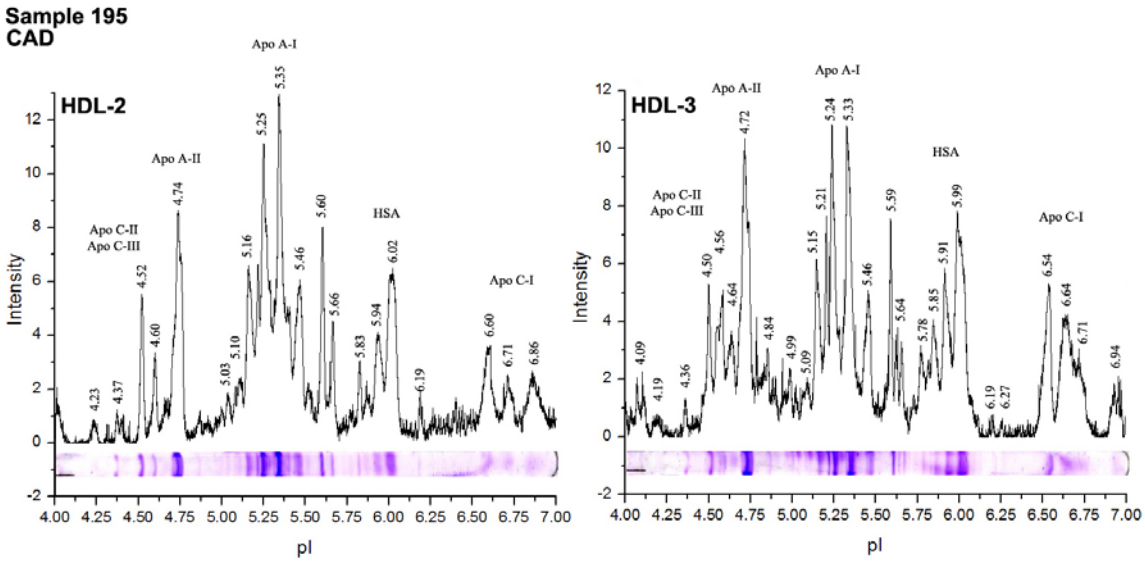

Figure A20. pI Values for Sample #195

VITA

Jeffery Devoyne Johnson Jr. graduated from Texas A&M University in May of 2004 with a B.S. in chemistry. He remained at Texas A&M University and in June of the same year he joined the Laboratory for Cardiovascular Chemistry under the direction of Dr. Ronald D. Macfarlane. Jeffery's research involved the improvement of existing DGU methods through study of the effects of altering heavy metal ions and counter ions in EDTA complexes. These efforts were expanded when his research evolved into the analysis of apolipoproteins of high density lipoprotein with a focus on atherogenic markers by various methods including: mass spectrometry, CE, and gel isoelectric focusing. He defended his research in the fall of 2008 and received his Ph.D. in December of 2008. The author can be contacted at the following address:

Chemistry Department
c/o Dr. Ronald D. Macfarlane
Texas A&M University
College Station, TX 77845-3255